NEW SUPPORTED TRANSITION METAL COMPLEXES: SYNTHESIS, CHARACTERIZATION AND APPLICATION AS CATALYSTS FOR OXIDATION/HYDRODESULPHURIZATION REACTIONS

Thesis submitted to
Cochin University of Science and Technology
in partial fulfilment of the requirements
for the Degree of

Doctor of Philosophy

in

Chemistry

Under the faculty of science

by

ANAS K

DEPARTMENT OF APPLIED CHEMISTRY
COCHIN UNIVERSITY OF SCIENCE AND TECHNOLOGY
KOCHI-22, India

April 2003

.....to my beloved parents

April 25, 2003

CERTIFICATE

This is to certify that the thesis entitled *"New supported transition metal complexes: synthesis, characterization and application as catalysts for oxidation/hydrodesulphurization reactions"* submitted for the award of the degree of Doctor of Philosophy of Cochin University of Science and Technology, is a record of *bona fide* research work carried out by Mr. Anas K under my supervision in the Department of Applied Chemistry.

Prof. K. K. Mohammed Yusuff

DECLARATION

I hereby declare that the thesis entitled *"New supported transition metal complexes: synthesis, characterization and application as catalysts for oxidation/hydrodesulphurization reactions"* submitted for the award of the Ph.D. Degree, is based on the original work done by me under the guidance of Dr. K. K. Mohammed Yusuff, Professor of Catalysis, Department of Applied Chemistry, Cochin University of Science and Technology, and that it has not formed part of any thesis submitted previously for the award of any degree.

Anas K

Kochi-22

25-04-03

Acknowledgement

Man is but a mere mortal and his simple tasks become major achievements due to the encouragement and support of his immediate society.

I would like to express my deep sense of gratitude to Dr. K. K. Mohammed Yusuff, Professor of Catalysis, Department of Applied Chemistry, Cochin University of Science and Technology, Cochin, for his efficient guidance, pertinent encouragement, inspiring discussions and valuable suggestions throughout this investigation.

I express my sincere thanks to Dr. S. Sugunan, Head, Department of Applied Chemistry, CUSAT, for providing necessary facilities for carrying out this research.

I invariably feel short of words to express my heartfelt gratitude and profound thanks to Dr. R. Sreekala, Res. Supdt, Sud-Chemie India Ltd., for her help and encouragement throughout this investigation. The sisterly affection she bestowed upon me is gratefully remembered.

I express my gratefulness to Dr. K. K. Abdul Rashid, Chief Manager, R&D Division, Sud-Chemie India Ltd., for his help and interest during various stages of this research.

I sincerely appreciate the help rendered by Dr. N. Sridevi, throughout this work. I also remain thankful to all the teaching and non teaching staff of this department.

I remain thankful to my labmates, Dr. Suja N. R, Mrs. Vineehta C. P., Mrs. Jyothi Maryam John, Dr. Rani Abraham, Dr. Preetha G. Prassad, Dr. S. Mayadevi, and Mrs. Jaleja P for providing a competitive and enjoyable atmosphere throughout my association in this department.

I express my deep sense of gratitude to Ms. Daly Davis for her help and encouragement during the final stages of this thesis preparation. I always remember my friends, Mr. Sunny Abraham, Dr. Suja Haridas, Dr. Renuka, Ms. Jean John, Ms. Neena Susan, Ms.Vidya and Mr. Robinson for their nice companionship and help at different stages of this work.

I am thankful to my colleagues, Mr. Manu and Mr. Baiju for their help and understanding. I also remember with gratitude to all the staff and workers of the R&D Division of Sud-Chemie India ltd., Binanipuram, Alwaye.

I take this opportunity to express my deep felt thanks to the authorities of Regional Sophisticated Instrumentation Centre (RSIC), IIT, Bombay, Central Drug Research Institute, Lucknow and IISc, Bangalore for providing me with their instrumental facilities.

Finally, I am very much indebted to my beloved parents, siblings and other members of the family for their love, patience, interest and encouragement.

Anas K

PREFACE

Catalysis is a common theme in chemistry and has even been considered as its own sub discipline. ; Catalysis are typically divided into homogeneous, heterogeneous and more recently bio catalysis. Metal complexes play a vital role as homogeneous catalysts for various reactions. One of the main advantages of metal complex catalysts is that the performance of the catalyst can be varied by altering the nature of the ligands. However, their application to large and small scale chemical process is restricted due to their homogeneous nature. It has been recognized that one of its central problem is the separation of the catalyst from the product of the reaction. Leaching of the catalyst and thermal decomposition lead to unacceptable losses in activity and selectivity. In their quest for more efficient catalysts, chemists often want to make use of the advantages of both the homogeneous and heterogeneous systems. Heterogenisation of homogeneous systems can be achieved by supporting the metal complexes on various inorganic and organic supports. Zeolites, silica, alumina and organic polymers are the commonly used supports. Molecules can be encapsulated inside the supercages of the zeolite based on their size and shape selective properties. In addition to the space constraints imposed by the zeolites, the net negative charge of the zeolite framework, and the distribution of the positive charge of the cation can lead to the specific interaction with encapsulated complexes, which in turn can induce structural and functional modification as compared to solution activities. Alumina is also an interesting support material, which can play a double role, acting as a binding agent in catalyst manufacture and as a carrier in the ultimate product. Transition metal complexes supported on alumina as a precursor for the catalyst preparations is getting wider attention of researchers in this field.

This thesis deals with the synthesis and charcterisation of some supported transition metal complexes and their catalytic properties. Two industrially important reactions were carried out: i) cyclohexanol oxidation and ii) hydrodesulphurization of diesel. Thesis is divided into nine chapters. An overview of the heterogenised homogeneous systems is given in Chapter 1. Chapter 2 deals with the materials and methods used for the preparation and characterisation. Details regarding the synthesis and characterisation of zeolite encapsulated transition metal complexes are given in Chapter 3 to Chapter 7. In Chapter 8, the results of catalytic activity studies of the cyclohexanol oxidation using the zeolite encapsulated complexes are presented. Details of preparation of hydrodesulphurization catalysts through the molecular designed dispersion method, their characterization and catalytic activity studies are presented in Chapter 9. References are given at the end of the thesis.

CONTENTS

HETEROGENISATION OF HOMOGENEOUS CATALYSTS: AN OVERVIEW

Catalysis is a key technology for the future developments and for solving the challenges regarding limited resources, growing population and environmental problems. Activity, selectivity and recycling are the essential features that have to be considered for the successful applications of catalysts. Catalysis is a kinetic phenomenon and traditional appreciation of catalysis is in terms of rate enhancement and energy savings. In practice, it involves the interaction of as many fields such as organic chemistry, surface chemistry, chemical kinetics, thermodynamics, solid state physics, ceramics and physical metallurgy. As more and more catalysts and catalytic process are available, the emphasis of research in this field has shifted to achieve more selectivity. Selectivity of catalysts is as old as the first appearance of enzymes on the face of the earth.

Catalytic processes are generally more selective, and capable of optimal utilization of raw materials. Unlike the stoichiometric oxidations with traditional oxidants such as permanganate and dichromate, the catalytic process does not produce large quantity of inorganic effluents which are difficult to dispose off. In view of the growing concern over the environmental problems, chemical industries are forced to adopt various catalytic techniques for their exhaust and effluent control. An important class of catalysts used with a view to environmental protection is auto-exhaust catalysts. Here noble metal catalysts supported on monoliths are used for the treatment of nitrogen oxides (NOx) and carbon monoxide to harmless carbon dioxide and dinitrogen.

The subject of catalytic reactions actually embraces the three traditionally different fields of catalysis: homogeneous, heterogeneous and biological (enzymatic) catalysis. These three areas have been generally developed as virtually separate disciplines with research in one area having little apparent relevance to that in the other two. As a result, greater emphasis must be placed on the development of new and improved catalytic processes.

1.1 Homogeneous catalysis by metal complexes

About 90% of organic chemicals are developed from petroleum and the majority of petrochemical processes are catalytic. Among these the most important reactions are catalytic oxidations[1,2]. Metal complexes play an important role in the control of selective/partial oxidation of alkenes, olefins and aromatic hydrocarbons to useful products. Hydroformylation or Oxo process, discovered by Roelin in 1938, for the production of an aldehyde from carbon monoxide and hydrogen, is the oldest and largest volume homogeneous catalytic oxidation reaction by metal complexes[3]. Eventhough, a serious study and applications of homogeneous catalysis of liquid-phase oxidation had originated in the late 1950s, the production of useful chemicals like terephthalic acid and acetaldehyde (Waker Process)[4] were reported only in 1959. Since then a large number of homogeneous catalysts were reported for oxidation reactions[5-9]. Palladium complexes containing *p*-triphenylphosphinemonophosphate was found to be active for the biphasic catalytic carbonylation of benzyl alcohol[5].

Epoxidation reactions are important in organic synthesis because the product epoxide can be converted into a variety of products. Oxochromium(V) complexes formed from chromium(III)-Salen is an active catalyst for the alkene epoxidation. These complexes can effect the direct epoxidation of norbornene[10]. A few molybdenum and cobalt complexes were found to epoxidise alkene[11-15]. The increasing demand for enantiomerically pure pharmaceuticals has fueled the search for asymmetric epoxidation catalysts, which would introduce one or two new stereocenters upon reaction with an olefin of appropriate symmetry. Asymmetric epoxidation reactions are thus very important from the point of view

of synthetic strategy. Manganese(II) Schiff base complex of chiral salen ligand was found to be active for the epoxidation of olefin[16]. Enantioselective ring opening of meso aziridines has been catalyzed by chromium(III) complexes of tridentate Schiff base derived from 1-amino-2-indanol[17]. Asymmetric cyclo addition reaction using chiral transition Schiff base complexes has also been studied[18]. Vogt *et. al,* reported the asymmetric nickel-catalyzed hydrocyanation of vinylarenes by applying homochiral xantphos(stereogenic diphosphene) ligands. An enantioselectivity of 63% was obtained when 4-isobutylstyrene was used as the substrate[19].

Eventhough transition metal complex catalysts are found to have better catalytic activity and selectivity, the separation of catalyst and reaction product from the reaction system is not that easy. Another disadvantage of the transition metal complexes is their instability to withstand high operation temperatures. A broad range of techniques for cost effective separation - such as catalysis in water, dendrimeric catalysis, and heterogenisation of homogeneous metal complexes are used and many more techniques are under investigation.

During the last few years there is an increasing interest in the application of dendrimers in catalysis. Dendirmers are highly branched regularly repeating macromolecules constructed via an interactive sequence of reaction steps[20]. The combination of organometallic and dendrimer chemistry has led to the development of interesting metallodendrimers which have proven to be of use in a variety of applications such as catalysis, electron transport, nano-reactors, drug or gene delivery agents, enzyme mimics, etc[21,22]. Numerous metallodendritic catalysts with active sites on the outer surface or at the core of the molecule have been reported[21,22]. Such catalysts are found to have advantages over monomeric homogeneous and heterogeneous catalysts in some of the applications. They can easily be recovered and separated from the reaction medium by chromatography or nanofiltration. Dendrimer-porphyrin Mn(III) complexes are found to have greater regioselectivity than the corresponding parent 5,10,15,20-tetrephenyl-porphyrinatomanganese(III) cation towards the epoxidation of alkenes[23]. Garber

et al. reported a dendritic analogue of ruthenium carbene catalyst for olefin metathesis[24]. First, second and third generation poly(amido)amine dendrimers with Co-Salen complex catalyse asymmetric ring opening reactions of olefins[25]. However, these types of catalysts suffer from severe limitations. The catalytic units placed in a densely packed surface (of a higher generation dendrimer) can interfere with each other, thereby decreasing the activity. On the other hand, catalytic sites residing at the core (focal point) of the dendrimer (or dendritic wedge) can be used to change the solubility properties of the catalyst and may result in beneficial interactions between the dendritic branches around the catalyst and the substrate. However, when the catalytic site is located inside a higher generation dendrimer, the branches can even prevent access of the substrate (as well as exit of products) and affect the catalysis reaction. The introduction of regio- and/or stereo control in a chemical reaction by using dendrimers with an encapsulated catalytic site is not yet straightforward. Apparently, the molecular network of dendrimers is too flexible to impose distinct spatial constraints on the course of the reaction. In fact, there is lot of scope for developing new metallodentritic catalysts with specific applications.

1.2 Heterogenisation of homogeneous systems – use of supports

Heterogenisation of homogeneous systems is an interesting area of research to exploit the advantage of both homogeneous and heterogeneous systems. Normally heterogenisation indicates the process of immobilisation of homogeneous transition metal complexes to an inert polymer or inorganic support. By anchoring the metal complexes on a solid surface, structurally organized catalytically active sites are generated. Such complexes exhibit higher activity and selectivity than their homogeneous counterparts with structurally disorganized active sites.

The inorganic supports used for anchoring are silica, alumina, zeolites and clays. The organic supports employed are polymers such as polystyrene, poly(4-vinyl pyridine) etc. Catalysts anchored to inorganic supports are sufficiently different in their chemical and physical properties when compared to

polymer supported species. The inorganic supports usually have the potential to tailor the catalyst structure to maximize selectivity and activity. Further, these complexes anchored on inorganic supports have preparative flexibility and stability. Among the various inorganic supports used, zeolite and aluminas are more important and are considered here in detail. Both the zeolite supported and alumina supported catalysts can act as bi-functional catalysts. The catalytic functions of these systems are often known to have contribution from the support.

1.2.1 Zeolites

Zeolites are crystalline aluminosilicates. Their crystal structures contain extensive cavities and channels. A zeolite with a particular topology is described by a three-letter code[26] irrespective of their chemical composition (Table 1.1). Zeolites are viewed as the "philosopher's stone" of modern chemistry[27]. They are widely applied as solid acid catalysts in oil refining and petrochemical manufacture[28]. Their use circumvents the effluent handling problems associated with conventional mineral acids such as sulfuric acid and hydrofluoric acid as well as Lewis acids such as aluminium chloride (for example in the alkylation of aromatic hydrocarbons)[29]. Moreover, crystalline zeolites require mild reaction conditions, and hence use of these catalysts leads to lower capital investment and increased flexibility in industrial applications[30]. Zeolites also find wide applications in fine chemical synthesis.

In fine chemical synthesis there is a marked trend towards replacement of stoichiometric amounts of inorganic oxidants, such as chromium(VI) and manganese(VII), with cleaner catalytic alternatives. Introduction of a redox metal center into molecular sieves considerably extends their catalytic potential[31-33]. The structural diversity of these systems including variation of the redox metal, incorporation of metal complexes, and the size and polarity of the micropores - provides the possibility of designing tailor-made solid catalysts ("mineral enzymes") for liquid phase oxidation with clean oxidants such as O_2, H_2O_2 and RO_2H. Heterogenised homogeneous system, as well as a novel redox-active

molecular sieve can easily be achieved through zeolite encapsulated transition metal complexes[34-37].

Table 1.1
Pore dimensions and the codes of various zeolites

Structure type	Trivial names	Pore diameter [Å]
LTA	Zeolite A	4.1
MFI	ZSM-5, TS-1, VS-1	5.3 x 5.6; 5.1 x 5.5
MEL	ZSM-11, TS-2, VS-2	5.3 x 5.4
MTT	ZSM-23	4.5 x 5.2
EUO	EU-1	4.1 x 5.7
AEL	$AlPO_4$-11	3.9 x 6.3
-	ZSM-48	5.5
-	MCM-22	5.6
MTW	ZSM-12	5.5 x 6.2
TON	Theta -1, ZEM-22	4.4 x 5.5
MOR	Mordenite	6.5 x 7.0; 2.6 x 5.7
	NCL-1	6.5-7.0
BEA	Zeolite-β	7.6 x 6.4 5.5 x 5.5
AFI	$AlPO_4$-5	7.3
EMT	Hexagonal faujasite	7.4; 7.4 x 6.5
FAU	Zeolite X or Y	7.4
AET	$AlPO_4$-8	7.9 x 8.7
CLO	Cloverite	13.2 x 4.0
VFI	VPI-5	12.1
-	MCM-41	15-100

Zeolite encapsulated transition metal complexes

The desire to mimic bio systems has prompted an extensive area of research work, involving the metal complexes of synthetic porphyrin, phthalocyanines and Schiff bases. Many models of enzyme active sites, especially for monoxygenase enzymes of the cytochrome P-450 family have been synthesised[38,39]. Comparative studies on the selectivity and stability associated with both synthetic models and natural systems, in the biomimetic oxidation of hydrocarbons, led to the conclusion that selectivity arises not only from the steric effects imposed by the environment of the enzyme active site upon substrate approach[39-41], but also from specific binding at the active site. Therefore, this field of research has been the subject of intense efforts to mimic, in a first approach, the protein cavity of natural enzymes, and of designing synthetic superstructured porphyrin models with a controlled steric environment such as picnic-basket porphyrins, strapped porphyrins, etc[42]. A similar conceptual approach has been developed and is based on mimicking the protein portion of natural enzymes by a size- and shape-selective framework of a mineral matrix such as clays and zeolites. These inorganic materials would provide the best arrangement for the catalytically active centers and can direct the substrate towards these centers[43-46]. Zeolite encapsulated transition metal complexes are generally referred to as "ship-in-a-bottle complexes" or zeozymes. For encapsulation of large complexes, zeolite with FAU or EMT (hexagonal faujasite) structures have been used in most cases. They posses a supercage (diameter 13Å) that can readily accommodate large metal complexes of ligands such as phthalocyanines, porphyrins, aromatic Schiff bases, amino acids etc. The zeolite encapsulation has both advantages and disadvantages. The primary advantages are the uniform dispersion of metal ions throughout the solid and prevention of polynuclear cluster formation of metal ions. Furthermore, the frame work structure of many zeolites, including the dimensions and arrangements of the cages are roughly equivalent to those that are encountered in enzyme catalysis, thus making some possible comparisons. Available space restricts the number of active complexes to one per supercage, and pore windows are not large enough to allow them diffuse and oxidise each other.

Zeolites effectively function as the solvent and as the counter ion in the formation of metal complexes. The window size in a zeolite restricts the size of the ligand that can be used and from this point of view, the use of zeolite is disadvantageous. For example, the catalytically useful ligand, triphenylphosphine is much too large to fit into a Y-type zeolite[47]. Furthermore, the encapsulation is generally limited to cationic complexes since the zeolite structure is anionic. In practical catalysis, diffusion may be a problem, particularly when many of the cavities are nearly filled with large complexes.

Methods of encapsulation

The most widely applicable synthetic methods for encapsulation are a) intrazeolite synthesis by complexation b) intrazeolite ligand synthesis and complexation and c) template synthesis

a) Intrazeolite synthesis by complexation: In this case the ligand is small enough to diffuse through the zeolite pores to form complexes with metal ion in the cages, but the metal complexes once formed are generally too large to diffuse out. The starting material is a transition metal ion-exchanged zeolite in which the metal ion is surrounded by H_2O, HO^- or oxide ions of the zeolite lattice. These weak ligands can usually be replaced by coordinating ligands. Encapsulated complexes of bis(salicylaldehyde) ethylenediimine (Salen) have been prepared by the interaction of Salen into transition metal exchanged faujasites[48]. Bipyridyl complexes of Fe, Mn, Cu and Ru were also prepared by this method[49-52].

b) Intrazeolite ligand synthesis and complexation: The metal complex is synthesized inside the zeolite cavity from smaller components of the ligand or by assembling it from smaller species around the transition metal ions inside the zeolite cavities. The synthesis of tetraphenylporphyrins as well as iron and manganese 5,10,15,20-tetramethyl prophyrin in FAU zeolite has been prepared using this method[53,54]. In the case of phthalocyanine complex the metal is introduced into the zeolite, through ion exchange in the form of carbonyl complex or metallocenes, followed by 1,2-dicyanobenzene, which reacts at elevated

temperatures to form the metal phthalocyanine in the pores[46]. The presence of unchelated transition metal ions can be largely avoided by the use of metallocenes, although a large fraction of the phthalocyanine remains metal free.

c) Template synthesis: In this method, metal complex, which acts as a structure directing agent (template) during the hydrothermal synthesis, is added to the synthesis gel. A major restriction for this method is that the metal complex to be used as the templating agent must be stable during the phases of the zeolite synthesis, such as high pH values and temperatures. Therefore the complexes that can be made by this method are scanty. On the other hand, it has the advantage that the metal complex is with a predetermined coordination. Phthalocyanine complexes of Fe, Co, Cu, Ni and Mn have been reported to be incorporated in FAU zeolites by this method[61-65].

Catalysis by zeolite encapsulated transition metal complexes

Detailed investigations on the catalytic behaviour have been reported for the zeolite encapsulated complexes of phthalocyanine, porphyrin, carbonyls, Schiff bases, bipyridienes, amines etc[43,55-67]. Zeolite encapsulated iron phthalocyanine (FePc) complexes are reported to be selective in oxidation of alkenes to alcohols and ketones under ambient condition with iodobenzene[43,55], or *tert*-butylhydroperoxide[56]. Encapsulated iron-phthalocyanine were found to be active in the oxidation of cyclohexane to cyclohexanone and cyclohexanol and the selectivity towards chclohexanone was high (95%) in comparison with that for the 'neat' analogue. The homogeneous complexes were found to be oxidatively destroyed under the reaction conditions and therefore are not regenerable[57]. Jacbos *et. al.*, reported the oxidation of cyclohexanone to adipic acid, using zeolite encapsulated complex[58]. Increased turnover number based on iron with the lower loading of FePc zeolites was observed in this reaction. This result was interpreted as due to the very effective site isolation within the cages, which prevents any bimolecular pathways to phthalocyanine catalyst destruction[59,60]. However, the catalytic oxidation reaction slows down due to the clogging of the pore system of zeolite with reaction products, thus preventing further access of reagents and

substrate to the active site. Similarly zeolite encapsulated phthalocyanine complexes of cobalt[61,62], copper[63,64], nickel, manganese, ruthenium, and osmium[65] were synthesized and characterised. CoPc encaged in zeolite EMT is an active catalyst for the oxidation of ethylbenzene with molecular oxygen[66], where as encapsulated chloro- or nitro phthalocyanine of Cu, Fe and Co are found to be effective in oxyhalogenation of benzene, toluene, phenol, aniline, anisole and resorcinol[63] under ambient conditions. Seelan *et. al*[64] ., reported the epoxidation of styrene using zeolite encapsulated copper phthalocyanine complex. Recently phenol hydroxylation activity of encapsulated phthalocyanine complex of V, Co and Cu have been studied[67]. The encapsulated complexes exhibited enhanced phenol hydroxylation activity with H_2O_2 compared to the 'neat' complexes and a comparative study revealed that the activity and product selectivity of the encapsulated complexes depend mainly on the redox potential of the $M^{(n+1)}/M^{n+}$ couple of the central metal ion.

Jacobs *et. al.*, was able to develop an efficient mimic of cyctochrome P-450[68]. It comprises the encapsulation of iron phthalocyanine complex in the supercages of zeolite Y followed by embedding this inclusion compound in the polydimethylsiloxane membrane. This system is found to oxidise alkanes at a comparable rates with those of the true enzyme at room temperature.

Catalysts, which imitate the high specificity and activity of the enzymes have been prepared by supporting metalloporphyrins on a rigid support[69,70]. Site isolation of the active center by bonding to the support is assumed to prevent the formation of less reactive dimers, (e.g., (μ-oxo)metalloporphyrin dimers) thereby tuning the catalytic activity favorably. Catalytically active zeolite encapsulated metalloporphyrins (iron and manganese tetramethyl and tetraphenyl porphyrin) and zeolite encapsulated zinc porphyrin complex have been reported[53,71]. Encapsulated iron-porphyrins containing electron withdrawing substituent on the β-pyrole position are found to be highly active for alkane hydrolysis[72]. Cationic meso-tetrakis(1-methyl-4-pyridino) porphyrinato manganese(III) complex encapsulated in modified zeolite Y and MCM-41 are reported for high activity and

selectivity towards the epoxidation of styrene and cyclohexane by iodosylbenzene[73].

Catalytically active metal phthalocyanine[74] and porphyrins encapsulated inside large pore materials like MCM-41 have been reported[75]. The phthalocyanine complexes were found to retain their planar structure in MCM-41, while they are known to be distorted in zeolite Y[74].

Zeolite encagement of Schiff base complex is getting wider attention in the field of heterogenised homogeneous systems. A large variety of zeolite encapsulated Schiff base complexes were studied. Zeolite encapsulated metal-Salen complexes [Salen = N, N'-bis(salycylaldehyde)] are one of the well studied systems. Intrazeolite synthesis by complexation method was adopted for the preparation of Salen complexes, since this ligand offers the desired flexibility. The metal complexes of this ligand are of an appropriate size (~10-11Å), so once formed in the supercages of zeolite Y (~10 Å) the complex cannot escape through the 7 Å ring opening[48]. Thus a large variety of cobalt[48], manganese[76], iron[77], rhodium[78] palladium[79] Salen complexes were prepared within the Y-faujasite supercage.

Ratnasamy *et. al*[80]., reported the synthesis of substituted Cu(X_2-Salen) (where X = H, Cl, Br/NO_2) encapsulated in the cavities of zeolite NaX and NaY. These authors synthesised the complexes using two different srategies *viz.* intrazeolite synthesis by complexation and template synthesis method. The former method resulted in the inclusion of more complex than the latter owing to the low, but finite solubility of Cu-Salen in the synthesis medium. Substitution of the aromatic hydrogen atom of the Salen ligand by electron withdrawing groups like -Cl, -Br and -NO_2 in the above complex show an enhancement in retention and concentration of the complex in the zeolite cavities. Zeolite encapsulated Cu(Salen) shows a colour isomerism upon treatment with a specific solvent[81]. The green encapsulated complex which is inactive on treatment with MeCN turns red and is catalytically active in oxidation reaction. In the case of Cu(Salen)-NaY(red)

catalyst Cu(II) ion appears to posses vacant axial positions and hence the catalyst is active in oxidation reactions, whereas the green variety, with Cu(II) ion in either five-or six-coordination, is inactive. Thus, the catalytic activity of Cu(Salen)-NaY changes dramatically with change in the coordination geometry around the Cu(II) ion in the zeolite. Mn(III) complexes with substituted Salen (3,5,3'5'-tetrachloro- and 3,5,3',5, terabromo) ligand encapsulated in zeolite-X catalyse the aerobic oxidation of styrene[82]. Enhanced catalytic activity for the selective oxidation of cyclohexanol to cyclohexanone using H_2O_2 oxidant was reported for zeolite Y encapsulated Cu(Salen) complex[83]. A Co(Salen) complex prepared inside the pore structure of Y zeolite was found to exhibit affinity for dioxygen as the pyridine adduct[48]. These adducts have excellent resistance to autoxidation even at elevated temperatures. The EPR spectrum of VO-Salen complex encapsulated in zeolite Y shows a tetragonally distorted structure and the complex has been reported to be catalytically active for phenol hydroxylation with 99% selectivity towards dihydrosobenzene[84]. Asymmetric epoxidation of alkenes can be achieved using zeolite Y encapsulated Mn(III) complex of a chiral-Salen ligand [Salen - *trans*-(R,R)-1,2-bis(salicylideneamino)cyclohexane][85].

Ratnasamy *et. al*[86]., carried out EPR studies to get an idea about the geometry of the encapsulated Salen complexes of Mn and Cu. The EPR spectroscopy distinguishes the encapsulated complex from the corresponding 'neat' and surface-adsorbed counterparts. Neat complexes showed broad EPR spectra due to spin-spin interactions; whereas, the encapsulated species showed well resolved metal hyperfine features resembling spectra of dilute frozen solutions. The spin hamiltonian parameters reveal a distorted square pyramidal geometry and an increase in the in-plane covalency of metal-ligand bond as consequences of encapsulation. These studies suggest that the distortion in molecular geometry arising out of encapsulation and the consequent depletion of electron density at the metal site are responsible for the enhanced catalytic activity of the zeolite encapsulated copper and manganese Salen complexes.

Zeolite-Y encapsulated Co(II) complex of tetra-*tert*-butyl-Salophen (prepared from 3,5,-di-*tert*-butyl salicylaldehyde and 1,2,-diaminobenzene), was found to be an efficient oxygen-activating catalyst in the palladium-catalysed aerobic 1,4-diacetoxylation of 1,3-dienes[87]. This is an example for the combined use of homogeneous and heterogeneous catalysts to make catalysis more effective. The homogeneous part controls the selectivity of the organic transformation; whereas the heterogeneous part plays the role of oxygen activation. Zeolite encapsulated Co(Salophen) was also found to be active in the ruthenium catalyzed selective oxidation of benzyl alcohol to benzaldehdye with 99% selectivity[88]. Another advantage of the heterogeneous system over the homogeneous counterpart is the deletion of extra axial ligand such as triphenylphosphine. Copper(II) complex of N_3O_2 Schiff base derived from, acetylacetone and a triamine, encapsulated in the supercage of zeolite Y was reported[89]. Here encapsulation was accomplished by the adsorption of copper(II) acetylacetone in the supercage of zeolite followed by addition of an aliphatic triamine to effect Schiff base condensation with the adsorbed copper(II) acetylacetone.

Another important class of zeolite encapsulated complexes, which is of immense attention, is the one involving bipyridyl complexes. Zeolite encapsulated Mn(II) bipyridine complexes[50] catalyse selective epoxidation of alkenes without complications from competing process such as self-oxidation or catalase activity. The epoxides of cycloalkenes can be transferred to alkenedioic acids by acid catalysed ring opening and carbon-carbon bond cleavage. Mizuno and Lunsford[90] from EPR measurements indicated a temperature driven interconversion between low spin and high spin state of the cobalt(II) tri(bipyridyl) complex ion, $[Co(bipy)_3]^{2+}$, encapsulated in the supercages of zeolite-Y. This is an interesting observation because the normal trigonally distorted $[Co(bipy)_3]^{2+}$ complex ion, both in solution and in solid state, retains high spin ground state, irrespective of the temperature or the nature of the counter ion[91]. A molecular graphic analysis indicated that it is impossible to fit the $[Co(bipy)_3]^{2+}$ ion having the same trigonally distorted geometry of the 'free' state, without causing

it to bump into the walls of the supercage. Tiwary and Vasudevan[92] used a molecular mechanics calculation to determine the minimum energy geometry that the $[Co(bipy)_3]^{2+}$ ion would adopt on encapsulation. According to the calculation; the minimum energy structure is one in which the complex attains an orientation in such a way that large sections of the bipyridyl groups are accommodated within the windows of the supercage. This change in geometry in turn leads to a change in the spin state of the cobalt ion. Zeolite encapsulated bipyridine complexes of iron[93] and manganese[94] were also reported.

Another interesting feature of zeolite encapsulated bipyridine complexes, especially of the ruthenium complex, is their photocatalytic activity. The guest/host interactions significantly retard the energy wasting back-electron-transfer reactions of initial photo products[71]. It has been demonstrated that the intrazeolitic complexes which possess ligands bearing a peripheral nitrogen atom, such as Y-$Ru(bpy)_2(bpz)^{2+}$ (where bpz is 2,2'-bipyrazine), are susceptible to coordination of another molecule of Ru^{2+} complex[95,96]. This approach is expected to provide highly efficient photocatalysts for solar energy conversion in the light of the unique reactivity and special distribution of the appropriate components[97]. The bis-terpyridine complex, $[Ru(tpy)_2]^{2+}$ in free solution has a very short excited state lifetime and is practically nonluminescent. The entrapment within the zeolite supercage dramatically increases emission intensity and excited state lifetime at room temperature[98]. and the zeolite encapsulated ruthenium bipyridyl complexes are reported to be an efficient oxygen sensor material[99]. The efficiency of luminescence quenching by oxygen on going from surface-adsorbed to zeolite-encapsulated flurophores increases drastically. $Ru(bpy)_3^{3+}$ trapped in the supercages of zeolite-Y can oxidise intrazeolitic water to dioxygen slowly, but with high efficiency[100].

Amino acid complexes encapsulated in the supercage of zeolite-Y can play vital role as zeozymes. Weckhuysen *et. al.*[101,102], reported the immobilization of Cu(histidine) complexes in zeolite by a simple ion exchange procedure. Amino acids like histidine, are the key building units of natural enzymes; therefore, the so

obtained inorganic enzyme has an active centre, which closely resembles its natural enzyme counterparts. Amino acid complexes of copper have been encapsulated and studied in the oxidations of alcohols, alkanes and alkenes by peroxides. Surprisingly the TON of these reactions are the same as that of several natural enzymes[103].

Metal carbonyl clusters grafted on supports such as oxides and zeolites offer a great deal of advantage for preparing supported metal catalysts at molecular level. Metal carbonyl clusters have been synthesized by introduction of metals by ion exchange followed by carbonylation[104] or by introduction of volatile metal carbonyls followed by condensation reaction with carbon monoxide[105]. Synthesis of zeolite encapsulated carbonyl clusters of Rh, Fe, Ir, Pd and Mo have been attempted in the supercages of NaY[106-110]. There are reports[111,112] about intrazeolitic bimetallic clusters like $[Fe_2Rh_4(CO)_{16}]^{2-}$ and $Rh_{6-x}Ir_x(CO)_{16(x=0-6)}$. Detailed investigations are in literature about intrazeolite half-sandwich complexes of rhodium and iridium[113].

Zeolite encapsulated metal carbonyl clusters find wide applications in catalysis. The encapsulated osmium carbonyl clusters offer stability and selectivity for CO hydrogenation to give C_2-C_4 hydrocarbons[114]. RhFe bimetallic carbonyl clusters synthesized in NaY catalyse the formation of a mixture of ethanol and methanol[111]. Iron carbonyl complexes in a hydrated sodium-Y zeolite matrix are noted for their catalysis in water gas-shift reaction[115]. A novel, zeolite encapsulated μ_3-oxo Co/Mn cluster catalysts were reported to oxidise *p*-xylene to terephthalic acid[116]. Cobalt cyanide complex, after encapsulation, was reported to be the first anionic complex synthesized inside a zeolite cavity[117,118]. These complexes are important due to the reversible oxygen binding capacity.

Investigations on the feasibility of Zeolite-X encapsulated metal complexes of octaaza macrocyclic ligand for the selective aerobic oxidation of methane at 273K using *tert*-butylhydrogen peroxide (TBHP) as a promoter in acetonitrile or water solvent has been carried out. The catalytic activity of the encapsulated

macrocyclic complex was found to be better than that of the neat Salen/substituted Salen complexes[119]. There are recent reports on the inclusion of azido iron(III) cyclam complex [cyclam = 1,4,8,11-tetraazacyclotetradecane] by intrazeolite synthesis by complexation method[120]. This complex is promising as a potent precursor for the synthesis of catalytically active Fe(V) nitrido species.

Kazusaka *et. al.*, have reported a copper(II)-pyridine derivative complex, $(Cu(2\text{-ethylpyridine})_n)^{2+/+}$, encapsulated within the supercage of Y-zeolite[121]. The encapsulated complex was used for the oxidative coupling of 2,6-dimethylphenol. The reaction gave two main products: diphenoquinone (DPQ) and polyphenylenoxide (PPO). Cu-Py-NaY was found to exhibit very high selectivity to PPO in comparison with Cu-Py-SiO_2 or CuCl+Py, in spite of its low catalytic activity. Further, they also observed the complex to be easily reducible to Cu(I) under vacuum at 200^{0}C and this reduced state gets re-oxidized to Cu(II) upon exposure to oxygen.

A novel zeolite Y encapsulated binuclear copper complex of 3-formylsalicylic acid was reported to be very efficient for the partial oxidation of benzyl alcohol and ethyl benzene[122]. Some zeolite encapsulated amine complexes; such as tetrammine copper(II)[123], cobalt(II) ethylenediamine etc. have been reported[124]. The zeolite encapsulated cobalt ethylenediamine complexes bind oxygen reversibly[124]. However, according to Schoonheydt and Pelgrism the mono and tris complexes are not capable of binding oxygen whereas the bis complex form 1:1 superoxo-complex $[Co(en)_2(O)_2]^{2+}$ and the 2:1 monobridged peroxo-complex $[\{Co(en)_2\}_2(O_2)]^{4+}$ are able to bind with oxygen[125].

As a result of encapsulation of the complexes and owing to their site isolation, a number of generalisations can be made on analyzing the available data[126]:

- Turnover number increases when the catalyst is encapsulated.
- Turnover number decreases with increased loading of the zeolite with complex. This decrease is associated with pore blockage of zeolite cages.
- The dimensions and shape of the environment at the active site control shape and regio-selectivity, and reactant diffusion as well.
- High yields of oxygenated products are mostly obtained with pure and highly diluted entrapped complexes.

The recent development in the field of hetergoenization of homogeneous system is the use of heteropoly acid as an anchoring agent[127,128]. The heteropoly acid is attached to the support by the interaction of the acidic protons with the basic sites of the support. Either ion pairing or a direct bond between oxygen atoms of the heteropoly acid and the metal has been used for the anchoring of the metal complex.

Mukhopadhyay and Chaudhari reported the synthesis of heterognized Wilkinson's hydroformylation catalyst, $HRh(CO)(PPh_3)_3$, by tethering it to zeolite-Y though phosphotungstic acid as a tethering agent[129]. They report that the catalysts prepared were highly stable and reusable besides better activity. Zsigmond *et. al.*, heterogenized the rhodium complexes of L-prolinamide and N-*tert*-butyl-L-prolinamide by two different methods ("ship-in-a-bottle" and anchoring methods) and the complexes were used in the hydrogenation of simple and prochiral alkenes. The "ship-in-a-bottle" type heterogenized rhodium complexes were active in the hydrogenation of hex-1-ene, cyclohexene, and 1-methylcyclohexene. At the same time the heterogenized catalyst had all the expected advantages of the heterogeneous system, namely easy handling and recyclability. The anchored catalyst could also catalyse the same hydrogenation reactions and thus showed all the advantages of the heterogeneous catalysts. However, the latter one showed more activity in the above hydrogenation reactions than the "ship-in-a-bottle" type catalysts. The anchored catalyst showed

higher enentiomeric excess *(ee)* in the enantioselective hydrogenation of *trans*-2-methylpent-2-enoic acid than its encapsulated counterpart[130].

1.2.2 Alumina

The earlier concept of a support was that the support is an inert substance which can provide a mean of spreading out an expensive catalyst ingredient such as platinum for its most effective use, or a means for improving the mechanical strength of an inherently weak catalyst. However, the support material may actually contribute to the catalytic activity, depending upon the nature of reaction and conditions, and it may react to some extent with other catalyst ingredients during the manufacturing processes. Some substance such as colloidal alumina or colloidal silica may play a double role, acting as a binding agent in catalyst manufacture and as carrier in the ultimate product. Alumina in the η and γ-form are intrinsically weakly acidic, but these substances may be a truely inert carriers for many reactions[131]. In some cases, it can be used itself as catalyst. A large variety of alumina exists; different forms can be made distinguishable from one another by X-ray diffraction. However, the nomenclature used by different research workers for the various alumina hydroxides and alumina may vary.

Aluminas are generally prepared by dehydration of various aluminium hydroxides. Even if the hydroxide is a gel, it can be readily converted to a crystalline form on aging and/ or heating. The most important aluminas for use as carrier are γ-Al_2O_3 or η-Al_2O_3. These forms have high surface area and are relatively stable over the temperature range of interest for most common catalytic reactions. They are very similar in structure and indeed sometimes are not easily distinguishable. Both the forms have a crystallographic form in which the oxygen atom arrangement is similar to that in spinel ($MgAl_2O_4$). The η form of alumina is more distorted than the γ form. The η form is inherently more acidic than the γ form, which makes it more active for many acid-catalyzed reactions such as olefin isomerization[132].

A large number of mixed oxides exist in the spinel structure, which is expressed in the general form $M^{II}M_2^{III}O_4$. Some simple oxides also form this structure, for example, Mn_3O_4, Fe_3O_4 and Co_3O_4. Crystallographically, the atomic ratio of the total metal atoms to oxygen atom is 3:4 for a spinel but only 2:3 for alumina. Hence for aluminas such as η and γ a portion of the lattice positions are vacant and there are varying degrees of disorder. This may be the principle reason for the greater solubility and compound formation between heavy metal cations and γ-Al_2O_3 and a supported catalyst[131]. These supports may have little catalytic activities. Aluminates in general are formed more readily than silicates.

γ-Alumina is used as a support for a large number of catalysts. Platinum supported on γ-Al_2O_3 find wide application as catalysts. A high metal support interaction was reported for the Pt/Al_2O_3 catalysts[133]. Melchor *et al.*, reported the synthesis of chlorinated alumina supported Pt catalyst at 200 and 300^{0}C[134]. A greater enhancement in n-butane isomerization activity was observed for the sample calcined at 300^{0}C. After calcination, Pt is oxidized to $PtCl_2$, which reacts with $AlCl_3$ to produce $PtCl_2$ $2AlCl_3$ complex. This complex is mobile on the support and agglomerates in large particles. During the isomerization of n-butane, platinum is reduced in the metallic state leading to very low metal dispersion. Very small platinum clusters are also present, which are able to perform the hydrogenation of butanes and to decrease the coke formation. On pure alumina no reaction was detected except at high temperature, where coking of the catalyst takes place[135]. The catalytic monohalogenation of methane was achieved over either γ-Al_2O_3 supported solid acid /platinum metal catalysts[136]. The mechanism of the halogenation is considered to involve insertion of a surface-coordinated electrophilic halogen species or electron deficient metal site into a methane C-H bond. The resulting five-coordinate intermediate carbonium ion may undergo, subsequent cleavage - halogenolysis to give the monohalogenated methane. A bimetallic Pt-Pd cluster produced by laser vaporisation of bulk metal or alloys deposited on high surface area γ-Al_2O_3 is an effective catalyst for hydrogenation of toluene[137]. Ivanov *et. al.*, reported the n-pentane isomerization

using Pt catalysts supported on two different supports *viz.*, 12-tungstophosphoric heteropolyacid (HPWA) on alumina and fluorinated alumina[138]. It was shown that $Pt/HPWA/Al_2O_3$ system is almost inactive in isomerization as a result of the interaction of HPWA with basic site of the alumina support. On the contrary, the presence of acidic sites in fluorinated alumina can prevent HPWA destruction and favour the uniform distribution of HPWA on the support surface and hence enhancement of the activity and selectivity was observed for this catalyst in isomerization. Enantioselective hydrogenation of pyruvate over polymer-stabilized and alumina supported platinum nanocluster have also been reported[139].

The hydrogenation of isoquinoline to isomeric decahydroisoquinoline via 1,2,3,4-tetrahydroisoquinoline or 5,6,76,8-tetrahydroisoquinoline was kinetically studied over ruthenium catalysts supported on carbon and alumina[140]. The hydrogenation of carbondioxide was reported with ruthenium catalysts deposited on supports like SiO_2, Al_2O_3 and ZnO_2[141]. The acidic nature of alumina support exhibits a preference for nitrogen lone-pair during the reaction. A bimetallic Pt-Ru supported on alumina was used for the hydrogenolysis reaction of methyl cyclopentane[142]. Osawa *et. al.*[143], reported the synthesis of $Pt\text{-}Ru/\gamma\text{-}Al_2O_3$ catalysts for dehydrogenation of cyclohexane.

Alumina-supported rhodium catalysts find application in low pressure hydrogenation of allene[144]. Alumina supported molybdenum catalysts, synthesised using the facile reaction between $Mo(p\text{-}C_3H_5)_4$ and the surface acidity of -OH groups of alumina, are successful in bringing about propene and but-1-ene metathesis[145]. Supported cobalt molybdate for the vapor phase oxidation of toluene to benzaldehyde and benzoic acid[146] and a supported iridium catalyst[147] for the reaction of cyclopropane and deuterium were also reported[147]. The main reaction was ring opening, yielding a mixture of isotopic propanes. Evidence for duel function catalysis was obtained in this case: The deuterium exchange is shown to take place on the support and the ring opening on the metal surface. Dual functionality was observed for reaction of methylcyclopropane or

1,1-dimethylcyclopropane with deuterium over the same Ir/Al_2O_3 catalyst. A high selectivity for the exchange of primary hydrogen atom in various hydrocarbons over Ir/Al_2O_3 was considered to be a function of the support rather than of the metal. The rate of hydrogen generation from water with an alumina supported mixed semiconductor catalyst ($ZnS\text{-}CdS/Al_2O_3$) has been found to be much higher than with singly supported catalysts (ZnS/Al_2O_3 and CdS/Al_2O_3)[148].

A tremendous amount of work has been carried out on various alumina supported Co-Mo, Ni-Mo and Ni-W catalysts for hydrodesulphurization reactions[149-153]. Supported $PtMoO_x$ or $PdMoO_x$ on alumina were also studied for hydrodesulphurization activity[154].

Recently acid-base property of Al_2O_3, $In_2O_3\text{-}Al_2O_3$ and $Ga_2O_3\text{-}Al_2O_3$ prepared by sol-gel method has been evaluated[155], and observed that addition of Ga_2O_3 into alumina leads to decrease Lewis acid strength but increase the number of sites, while In_2O_3 addition causes a global decrease of Lewis acidic properties of alumina. Using CO_2, as a probe to study basicity, the number of surface basic sites on alumina was found to be decreased by the In_2O_3 and Ga_2O_3 addition.

Alumina supported transition metal complexes: precursors for catalysts

There has been some interest in the preparation of catalysts starting from transition-metal acetylacetonates (pentane-2,4-dionate). *Institut Francai's du Pétrole* (IFP) reported that in this way supported noble-metal catalysts could be prepared, which would have a high degree of dispersion and greater stability[156,157]. Results published by a group at the Technical University, Twente suggest that, monolayer catalysts can be prepared through this method, which are not easily obtainable otherwise[158,159]. Also, $MoO_2(acac)_2$ has been claimed as a precursor of choice in the preparation of hydrotreating catalysts[160], and $UO_2(acac)_2$ has been utilized to prepare uranium promoted hydrotreatment catalysts[161].

All acetylacetone (acac) complexes except $Ru(acac)_3$ and $Rh(acac)_3$ react with coordinatively unsaturated (c.u.s) Al^{3+} sites of $\gamma\text{-}Al_2O_3$ surfaces. There

appears to be correlation between the acid/base sensitivity of an acac complex and its reactivity towards the surface OH groups[160]. Complexes which are stable in the presence of H^+ and OH^-, such as $Pd(acac)_2$, $Pt(acac)_2$ and $Co(acac)_3$, react only with the c.u.s. Al^{3+}, with transfer of the acac ligands to Al^{3+}. Complexes which decompose in the presence of H^+ such as $MoO_2(acac)_2$ and $VO(acac)_2$, react not only with c.u.s. Al^{3+} sites but also with the basic OH groups. Of the complexes which are sensitive to H^+, but not to (any great extent to) OH^-, $Fe(acac)_3$ reacts only to a minor extent with the acidic OH groups of γ-Al_2O_3

The "designing" of a catalyst system requires a thorough control of the surface morphology, and for this purpose a novel synthesis method, the molecular designed dispersion (MDD) method has been developed[162-166]. This method consist of two steps: in the first step, a neutral transition metal acetylacetonate complex ($M^{n+}(acac)_n$) is anchored to the surface of a high-surface-area support. In a consecutive step, the adsorbed complex is decomposed in an oxygen containing atmosphere at elevated temperatures, yielding the supported transition metal oxide catalyst. Two methods were used for carrying out the deposition process: (1) by hydrogen bonding between an acetylacetonate ligand and the surface hydroxyls and (2) by a ligand -exchange mechanism, with formation of a covalent metal-oxygen-support bonding and loss of a ligand as acetylacetone (Hacac). Molecular designed dispersion involving the use of the acetyl acetonate (acac) complexes of Mo, Cu and V supported on silica/alumina and their interactions with the supports were thoroughly explored [167].

Baltes *et. al.*[168], carried out a detailed investigation to find out the influence of various parameters like support, preparation method, and the geometry of the complex on the activity of catalysts prepared through molecular designed dispersion method. They observed that alumina is clearly a superior support in comparison to silica. The planar geometry of the $Cu(acac)_2$ allows easy multilayer coverage even at low loading, whereas coordinatively saturated complexes such as $MoO_2(acac)_2$ are sterically hindered from approaching the support surface. The latter therefore shows a lower adsorption capacity under the same reaction

conditions. They also carried out two method of deposition: a liquid phase and a gas-phase method. The reaction conditions chosen during the deposition of the complex are seen to influence the surface structure of the final catalyst. Therefore, the molecular designed dispersion method is a very promising way of designing a catalyst system that satisfies the demands of a catalytic reaction.

1.3 Scope of the present investigation

For a better tomorrow, the development of eco-friendly catalysts is a challenge in front of the scientists. The catalysts should be easily separable, recyclable, and also the metal leaching from the catalyst should be nil. The pharmaceutical field is in search for catalysts for asymmetric synthesis. Moreover the poisonous effluent gases like carbon monoxide, nitrogen oxides, and sulfur oxides should be removed for a healthy and cleaner environment. Anchoring or encapsulation of inorganic complexes on various supports have been used to achieve the above mentioned goal of green chemistry.

Zeolite Y has been used for effective encapsulation of metal complexes. The channel structure of Y zeolite can impart size and shape selectivity. This can fine tune the coordination environment around the metal by modifying the electrostatic properties of the ligand. It can further control the access of active sites by properly regulating the diffusion of the reactant molecules. By preventing the dimerisation of the already included metal complexes and also by providing enough ruggedness, it can increase the life time of the catalyst. The encapsulated complex can act as biomodel compounds, as the zeolite matrix can provide a similar situation as that of the protein part of an enzyme. Metal Schiff base complexes are known to mimic biomolecules. Metal Salen complexes are well explored for their ability to act as structural and functional mode of many metalloenzymes.

Alumina supported transition metal complexes are gaining the attention of the researchers working on the development of active heterogeneous catalysts. These supported complexes can be calcined at an appropriate temperature to

produce metal oxide catalysts. This method of preparation is known as the molecular designed dispersion method and is well studied for the preparation of highly dispersed metal oxide catalysts.

The present investigation was taken up with the following objectives:

- To synthesize some zeolite encapsulated transition metal complexes of Schiff base ligands, which are able to fine tune the structure of metal complexes.
- To arrive at their structural features using various characterization techniques .
- To carry out oxidation reaction of cyclohexanol using the encapsulated complexes with a view to compare the catalytic activity of the prepared zeolite encapsulated complexes
- To develop a highly dispersed and active cobalt-molybdenum catalyst supported on alumina for hydrodesulphurization reactions.

With these objectives, zeolite encapsulated metal complexes of the following ligands were synthesized and characterized.

- N,N′-bis(quinoxaline-2-carboxalidene)-*o*-phenylenediamine (QOPD)
- Indole-3-carboxaldehyde semicarbazone (ICSCZ)
- Indole-3-carboxalidene-3-amino-1,2,4 triazole (ICAT)
- N,N′-bis(4-hydroxy-3-methoxy benzalidene)-*o*-phenylenediamine (VOPD)
- Curcumine (Cur)

Highly dispersed and active catalysts for hydrodesulphurization reaction, Co-Mo catalysts supported on alumina was prepared by making use of cobalt and molybdenum complexes of pyrrolidine-*N*-carbodithioate as the precursors for the catalyst.

EXPERIMENTAL TECHNIQUES

2.1 Introduction

Details regarding the reagents used, preparation of the ligands and the various analytical and physico-chemical techniques employed for the characterization of the metal complexes are presented in this chapter. Procedural details regarding the synthesis and characterization of the hydrodesulphurization catalyst are also presented in this chapter.

2.2 Reagents

Metal salts used were $CoCl_2.6H_2O$ (E. Merck, G.R), $NiCl_2.6H_2O$ (E. Merck, G.R), $CuCl_2.2H_2O$ (E. Merck, G. R), $(NH_4)_6Mo_7O_{24}.4H_2O$ (SRL, India)

o-Phenylenediamine (Loba Chemie), indole-3-carboxaldehyde (SRL, India), 3-amino-1,2,4-triazole (Aldrich, 95% pure) and vanillin (S. D. Fine-Chem Ltd.) were used as starting materials for the preparation of ligands. Unless otherwise specified, all other reagents were of analytical grade. All the chemicals were used as obtained except *o*-phenylenediamine. *o*-Phenylenediamine was purified as follows[169]:

o-Phenylenediamine was dissolved in water, and to this was added activated charcoal. The solution containing charcoal was then boiled and filtered. The crystals formed in the filtrate was separated, dried and kept in a desiccator.

2.3 Ligands

The following ligand are used for the preparation of zeolite encapsulated complexes:

- *N,N'*-bis(quinoxaline-2-carboxalidene)-*o*-phenylenediamine (QOPD)
- Indole-3-carboxaldehyde semicarbazone (ICSCZ)
- Indole-3-carboxalidene-3-amino-1,2,4 triazole (ICAT)
- *N,N'*-bis(4-hydroxy-3-methoxybenzalidene)-*o*-phenylenediamine (VOPD)
- Curcumine (Cur)

In addition to the above ligands, pyrrolidine-*N*-carbodithioate was used as the ligand for the preparation of precursor metal complex for hydrodesulphurization catalysts.

2.3.1 Preparation of quinoxaline-2-carboxaldehyde

Quinoxaline-2-carboxaldehyde was prepared by adopting the following procedure[170]. Glacial acetic acid (6 mL), *o*-phenylenediamine (21.6 g, 0.2 mol), hydrazine hydrate (5 mL, 0.1 mol) and a pinch of sodium bicarbonate were added to a solution of D-glucose (36 g, 0.2 mol) in water (54 mL), and the reaction mixture was heated under reflux for 5 h on a boiling water bath. The product, 2-(D-arabinotetrahydroxybutyl)-quinoxaline, which got precipitated on cooling the solution in ice, was filtered and washed with water. It was further purified by recrystallisation from hot water. The recrystallised 2-(D-arabinotetrahydroxy-butyl)quinoxaline (5g, 0.02 mol) was dissolved in water (300 mL) containing glacial acetic acid (10 mL), and was kept at room temperature with controlled stirring for 16h. This solution was filtered, and the filtrate was neutralized with sodium bicarbonate. The compound present in the neutral solution was extracted with ether. The ether extract after drying with anhydrous sodium sulfate was evaporated to dryness. The resulting residue was recrystallised from petroleum ether to give pure quinoxaline-2-carboxaldehyde.

2.3.2 Preparation of *N,N'*-bis(quinoxaline-2-carboxalidene)-*o*-phenylene diamine (QOPD)

Quinoxaline-2-carboxaldehyde (7.90g, 0.05 mol) in methanol (20 mL) was taken in a round bottom flask. A methanolic solution (20 mL) of *o*-phenylene-diamine (2.70g, 0.025 mol) was slowly added to this with stirring. The addition was continued till the precipitation of the Schiff base was completed. The yellow compound thus obtained was filtered, washed with methanol, recrystallised twice from methanol and dried in *vacuo* over anhydrous calcium chloride. The purity of the ligand was checked by TLC.

2.3.3 Preparation of indole-3-carboxaldehyde semicarbazone (ICSCZ)

Semicarbazide hydrochloride (0.01 mol, 1.15g) dissolved in minimum quantity of 0.01N NaOH was heated to boiling. The solution was cooled and tested for neutrality using pH paper. More acid or alkali was added to adjust the pH at 7. An ethanolic solution (100mL) containing indole-3-carboxaldehyde (0.01 mol, 1.45g) was then slowly added to the neutral solution of semicarbazide with continuous stirring. The mixture was refluxed on a water bath for 2h. Semicarbazone separated out on cooling was filtered, washed with ethanol and recrystallised from 1-propanol[171].

2.3.4 Preparation of indole-3-carboxalidene-3-amino-1,2,4-triazole (ICAT)

Indole-3-carboxaldehdye (1.45 g, 0.01 mol) dissolved in ethanol (10 mL), was mixed with 3-amino-1,2,4-triazole (0.84g, 0.01mol) in 1:1 ratio. The resulting solution was boiled for condensation reaction under reflux on a water bath for about 1h. Yellow crystals formed at room temperature was collected, washed with little ethanol, and then dried in *vacuo* over anhydrous $CaCl_2$.

2.3.5 Preparation of *N,N'*-bis(4-hydroxy-3-methoxybenzalidene)-*o*-phenylenediamine (VOPD)

Vanillin (7.60g, 0.05 mol) in methanol (20 mL) was taken in a round bottom flask. A solution of *o*-phenylenediamine (2.70g, 0.025 mol) in methanol(20 mL)

was slowly added to the solution of vanillin with stirring. The amine solution was added till the precipitation of the Schiff base was completed. The yellow coloured compound thus separated out was filtered, washed with methanol and recrystallised from methanol. The recrystallised Schiff base, VOPD was dried in *vacuo* over anhydrous calcium chloride. The purity of the ligand was checked by TLC.

2.3.6 Purification of curcumin

Curcumin (1,7-*bis*(4-hydroxy-3-methoxyphenyl)-1,6-heptadiene-3,5-dione) is the dominant pigment among the curcuminoids. The other pigments present are demethoxy curcumin, bis-demethoxy curcumin and traces of dihydrocurcumin. The curcumin obtained from Arjuna Aromatics Pvt. Ltd., Alwaye, was used after purification by chromatographic technique[172] using a silica gel (100-200 mesh) stationary phase and 5% methanol in chloroform as the eluent.

2.3.7 Preparation of pyrrolidine-*N*-carbodithioate

A 500 mL three-necked flask was equipped with a powerful electric stirrer and a separating funnel and an air condenser. An aqueous solution (~200 mL) of sodium hydroxide (40gm, 0.02M) and pyrrolidine (35.56g, 0.5M) was introduced, to the above flask that was well-cooled in a freezing mixture of ice and salt. Carbon disulfide (32 mL, 0.5M)) was added dropwise from the separating funnel and the mixture was stirred for about 2h. The solid that separated out was washed several times with petroleum ether and recrystallised from water.

2.4 Supports

2.4.1 Zeolite Y

Synthetic Y type zeolite with silica alumina ratio of 2.4 and surface area of 650 m^2/g was obtained from Süd-Chemie India Ltd., Baroda.

2.4.1.1 Preparation of metal exchanged zeolite Y

The zeolite Y was stirred with 0.1 mol dm^{-3} solution of sodium chloride for 24h at room temperature to convert any other ions (if present) into Na^+ ions. The sodium exchanged form (NaY) was then made chloride free by washing with distilled water. It was then dried at 100^0C. The sodium ions were conveniently replaced with bivalent transition metal ions, Co^{2+}, Ni^{2+} or Cu^{2+} by stirring NaY (5gm) with 0.01 mol dm^{-3} solution of respective metal chloride for 24 h. It was then filtered and dehydrated at 450^0C for 4h. Procedural details about the use of the metal exchanged zeolite for the preparation of encapsulated Schiff base complexes are given in appropriate chapters.

2.4.2 γ-Alumina

γ-Alumina extrusions of 1/20" dia having surface area of 245m^2/gm and 5%MoO_3 and γ-Alumina extrusions 1/20" dia without MoO_3 and a surface area of 245m^2/gm were obtained from Süd-Chemie India Ltd., Baroda and were used as supports for the preparation of the hydrodeulphurization catalysts..

2.5 Reagents for catalytic activity study

Cyclohexanol (Merck) and *tert*-butylhydroperoxide (Merck, 70%) were used for the catalytic activity study of cyclohexanol oxidation. Straight run diesel having a sulfur content of 0.9-1.0% from Kochi Refineries Ltd., was used for the hydrodesulphurisation activity studies. Solvents employed were either 99% pure or purified by known laboratory procedures. Details regarding the catalytic activity studies are included in the respective chapters.

2.6 Analytical methods

During the synthesis of metal complexes in the restricted spaces provided by pores, channels, or cavities, the following questions must be considered.

a] Does the organic ligand form the desired complex?

b] In what yield is the desired complex obtained?

c] Is the special environment of the derived compound inside the pores and cavities capable of imparting special properties to the entrapped systems?

d] Can one rule out the possibility of the derived compound to be on the surface of the solid?

e] Does the synthesis of the desired complex preserve the pore structure of the zeolite host?

In order to give an unequivocal answer to each of these questions, a battery of analytical techniques has to be used. The following analytical techniques are used in the present investigation:

2.6.1 Analysis of Si, Al, Na and transition metal ion in the zeolite

Zeolite encapsulated metal complex was accurately weighed ('x'g) and transferred to a beaker. Con. sulphuric acid (about 40 mL) was added and heated. It was cooled, diluted with water (200 mL) and filtered through an ash less filter paper. The residue was incinerated in a platinum crucible, cooled and weighed ('a' g). It was digested with hydrofluoric acid (10 mL) with three or four times to remove all the silica as H_2SiF_6[173] and the remaining solid finally ignited to 1000^0C and weighed('b' g). From this the percentage of silica (SiO_2) was calculated using the equation.

$$\% SiO_2 = \frac{(a - b)}{x} x100 \qquad .....(2.1)$$

The residue in the platinum crucible was then fused with potassium persulphate to form a clear melt and was dissolved in water, filtered and combined with earlier filtrate. The Al and transition metal ions in the solution were determined by AAS. Sodium contents were estimated by flame photometry. From the metal percentages obtained the ion exchange capacity was calculated. The unit cell formula[174] was also derived from these values. An atomic absorption spectrophotometer (Perkin Elmer 3110) was used for the metal estimation.

2.6.2 Elemental analysis

Microanalysis for carbon, hydrogen and nitrogen in the zeolite samples were done at RSIC, CDRI, Lucknow using Heraues Carlo Erba 1108 elemental analyzer.

2.6.3 Surface area analysis

Surface area of the samples were measured by multipoint BET[175] method using a Micromeritics Gemini 2360 surface area analyzer. Nitrogen gas was used as the adsorbate at liquid nitrogen temperature. The equation used in the determination is:

$$\frac{P}{V(P_0 - P)} = \frac{1}{V_m C} + \frac{(C-1)P}{V_m C P_0} \qquad \text{.....(2.2)}$$

V = Volume of the gas adsorbed at relative pressure P/P_0

V_m = Volume of the gas in the monolayer

P_0 = Saturation vapor pressure of the adsorbate at the experimental conditions

C = a constant related to heat of adsorption and liquefaction of gas

On plotting left side of the Eq. 2.2 against P/P_0 a straight line is obtained with slope $(C-1)/V_mC$ and intercept $1/V_mC$. From these values, V_m and the number of moles of nitrogen adsorbed, V_m can be calculated.

BET surface area is calculated using,

$$S_{BET} = X_m N A_m 10^{-20} \qquad \text{.....(2.3)}$$

N = Avagadro's number

A_m = Cross-sectional area of the adsorbate molecule in Å

Pore volume of the sample at $P/P_0 \sim 0.9$ is computed by converting the volume of nitrogen adsorbed at $P/P_0 \sim 0.9$ to volume of liquid equivalent to it using Eq. 2.4

$$V_{tot} = V_{ads} D \qquad \text{.....(2.4)}$$

where V_{tot} = total pore volume at $P/P_0 \approx 0.9$

V_{ads} = volume of the gas adsorbed at relative pressure 0.9

D = density conversion factor.

2.6.4 X-ray diffraction analysis

Metal exchanged zeolite and the encapsulated complexes were analysed by powder X-ray diffraction for comparing their crystallinity. X-ray diffractometer used in the present study is Rigaku-D. Max. C. Measurements were done with a stationary X-ray source, Ni filtered CuK_α radiation (λ = 1.5404) and a movable detector which scans the intensity of the diffracted radiation as a function of the angle 2θ between the incident and diffracted beam.

2.6.5 SEM analysis

The morphology of the samples was examined using JEOL-JSM-840A SEM (at IISc, Bangalore) to determine whether there are any surface adsorbed materials or any morphological change occurred during the conditions of encapsulation. The samples were coated with a thin film of gold to prevent surface charging and to protect the zeolite material from thermal damage by electron beam. Furthermore SEM can give an idea about how the soxhlet extraction is effective in removing surface adsorbed species.

2.6.6 Magnetic measurements

The magnetic susceptibility measurements were carried out at room temperature on a simple Gouy type balance. The Gouy tube was standardized using $Co[Hg(SCN)_4]$ as recommended by Figgis and Nyholm[176]. The effective magnetic moment was calculated using the following equation

$$\mu_{eff} = 2.84(X'_m T)^{1/2} \text{ BM} \qquad \text{.....(2.5)}$$

where T = absolute temperature

X'_m= molar susceptibility corrected for diamagnetism of all atoms present in the complex (using Pascal's constant) and that of zeolite framework per unit metal.

2.6.7 FTIR spectra

Infrared spectroscopy is a useful technique to get an idea about the coordination of the ligands. It can also be used for the confirmation of encapsulation of complexes inside the zeolite cages. The mid IR region of the spectrum is very useful in structural analysis of zeolite as it contain the fundamental vibrations of the framework. Further, each zeolite exhibits a typical IR pattern[177]. Infrared spectra of the ligand and the encapsulated complexes in the region 4000-400 cm^{-1} were recorded by KBr techniques using Perkin Elmer 881, IR Spectrophotometer (at RSIC, CDRI, Lucknow).

2.6.8 Diffuse reflectance spectra

The diffuse reflectance spectra were recorded at room temperature in the range 250-850 nm with NaY sample as reference using Ocean Optics, Inc. SD 2000, Fiber Optic Spectrometer with a charged coupled device (CCD) detector. The spectra were computer processed and recorded. If it was plotted as percentage reflectance versus wavelength, Kubelka-Munk[178,92] analysis has to be performed to get the spectra in the absorbance mode.

The Kubleka-Munk equation is as follows

$$\text{Log}\frac{(1-r_\alpha)^2}{2r_\alpha} = \text{Log}k - \text{Log}\,S \qquad \text{.....(2.6)}$$

$r_\alpha = R_\alpha$ (sample)/ R_α (Standard). Here the standard used is the sodium form of the zeolite Y. R_α (sample) = the diffuse reflectance of the sample. R_α is taken as 1 for the standard. K = absorption coefficient and S = scattering coefficient.

Therefore the Kubelka-Munk factor, F(R) is given by Eq. 2. 7

$$F(R) = \frac{(1-r_\alpha)^2}{2r_\alpha} = \frac{k}{S} \qquad \text{.....(2.7)}$$

A plot of $(1-r_\alpha)^2/2r_\alpha$ as a function of wavelength gives the corrected absorption curve. But in the present case, the software of the spectrophotometer does the necessary calculation and plots the spectra directly in the absorbance mode.

2.6.9 EPR spectra

EPR is a useful technique to find out the coordination environment of metal ions. The EPR spectra of the powdered copper(II) encapsulated complexes were recorded at liquid nitrogen temperature using a Varian E-109 X/Q band spectrometer (at RSIC, IIT Mumbai). The standard used was TCNE (tetracyanoethylene, g = 2.0027). Magnetic moment (μ_{eff}) values can also be obtained from the EPR parameters by substituting $g_{\parallel}$ and $g_{\perp}$ in the Eq. 2.8 [179].

$$\mu^2_{eff} = g_{\parallel}^2/4 + g_{\perp}^2/4 + 3KT/\lambda_0(g-2) \qquad .....(2.8)$$

The bonding parameter P can be calculated using the equation given below

$$P = (A_{\parallel} - A_{\perp})/(g_{\parallel} - 2) - 5/14(g_{\perp} - 2) - 6/7 \qquad .....(2.9)$$

2.6.10 TG analysis

Thermogravimetric (TG) analysis of the samples were carried out on a TGAQ50 V2.34 thermal analyzer (TA instruments make) at a heating rate of 20^0C min^{-1} in an atmosphere of nitrogen (flow rate, 60ml min^{-1}), to know about the thermal stability of the encapsulated complexes

2.6.11 Gas chromatography

The catalytic activity studies were performed with a Chemito 8510 Gas Chromatograph equipped with a flame ionization detector (FID). A carbowax column was used for separating various components in the reaction mixture.

2.7 Alumina supported catalysts

Alumina supported Co-Mo catalysts were prepared with a view to develop a catalyst with a high diesel hydrodesulphurization activity. The details regarding the preparation are given in Chapter 9

2.7.1 Analysis of metal content of alumina supported catalysts

The samples (0.5g) were accurately weighed into a beaker. It was then extracted with concentrated sulphuric acid. Cobalt and molybdenum were estimated using atomic absorption spectrophotometer.

2.7.2 Laser Raman spectroscopy

Laser Raman Spectroscopy (LRS) is an effective tool in studying the morphology of alumina supported molybdenum catalysts, since LRS is essentially free of contribution from the alumina support[180]. The Raman measurements were performed in a 90^0 geometry using a Jobin Yvon TRIAX 550 triple grating spectrometer equipped with a cryogenic charge-coupled device camera, and diode-pumped frequency doubled solid state Nd:YAG laser of 532 nm (Model DPSS532-400, Coherent Inc. USA). The scattered light was collected using microscope objective (10x/0.25) and fiber optic cable. A super notch filter (Kaiser Optical Systems, Inc.) was used to eliminate the Rayleigh scattering and residual laser light. The incident laser power was kept below 20mW focused in a diameter of ~50μm to avoid the laser heating of the sample.

2.7.3 Molybdenum dispersion by oxygen chemisorption

Estimation of the percentage molybdenum dispersed on the surface of alumina will give an idea about the active phases available for the reaction. A modified method of Liu *et. al.*[181], was employed for the determination of metal dispersion. The method is as follows.

A microcatalytic reactor was loaded with the catalyst (equal sized particle) and was connected to a manual gas sampling valve. In the initial stage hydrogen

was allowed to flow through the reactor at a rate of 30 mL per minute. The reduction was carried out at a temperature of 500°C for one hour. After completing the reaction the carrier gas was switched over from hydrogen to helium. The temperature was raised to 525°C and maintained for fifteen minutes. The residual hydrogen on the catalyst was thus removed. The reactor was then cooled to room temperature. The reactor after cooling was immersed in a container with a mixture of dry ice and acetone to maintain a temperature of -78°C. This is done to avoid the catalyst's susceptibility to bulk phase oxidation and to minimize the interference of cobalt in the chemisorption of oxygen. About 1.0 mL of oxygen was then injected through a manual gas-sampling valve, just upstream of the catalyst bed. The oxygen that was not adsorbed on the catalyst was carried by the helium carrier to the thermal conductivity detector (TCD) of a gas chromatograph (CHEMITO 8510) for analysis. Two or three injection of oxygen (1.0 mL) were given through the catalyst till 100% of oxygen slip occurs. The number of reduced molybdenum atoms on the catalyst surface was calculated from the number of oxygen atoms adsorbed by the catalyst, by assuming a stoichiometry 1:1. Percentage of molybdenum dispersion can be calculated as follows.

$$\text{Molybdenum dispersion} = \left[\frac{\text{No. of oxygen adsorbed}}{\text{No. of molybdenum in the catalyst}}\right] \times 100 \qquad \ldots(2.10)$$

2.7.4 Temperature programmed reduction

Temperature programmed reduction (TPR) is used to investigate the surface structure and reducibility of the catalysts. TPR was carried out according the following procedure[182]. About 1 gm of the catalyst sample (9 x 12 mesh) was loaded in a microcatalytic quartz reactor of 3mm diameter and 300mm length coupled with a thermal conductivity detector (TCD). About 2ml glass beads were packed at the top and bottom of the catalyst. The catalyst is preheated in a current of nitrogen at 420°C for 30 min and cooled to room temperature. Temperature programmed reduction was carried out in the range ambient to 700°C in a stream of argon/hydrogen gas mixture (95:5) flowing at a rate of 40 mL min^{-1}. Using a

linear temperature programmer, heating rate was maintained at 10°C min^{-1}. Hydrogen consumption was monitored using TCD. The experimental setup for temperature programmed reduction is given in Figure 2.1.

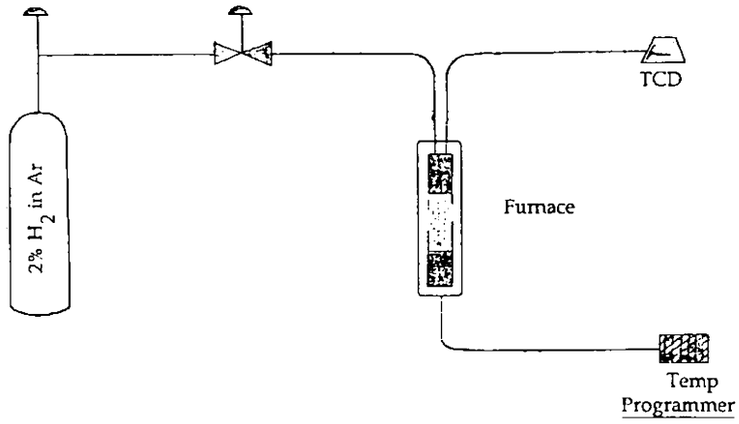

Figure 2.1 Experimental set up for the TPR

2.7.5 X-ray fluorescence spectrometry

The sulphur content in the diesel was determined using X-ray fluorescence spectrometry. Oxford, Lab-X 2000 spectrophotometer was used for this purpose.

ZEOLITE ENCAPSULATED METAL COMPLEXES OF *N,N'*-bis(QUINOXALINE-2-CARBOXALIDENE)-*O*-PHENYLENEDIAMINE

3.1 Introduction

Quinoxalines are bicyclic, heterofused systems widely distributed in nature. Numerous synthetic quinoxalines are also reported. Quinoxalinoyl residues are present in several biologically active polypeptides such as levomycin, actinoleukin and echinomycin[183]. Quinoxaline derivatives play an important role in the synthesis of the antibiotic peptide triostin[184]. Quinoxaldehydes are found to form Schiff bases with organic amines. Complexes of Schiff base derived from quinoxaline-2-carboxaldehyde are also reported[185,186]. A search through the literature has revealed that zeolite encapsulated complexes of Schiff bases derived form quinoxaline-2-carboxaldehyde and *o*-phenylenediamine have not yet been reported. Metal complexes derived from Schiff base ligands have wide applications. Many of them are found to have immense catalytic and bio-mimetic property. The details regarding the synthesis and characterization of zeolite encapsulated cobalt, nickel and copper complexes of this Schiff base are presented in this chapter. The structure of the ligand is given in Figure 3.1.

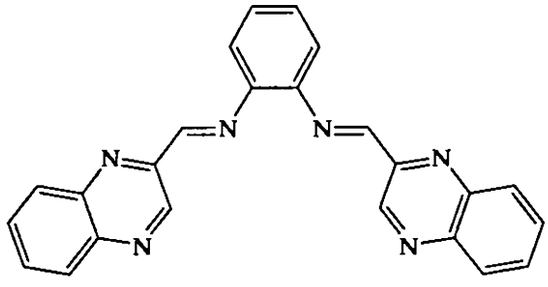

Figure 3.1 Structure of *N,N'*-bis(quinoxaline-2-carboxalidene)-*o*-phenylenediamine (QOPD)

3.2 Experimental

3.2.1 Materials

The details regarding the synthesis and purification of the ligand and the preparation of metal exchanged zeolite are given in Chapter 2. These metal exchanged zeolites were used for synthesizing the complex in the super cage.

3.2.2 Synthesis of zeolite encapsulated complexes of *N,N'*-bis(quinoxaline-2-carboxalidene)-*o*-phenylenediamine (QOPD)

Zeolite encapsulated cobalt(II), nickel(II) and copper(II) complexes of QOPD were prepared from the metal exchanged zeolite using the intrazeolite synthesis by complexation method. In this method, metal exchanged zeolite (5g) was heated with excess (2g) of QOPD at 125^{0}C for 16h in a closed glass ampoule to effect complexation. During heating, QOPD ligand diffuses into the zeolite and undergoes complexation with metal ion to form complexes, which are too large to exit the supercages. The resulting material was soxhlet extracted with chloroform and then with methanol to remove unreacted ligand and surface complexes. It was then stirred with 1.0 M sodium chloride solution to re-exchange the uncomplexed metal ion and was finally dried at 120^{0}C.

3.2.3 Analytical methods

Various physicochemical characterization techniques were employed to characterize the prepared metal complexes. Details of these techniques used are given in Chapter 2.

3.3 Results and discussion

3.3.1 Metal exchanged zeolites

Zeolites containing transition metal ions are widely studied[187,188]. These ions, introduced into the zeolite by ion exchange, can occupy specific coordination sites after dehydration. The resulting coordination to the lattice oxygen is often

unsaturated, leaving the possibility of adsorption of small molecules to the metal site. The knowledge of the coordination and electronic structure of the transition metal centers is important for the investigation of the catalytic potential of the materials.

3.3.1.1 Chemical analysis

The analytical data for the metal exchanged zeolite are given in the Table 3.1. The Si/Al ratio of NaY is 2.38, which is found to be retained even after the metal exchange indicating the absence of any dealuminaton. It is reported that high concentration of metal chloride solution may affect the framework of the zeolite. To avoid dealumination and destruction of framework structure, dilute solutions of metal ions have been recommended[189]. Therefore, very low concentration of the metal chloride solutions (0.005M) were used for ion-exchange Furthermore, pH of the solution was adjusted to 4.0-4.5.

Table 3.1
Analytical data of metal exchanged zeolites

Metal exchanged zeolite	%Si	%Al	%Na	% Metal
NaY	25.60	10.76	7.90	-
CoY	24.46	10.38	6.90	3.33
NiY	24.37	10.47	6.70	1.87
CuY	24.75	10.37	7.01	3.48

The degree of ion-exchange and unit cell formulae of the metal exchanged zeolites could be derived from the analytical data (Table 3.2). The maximum ion exchanged capacity is observed for CuY. The order of ion exchange capacity is CuY~CoY>NiY. The unit cell formula is a representation of the composition of a unit cell in the metal exchanged zeolites.

Table 3.2
Composition of metal exchanged zeolites

Sample	Degree of ion exchange	Unit cell formula
NaY	-	$Na_{56}(AlO_2)_{56}(SiO_2)_{136}\ nH_2O$
CoY	29.39	$Na_{39.5}Co_{8.2}(AlO_2)_{56}(SiO_2)_{136}\ nH_2O$
NiY	16.43	$Na_{46.8}Ni_{4.6}(AlO_2)_{56}(SiO_2)_{136}\ nH_2O$
CuY	28.99	$Na_{39.8}Cu_{8.1}(AlO_2)_{56}(SiO_2)_{136}\ nH_2O$

3.3.1.2 X-ray diffraction analysis

X-ray diffraction (XRD) gives information about the location of the transition metal ions in the zeolite unit cell[190,191]. However, detailed information about the coordination of the metal cannot be obtained, since it is difficult to distinguish the metal atom from the silicon and aluminium atoms. Moreover the site structure is an average of occupied and non occupied sites. X-ray diffraction patterns of the zeolite samples are given in Figure 3.2. A comparison of the patterns indicates no destruction of the structure of the host zeolite upon the introduction of metals. Moreover, the XRD patterns are very similar to those reported in the literature[192]. So it is clear that the crystalline structure was almost preserved in the metal exchanged zeolites.

3.3.1.4 FTIR spectra

A systematic investigation of the frame work structures of many synthetic zeolites has been carried out in the 200-1300 cm^{-1} region (the mid-ir region) by Flasigen *et. al,*[193]. The mid-infrared region of the spectrum is useful, since it contains the fundamental vibrations of framework alumina or silica. The spectral bands of zeolite can be grouped into two classes; (1) the bands, which are due to

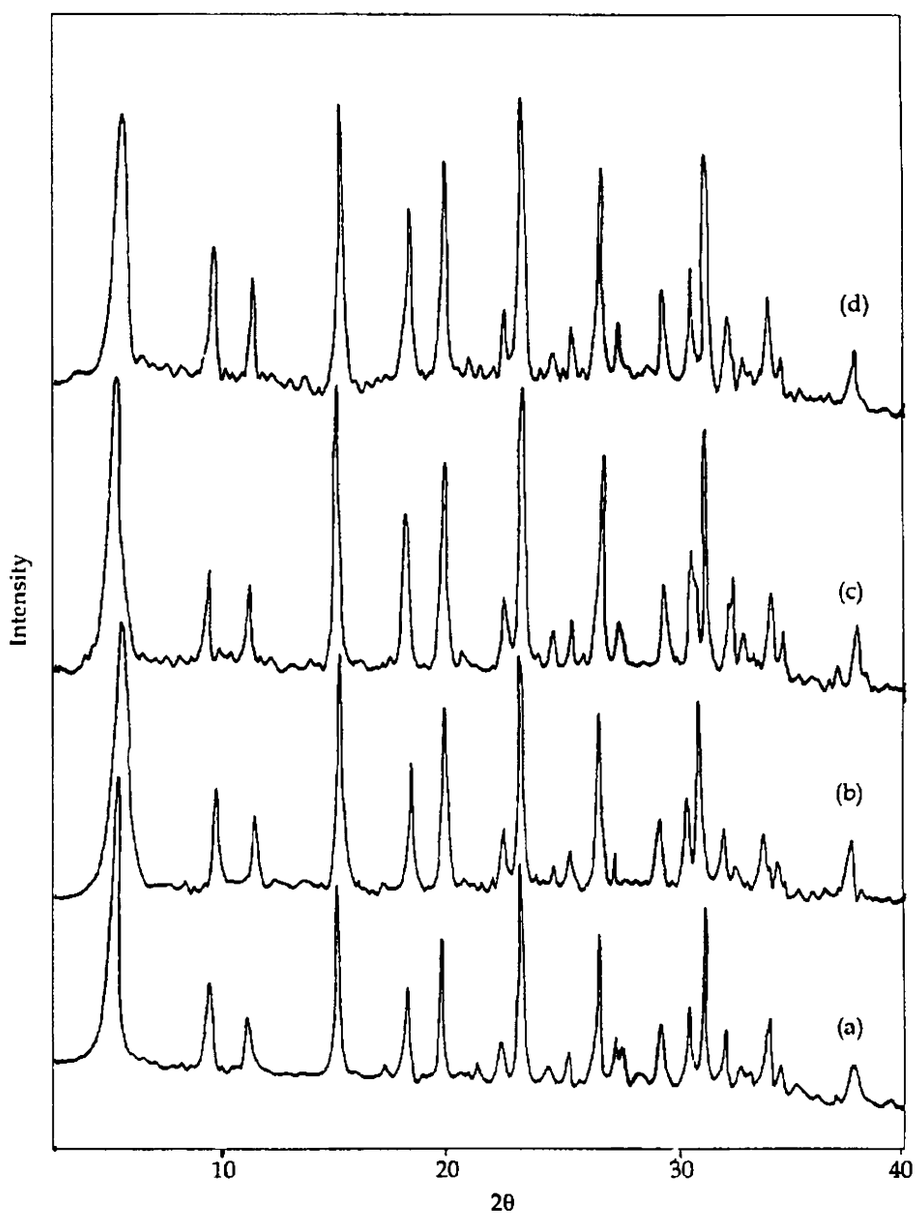

Figure 3.2 XRD Patterns of (a) NaY (b) CuY (c) NiY (d) CoY

the internal vibration of the TO_4 tetrahedron, (the primary unit of the structure), and (2) the bands which may be related to the linkage between tetrahedra. Class 1 vibrations are not sensitive to other structural vibrations and Class 2 vibrations are sensitive to the overall structure. The mid-IR assignments of the zeolite Y are given in Table 3.3. All the metal exchanged zeolites exhibit an IR spectra which is almost same as that of zeolite-Y, which also shows that the zeolite framework remains intact on metal exchange. The IR spectra of the NaY zeolite and copper exchanged zeolite are given as a typical case in Figure 3.3.

Table 3.3
IR assignment of zeolite Y (NaY)

Internal tetrahedral (cm^{-1})	External linkage (cm^{-1})	Assignment of bands
1250-950	1150-1050 Sh	Asym. Stretch
720-650	750-820	Sym. Stretch
500-420	-	T - O bend
-	650-500	Double ring
-	420-300	Pore opening

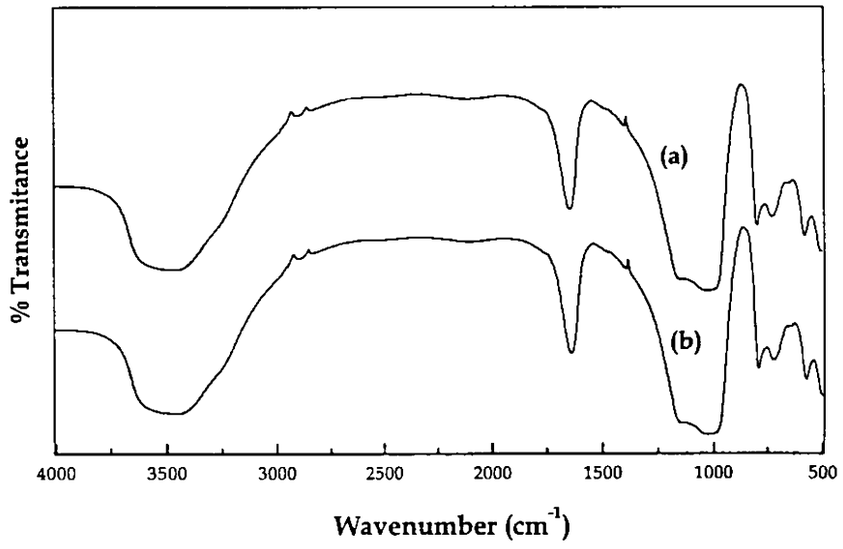

Figure 3.3 FTIR Spectrum of (a) NaY and (b) CuY

3.3.2 Y Zeolite encapsulated QOPD complexes

Y zeolite encapsulated QOPD complexes of cobalt, nickel and copper were synthesized using intrazeolite synthesis by complexation method (see section 3.2.2). The complexes were characterized using various techniques like chemical analysis, SEM, XRD, surface area, pore volume, magnetic moment measurements, electronic spectra, FTIR and EPR spectroscopy. Thermal behaviour of the zeolite complexes in inert atmosphere was studied using TG.

3.3.2.1 Chemical analysis

The analytical data of the zeolite complexes are given in Table 3.4. The percentage silica was determined according to the procedure described in Chapter 2 and metal percentage was determined by AAS analysis. The silica-alumina ratio for the entrapped complex is around 2.39. This proves that the zeolite framework is unaltered even after encapsulation. The metal content of the encapsulated complex is less compared to the corresponding metal exchanged zeolites, which suggests that a portion of the metal that remain uncomplexed is re-exchanged with the Na^+ ion. However, some uncomplexed metal may still remain in the zeolite cage after back exchange. The carbon percentage of the zeolite encapsulated complexes gives only a qualitative idea about the entrapment of the complex inside the zeolite cavity. The values indicate that the metal to ligand ratio is 1:1.

Table 3.4
Analytical data of encapsulated complexes

Sample	%Si	%Al	%Na	%Metal	%C
YCoQOPD	24.31	10.22	7.20	0.79	3.40
YNiQOPD	24.60	10.25	7.02	0.59	2.75
YCuQOPD	24.35	10.23	6.70	2.10	9.00

3.3.2.2 SEM analysis

Scanning electron micrograph is an effective tool to investigate the effectiveness of the purification process to remove extraneous materials on the zeolite. SEM can also be used to measure the particle size. SEM of YCuQOPD before and after the Soxhlet extraction (Figure 3.4) using chloroform and methanol shows the removal of the surface adsorbed species. Soxhlet extraction with a suitable solvent can thus successfully remove the surface complexes.

3.3.2.3 X-ray diffraction analysis

The XRD patterns of the encapsulated complexes are given in Figure 3.5. They appear similar to those of the corresponding metal exchanged zeolites and the parent zeolite. Therefore the zeolite framework structure was not altered during the encapsulation of the complexes. It was reported that the location of large, transition-metal complexes either within or on the external surfaces of faujasite-type zeolites can be determined from an analysis of the XRD pattern[194,49]. An empirically derived relationship exists between the relative peak intensities of the 331, 311 and 220 reflections and location of small cations. Cations are randomly distributed within the lattice if $I_{331} > I_{220} > I_{311}$, but if $I_{331} > I_{311} > I_{220}$, the cations assume positions at site in side the β- cage. This indicates that significant cation redistribution occurred following complex formation within the zeolite supercages.

3.3.2.4 Surface area and pore volume

The surface area of porous solids like zeolite is mainly internal surface area and blocking of the pores due to the formation of metal complexes decreases the surface area. Such extent of reduction in surface area of zeolite has been reported by Balkus and Gabrielov[37]. There are reports on the reductions in surface area of NaY zeolite from 699 m^2/g to 378 m^2/g as a result of the encapsulation of the cobalt phthalocyanines[60].

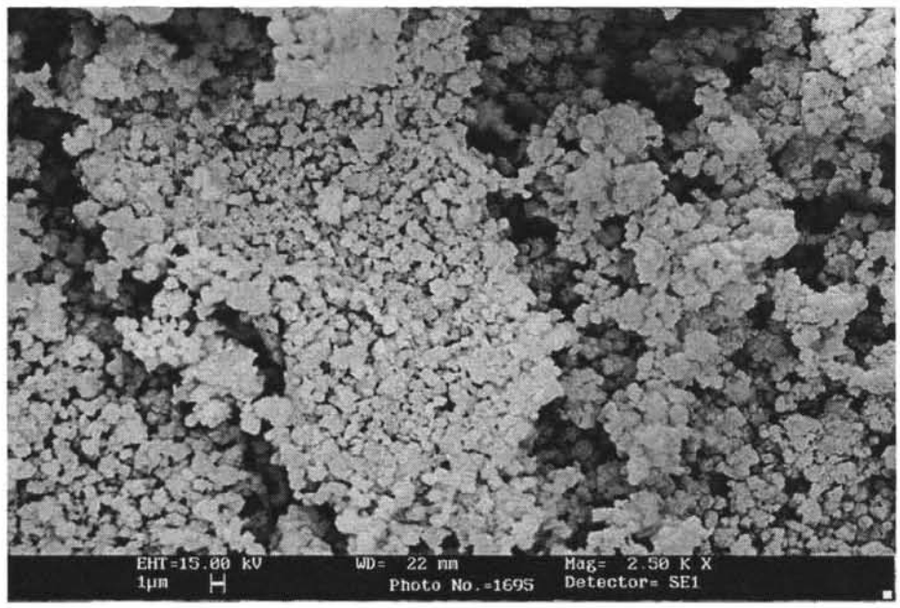

(a)

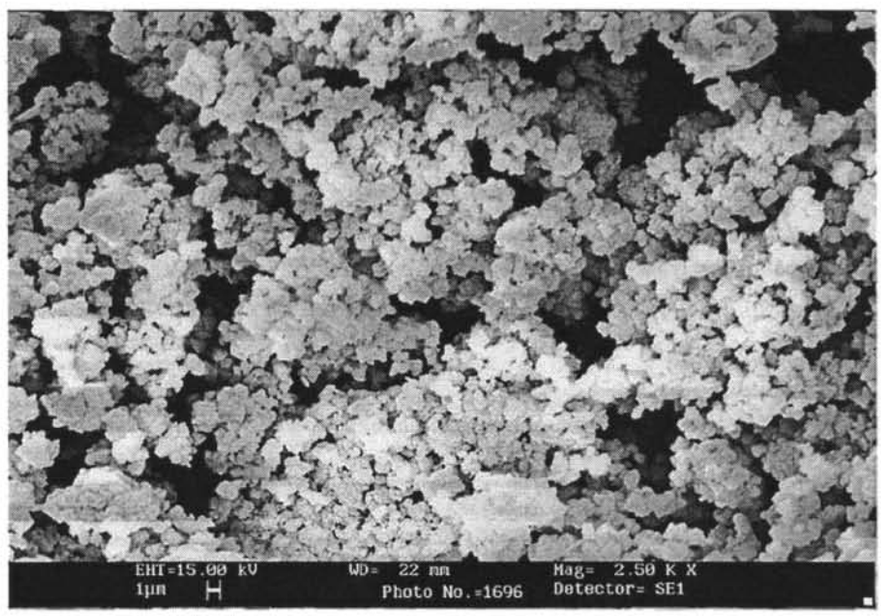

(b)

Figure 3.4 Scanning Electron Micrograph of YCuQOPD
(a) before (b) after soxhlet extraction

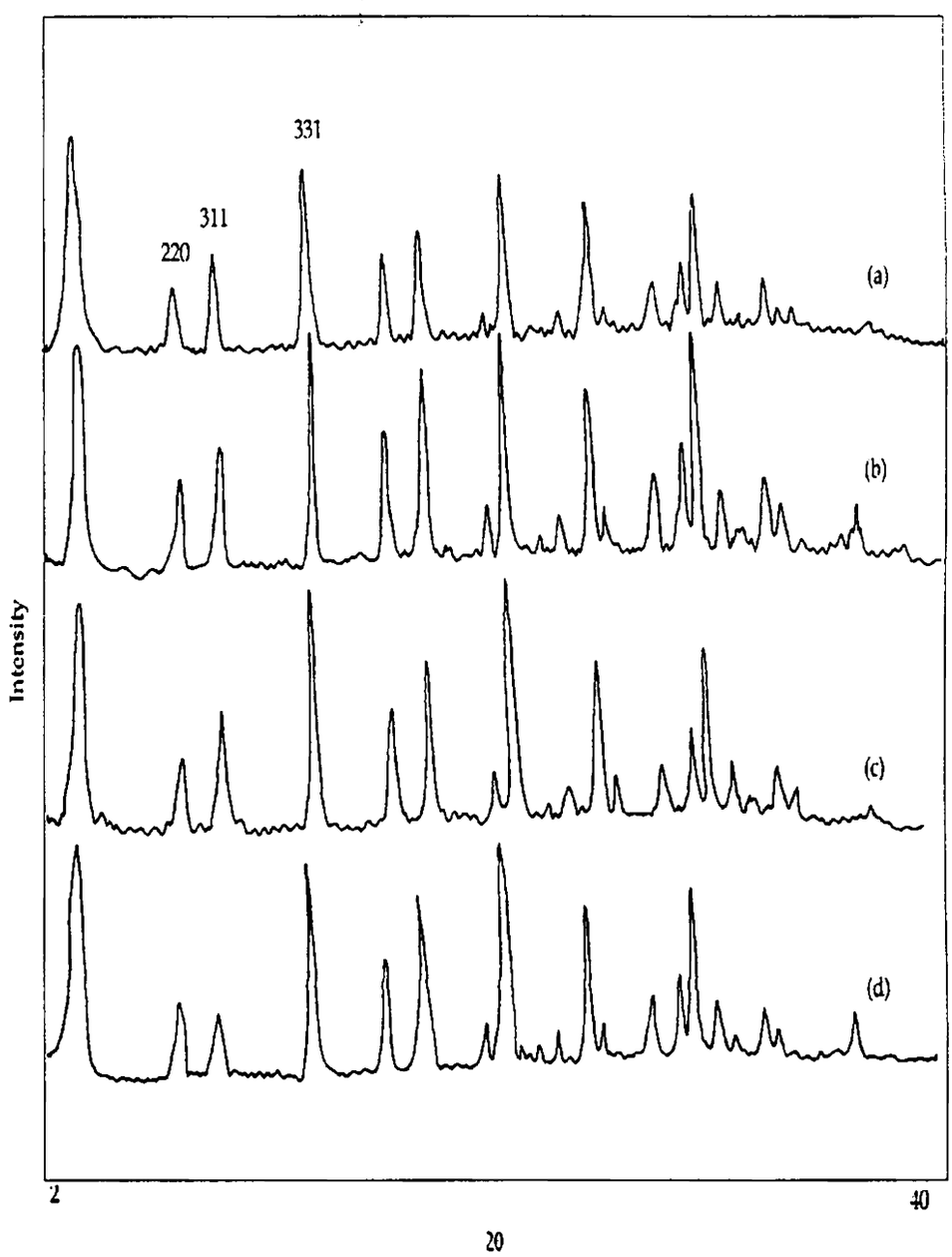

Figure 3.5 XRD Patterns of (a) YCoQOPD (b) YNiQOPD (c) YCuQOPD and (d) CuY

Surface area and pore volume analysis of the samples determined by BET method are presented in Table 3.5. A drastic decrease in surface area and pore volume was observed in the case of zeolite encapsulated complexes, which can be considered as the result of pore blocking due to encapsulation.

Table 3. 5
Surface area and pore volume data of the zeolite encapsulated complexes

Metal ion	Surface area (m^2/gm)		Pore volume (cc/g)	
	MY	Complex Y	MY	Complex Y
Co	640	470	0.26	0.18
Ni	635	490	0.25	0.19
Cu	640	453	0.24	0.17

3.3.2.5 FTIR spectra

Infrared spectroscopy is useful technique for the identification of the complex formation within the zeolite, and the spectra can be used to gain information about the donor atom which is coordinated to the metal. The IR spectra of the ligand and the encapsulated complexes are given in Figure 3.6 and Figure 3.6a respectively. The spectral data are given in Table 3.6.

The spectra of the encapsulated complexes are dominated by the peaks due to the zeolite. The stretching due to the zeolite OH groups is spread over the region from 3500 - 3700 cm^{-1}. The band at 1000 cm^{-1} of the zeolite encapsulated complexes is due to the asymmetric stretching vibrations of $(Si/Al)O_4$ units of zeolite host. The broad bands at the region 1000, 1650 and 3500 cm^{-1} of the zeolite obscure some of the bands of metal complexes. In the spectrum of QOPD ligand, the bands at 1596 and 1060 cm^{-1} are attributed to the stretching mode of C=N and C-N respectively. On complexation the band at 1596 cm^{-1} is found to be shifted to lower frequencies, which shows that azomethine nitrogen is coordinated to the metal.

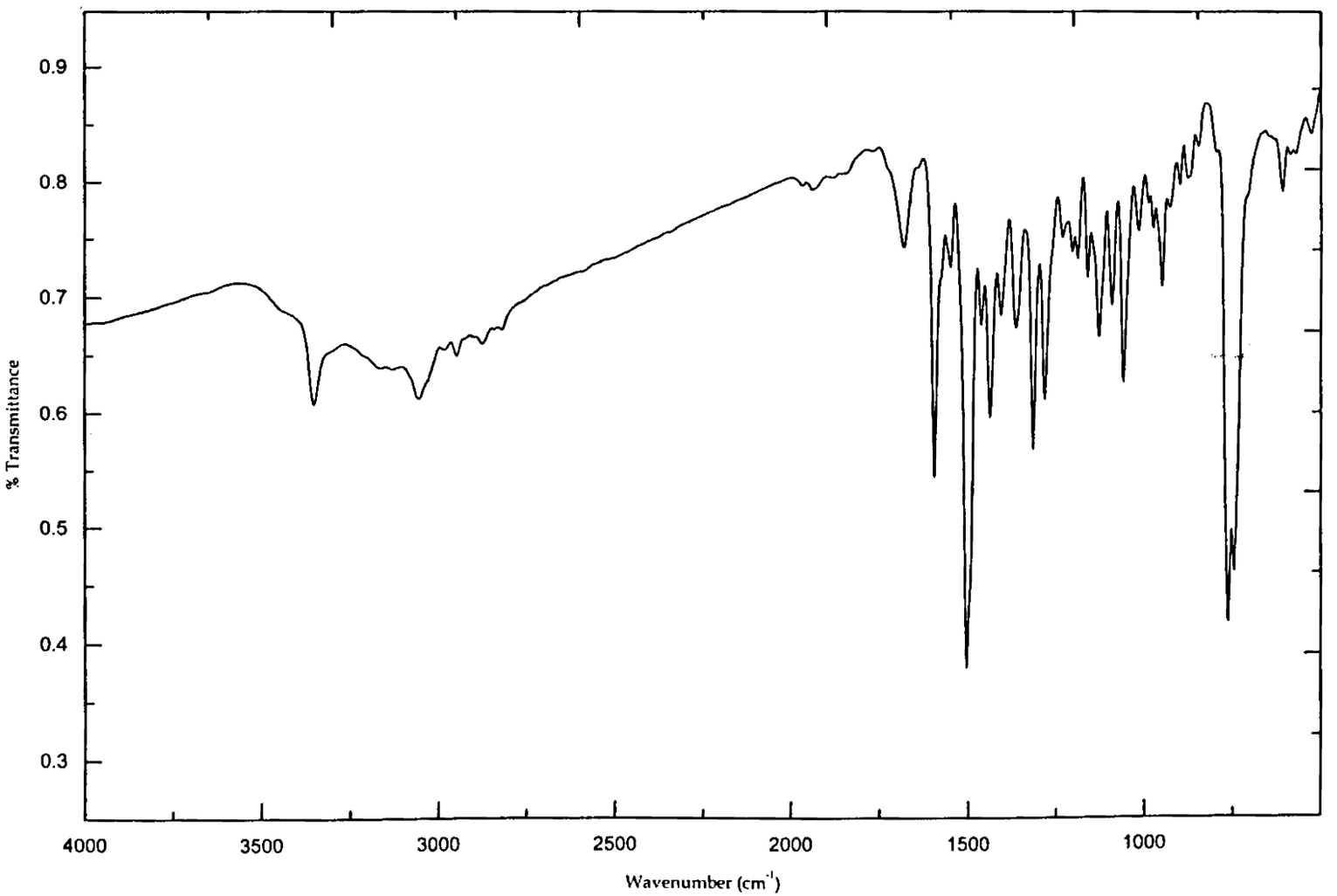

Figure 3.6 FTIR Spectrum of QOPD

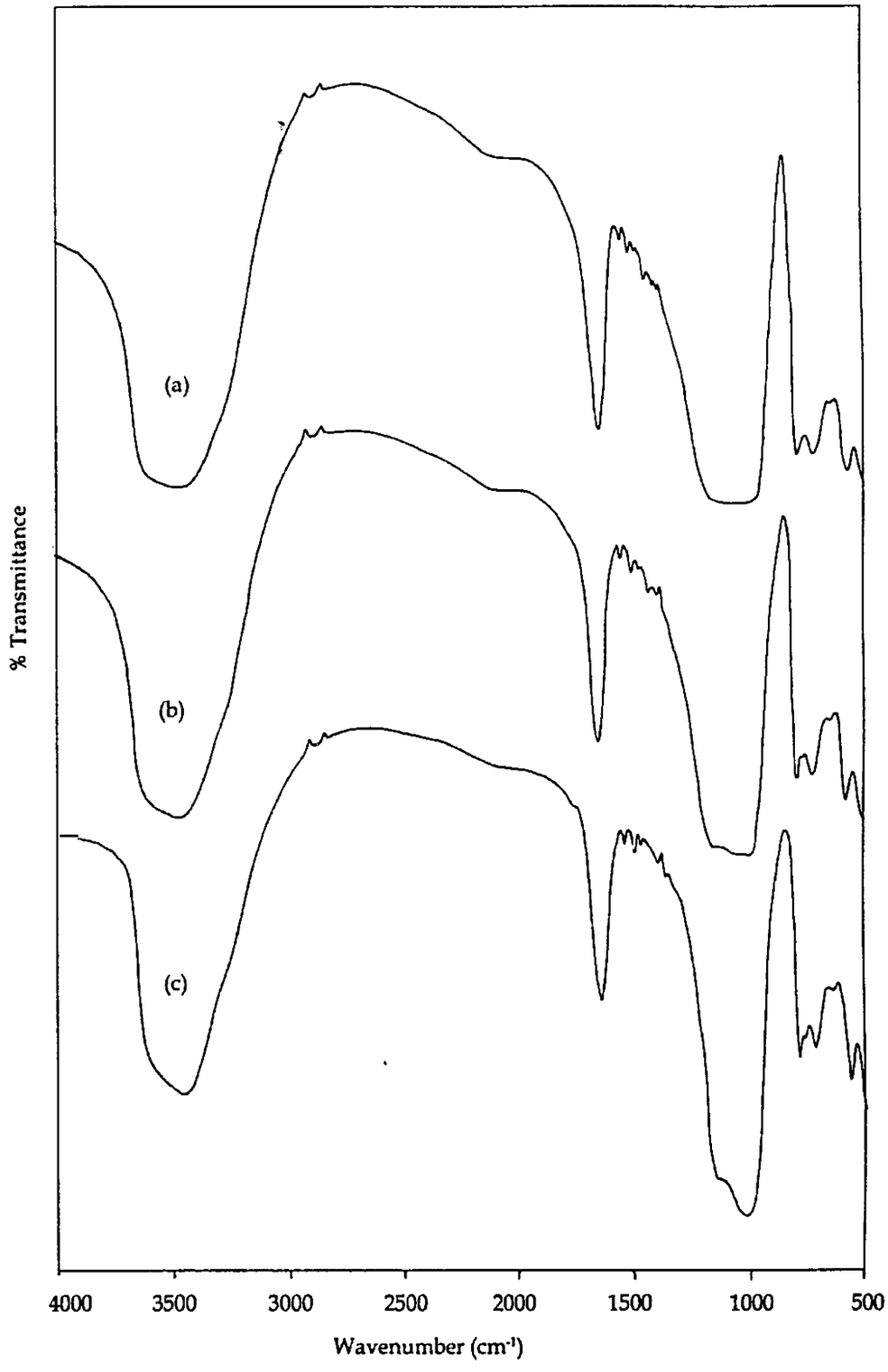

Figure 3.6a FTIR spectra of (a) YCoQOPD (b) YNiQOPD (c) YCuQOPD

Table 3.6
IR Spectral data of MY, QOPD and zeolite complexes

MY	QOPD	YCoQOPD	YNiQOPD	YCuQOPD
575		575	575	573
	763			
757		724	725	726
	950			
1020		1023	1023	1024
	1060			
	1130			
	1504	1500	1502	1506
	1548	1542	1546	1542
	1596	1575	1570	1568
1644		1637	1636	1631
	1681			
	1713	1710	1710	1712
	2369	2367	2368	2368
	2668	2668	2670	2672
	2726	2725	2725	2725
	3351			
3464		3465	3460	3465

3.3.2.6 TG analysis

Thermal analysis is an effective tool to study the decomposition pattern of the metal complexes. Thermogravimetric analysis provides a quantitative measurement of any weight change associated with a transition. The change in mass is a result of the rupture and/or formation of chemical bonds at higher temperature and removal of volatile product. The thermal stability of complexes is believed to be enhanced on heterogenizing them especially by encapsulating in zeolite pores[195]. The TG/DTG data provide the decomposition temperature range

and the decomposition peak temperature. Changes in the TG patterns as compared to that of metal exchanged zeolite indicate the encapsulation of complexes.

TG of all the samples were recorded at a heating rate of 10^0C/min. in nitrogen atmosphere. The TG patterns of NaY, metal exchanged zeolite and zeolite encapsulated complex are given in Figure 3.7 and the DTG of the zeolite encapsulated complex is given in Figure 3.7a. All the encapsulated complexes show a pattern of TG different from that of the metal exchanged zeolite and parent NaY. A weight loss of about 10% is observed in the temperature range of all the three QOPD complexes. Such a weight loss is observed in the case of metal exchanged zeolite also. Therefore this may be due to the intrazeolite water molecule. The copper complex shows a two stage decomposition pattern, whereas cobalt and nickel show single stage weight loss. This single stage weight loss can be attributed to the simultaneous removal of water and decomposition of encapsulated complex. The second peak in the copper complex was broad and with a DTG minimum around 450-550^{0}C. Weight loss in this case corresponds to the decomposition of ligand. The broad peak is an indication of slow combustion of QOPD inside the cages. If the complex is in the zeolite surface the peak due to the complex decomposition might be a sharp one. Based on the TG data the observed stability of the complexes is in the order YCuQOPD> YNiQOPD~YCoQOPD.

Table 3.7
TG/DTG Data

Sample	Weight loss: Stage I			Weight loss: Stage II		
	Temp range(^{0}C)	Peak temp (^{0}C)	% Mass loss	Temp range(^{0}C)	Peak temp (^{0}C)	% Mass loss
YCoQOPD	60-220	99	9.2	-	-	-
YNiQOPD	60-232	111	10.1	-	-	-
YCuQOPD	60-240	114	9.0	460-575	485	13.9

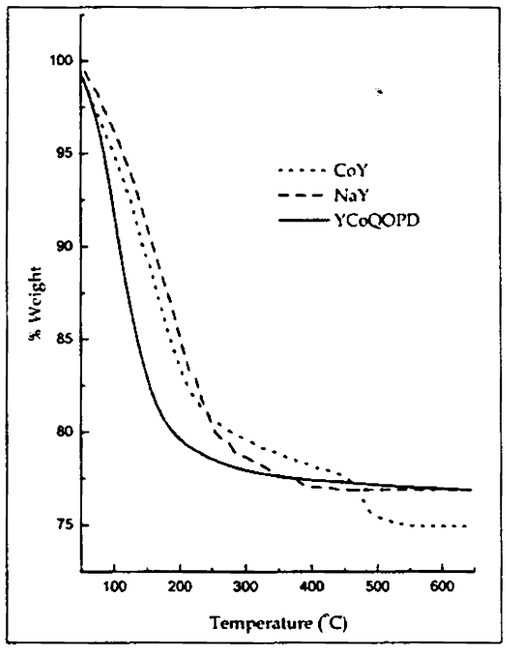

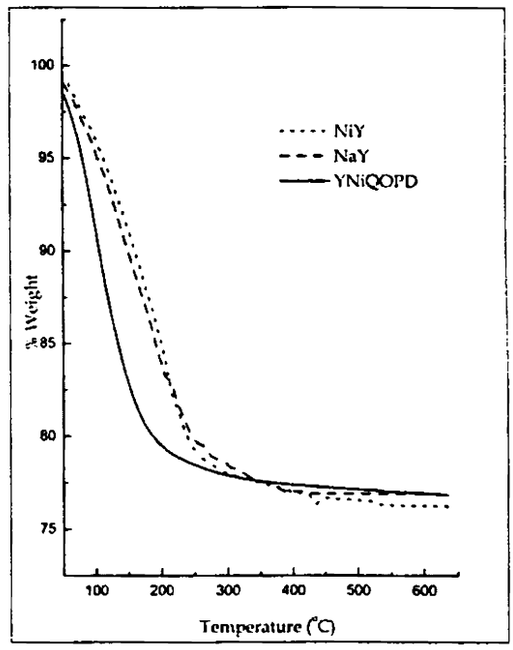

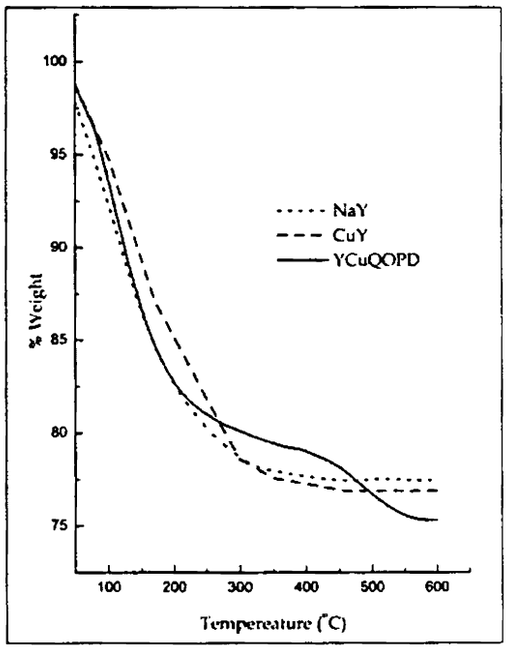

Figure 3.7

TG patterns of NaY, MY and zeolite encpasulated QOPD complexes

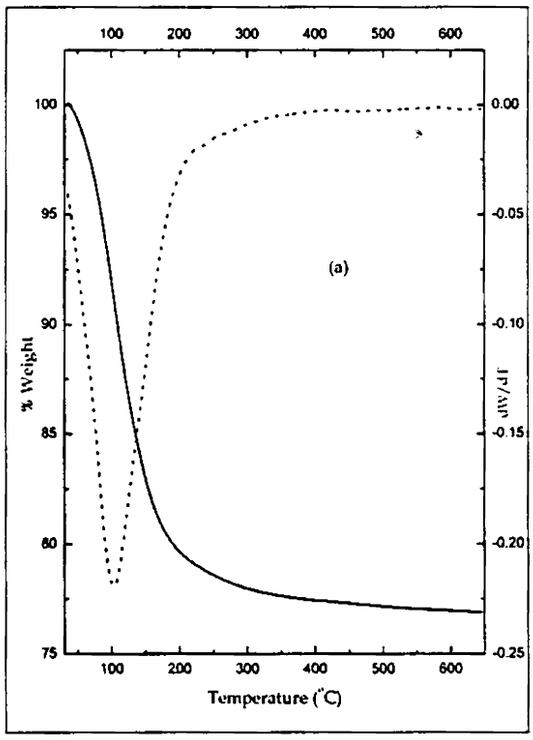

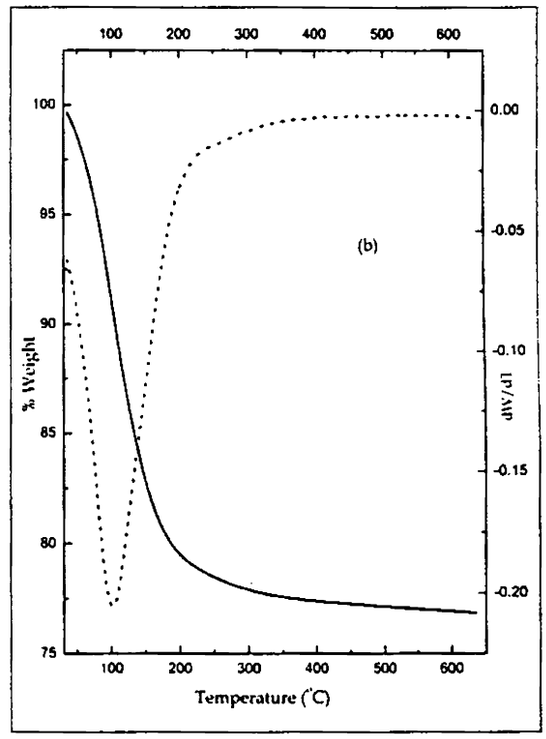

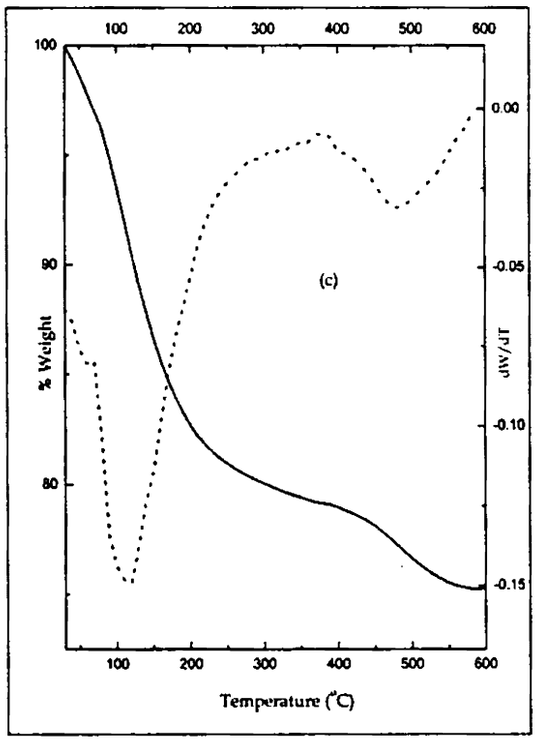

Figure 3.7a

TG/DTG patterns of (a) YCoQOPD
(b) YNiQOPD (c) YCuQOPD

3.3.2.7 Electronic spectra

Electronic spectroscopy provides a way to study the coordination environment of transition metal complexes in zeolites. The energy of the d-d transitions depends on the number and position of the ligands surrounding the transition metal ions. As such, these spectra provide a 'fingerprint' of the specific metal environment in the zeolite. The electronic spectra of the encapsulated complexes can only be measured experimentally by diffuse reflectance spectroscopy (DRS) since the complexes are insoluble[196]. Diffuse reflectance spectroscopy detects the d-d transitions in the near IR and visible region, and the ligand metal interactions through the ligand to metal charge transfer transitions in the UV region[197-199]. The electronic spectra of the encapsulated complexes are given in the Figure 3.8 and the plausible transitions assigned for the complexes are given Table 3. 8.

Six coordinate complexes of cobalt(III) are invariably low spin and diamagnetic. It is possible to observe spin-allowed d-d bands in the visible region of the spectra of low-spin cobalt(III) complexes. The bands observed at 17670 and 22730 cm^{-1} for YCoQOPD could be attributed to $^1A_{1g} \rightarrow {}^1T_{2g}$ and $^1A_{1g} \rightarrow {}^1T_{2g}$ transitions, which is characteristic of cobalt(III) low spin octahedral complex[200]. The geometry assigned for the complex on the basis of electronic spectra is in agreement with the EPR and magnetic data also.

The nickel(II) species are of special interest since these species exist in almost all the coordination numbers. In a cubic field three spin allowed transitions are expected because of the splitting of the free ion, ground ^3F term and the presence of the ^3P term. Spectra of octahedral nickel(II) complexes[201] usually consist of three bands in the region 8000 to 13000 cm^{-1}. 15000 to 19000 cm^{-1}, and 25000 to 29000 cm^{-1}. These transitions are seen in the present encapsulated nickel(II) complexes.

Table 3.8
Electronic spectral data

Sample	Absorption Max.		Tentative assignments
	(cm^{-1})	(nm)	
YCoQOPD	17670	565	$^1T_{2g} \leftarrow {}^1A_{1g}$
	22730	440	$^1T_{1g} \leftarrow {}^1A_{1g}$
	26315	380	Charge transfer
YNiQOPD	12500	800	$^3T_{2g}(F) \leftarrow {}^3A_{2g}(F)$
	17680	595	$^3T_{1g}(F) \leftarrow {}^3A_{2g}(F)$
	26020	385	$^3T_{1g}(P) \leftarrow {}^3A_{2g}(F)$
	32840	305	Intraligand transition
YCuQOPD	15220	660	$^2A_{1g} \leftarrow {}^2B_{1g}$
	17515	570	$^2B_{2g} \leftarrow {}^2B_{1g}$
	21325	470	$^2E_g \leftarrow {}^2B_{1g}$
	25730	390	Charge transfer
	32360	310	Intraligand transition

A single band spectrum might be expected in the electronic spectrum of copper(II) complex, since the d^9 configuration can be thought of as an inversion of d^1. However, the d^9 ion is characterized by large distortion from octahedral symmetry and the band is unsymmetrical, being the result of a number of transitions which are by no means easy to assign unambiguously. Because of these reasons electronic spectroscopy cannot be used as a tool for identifying structure of copper complex. Certainly in the absence of X-ray crystallography, ESR should be regarded as essential to compliment electronic spectroscopic data. Since the ground state in an octahedral field is the Jahn-Teller unstable ^2E_g, very

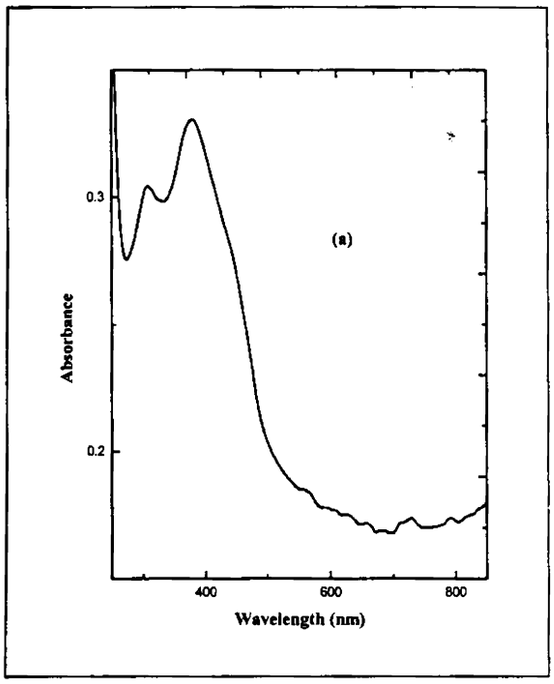

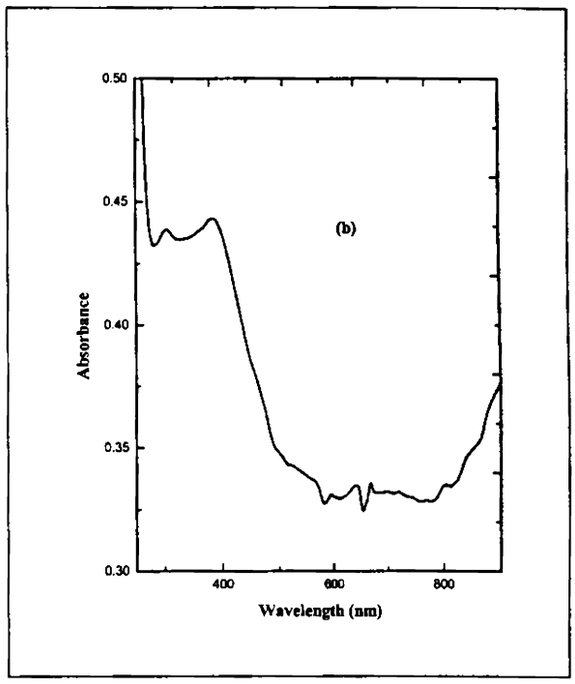

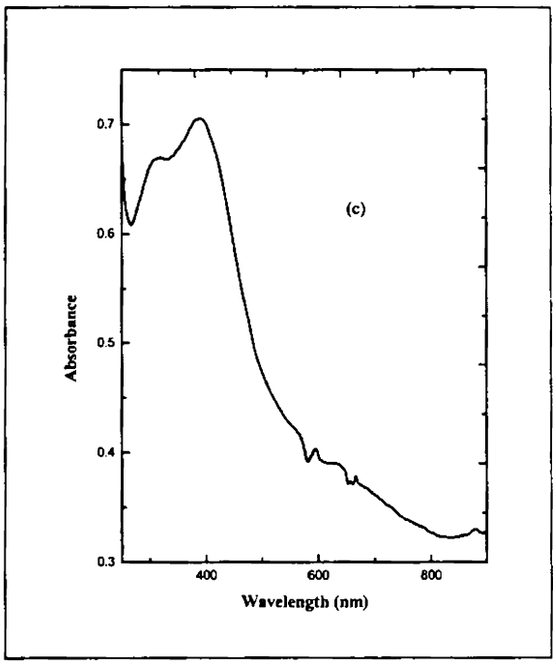

Figure 3.8

Electronic spectra of

(a) YCoQOPD

(b) YNiQOPD

(c) YCuQOPD

few regular octahedral copper(II) complexes do exist. It was reported that a high degree of distortion may even lead to a square planar (D_{4h}) geometry[202].

The electronic spectra of the YCuQOPD complex is given in Figure 3.8. The bands observed for the complexes at 15200, 17500 and 21300 cm^{-1} corresponds to $^2B_{1g} \rightarrow {}^2A_{2g}$, $^2B_{1g} \rightarrow {}^2B_{2g}$ and $^2B_{1g} \rightarrow {}^2E_g$ transitions respectively and these are in agreement with those reported for a square planar geometry[203].

3.3.2.8 Magnetic measurements

Magnetism has been of considerable utility in establishing the structure of many complexes[204]. The strong and weak field complexes of several transition metal ions differ in the number of unpaired electrons in the complexes. Therefore it is possible to easily distinguish spin-paired from spin-free complex. Determining the number of unpaired electron can also give information regarding the oxidation state of a metal ion in a complex.

The magnetic moment values of zeolite complexes were measured using the Gouy method at room temperature. The magnetic moment determination by this method cannot be considered as very accurate, since the application of diamagnetic corrections due to the zeolite support and the paramagnetic contribution of the traces of iron impurity are not perfect. The molecular weight of the zeolite encapsulated complexes were determined based on the unit cell formulae calculated using the elemental analysis. However this method gives a qualitative idea about magnetic moment of the complexes formed inside the zeolite. The magnetic moment data of the complexes were calculated and are presented in Table 3.9.

In an octahedral field Ni(II) (d^8) has a nondegenerate ground state, ^3A-($t_{2g}^6e_g^2$), and no contribution from spin orbit coupling is expected. The measured moments are in the range 2.8 to 3.3 BM, and are very close to spin-only value of 2.83. Values of octahedral complexes slightly above the spin-only value arise from slight mixing of a multiplet excited state in which spin-orbit coupling is

appreciable. An octahedral geometry was assigned for the YNiQOPD complex, based on the observed magnetic moment value of 3.0 BM. It appears that the other coordination sites of the octahedral nickel(II) are bonded to the water molecules or to the zeolite framework oxygen atoms.

Structure of copper complexes cannot be assigned stereochemistry based on the room temperature magnetic moment value alone. Usually the magnetic moment values of the copper(II) complexes are in the range 1.75-2.2 BM[200]. A magnetic moment value of 1.9BM was observed for the YCuQOPD complex.

Table 3. 9
Magnetic moment data of the encapsulated QOPD complexes

Complexes	Magnetic moment (BM)	Unit Cell
YCoQOPD	-	$Na_{50}Co_{1.98}(AlO_2)_{56}(SiO_2)_{136}nH_2O$
YNiQOPD	3.0	$Na_{53.04}Ni_{1.48}(AlO_2)_{56}(SiO_2)_{136}nH_2O$
YCuQOPD	1.9	$Na_{56.23}Cu_{4.88}(AlO_2)_{56}(SiO_2)_{136}nH_2O$

3.3.2.9 EPR spectra

EPR spectroscopy is ideal to probe both molecular and electronic structural information of the paramagnetic ions and the effect of molecular confinement of the complexes inside the zeolite cage. An EPR spectrum of the zeolite encapsulated copper complex is given in Figure 3.9. The data obtained from the spectra of YCuQOPD is given in Table 3.10. The spectra of the zeolite-Y encapsulated copper complexes are characterized by an axial spin Hamiltonian. The resolution in the copper hyperfine features confirm that the encapsulated metal complexes are isolated and present as monomeric species[86]. The $g_{||}$ value in the case of zeolite encapsulated complex is found to be higher than the usually reported value. Sakaguchi and Addison[205] attributed such a higher value for a tetrahedral distortion of a square planar chromophore or due to increasing

positive charge on donor atom. The higher value of $g_{\parallel}$ is also an indication of the decreased covalence of the metal-ligand bond due to increased delocalization. They also suggest that the ratio $g_{\parallel}/A_{\parallel}$ may be conveniently used as an empirical index of tetrahedral distortion. This quotient ranges from 105 to 135 cm for square planar structures. The $g_{\parallel}/A_{\parallel}$ value of 134 suggests a square planar geometry for the complex. For the Cu(II) complexes with the unpaired electron in the B_{1g} orbital, the density of the unpaired electron at the central atom can be computed from the following equation

$$\alpha^2 = (A_{\parallel}/P) + (g_{\parallel} - 2) + {}^3/_7(g_{\perp}-2) + 0.04$$

where $1-\alpha^2$ measures the covalence associated with the bonding of the Cu^{2+} ions to the ligand and P = 0.036 cm^{-1}. The α^2 values of YCuQOPD is 0.82 which indicates the Cu^{2+} ion to be in an ionic environment.

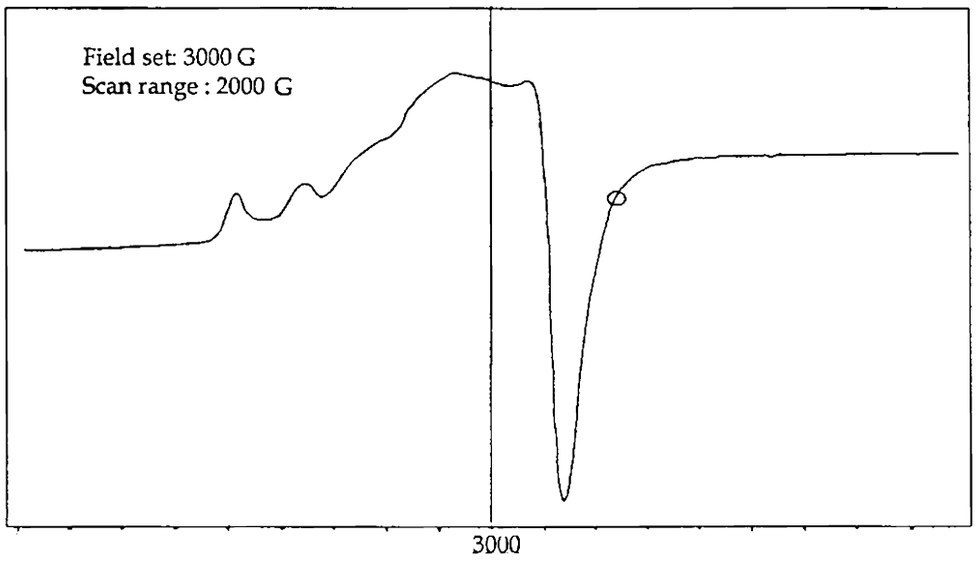

Figure 3.9 EPR spectrum of YCuQOOPD

Table 3.10
EPR Spectral data of YCuQOPD

EPR parameter	YCuQOPD
$g_{\|\|}$	2.36
$A_{\|\|}$	177.40cm^{-1}
$g_{\|\|}/A_{\|\|}$	134 cm
$g_{\perp}$	2.05
α^2	0.82

The YCoQOPD complex was found to be EPR silent. This again suggests a low-spin octahedral cobalt(III) complex.

ZEOLITE ENCAPSULATED METAL COMPLEXES OF INDOLE-3-CARBOXALDEHYDE SEMICARBAZONE

4.1 Introduction

The coordination chemistry of chelating agents with oxygen-nitrogen donor sites has been an area of interest for a number of years. These types of compounds include Schiff base complexes derived from semicarbazide, amino acids, amino phenols etc[206-208]. The oxygen atoms are coordinated in most cases to a transition metal ion to secure the stability of the complex. Semicarbazones act as a bidentate or tridentate ligand depending on the aldehyde residue attached to the semicarbazide moiety. In view of the interesting properties of semicarbazone complexes zeolite encapsulated cobalt(II), nickel(II) and copper(II) complexes of the Schiff base indole-3-carboxaldehyde semicarbazone (Figure 4.1) have been prepared and characterized. The details regarding the synthesis and characterization studies are presented in this chapter

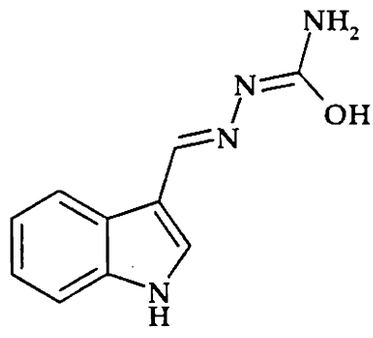

Figure 4.1 Structure of Indole-3-carboxaldehyde semicarbazone (ICSCZ)

4.2 Experimental

4.2.1 Materials

Details regarding the preparation of the metal exchanged zeolites are given in Chapter 2. These metal exchanged zeolite are further used for the encapsulation of the Schiff base complexes using the intrazeolite synthesis by complexation method.

4.2.2 Synthesis of zeolite encapsulated complexes of indole-3-carboxaldehyde semicarbazone (ICSCZ)

Zeolite encapsulated cobalt(II), nickel(II) and copper(II) complexes of ICSCZ were prepared from the metal exchanged zeolite using the intrazeolite synthesis by complexation method. In this method, the ligand diffuses into the zeolite and undergoes complexation with metal ion to form complexes which are too large to exit the supercages. The diffusion of the ligand is facilitated by heating the metal exchanged zeolite (5g) with excess of ligand (1.85g) at 130^{0}C for 16h in a closed glass ampoule. The resulting material was soxhlet extracted with methanol to remove unreacted ligand and surface complexes, stirred with 1.0 M sodium chloride solution to re-exchange the uncomplexed metal ion and was finally dried at 120^{0}C.

4.2.3 Analytical method

Details regarding the various analytical methods and characterization techniques used are given in Chapter 2.

4.3 Results and discussion

Zeolite Y encapsulated cobalt(II), nickel(II) and copper(II) complexes of the Schiff base, indole-3-carboxaldehyde semicarbazone was synthesized and characterized by various techniques like chemical analysis, XRD, surface area, pore volume, magnetic moment measurements, electronic, FTIR and EPR spectroscopy and TG analysis.

4.3.1 Chemical analysis

The amount of silica, alumina and the Si/Al ratio are very important criteria in maintaining the crystallinity and stability of the zeolites. The analytical data of the zeolite complexes are given in Table 4.1. The percentage silica was determined according to the procedure described in Chapter 2 and metal percentage was determined by AAS analysis. The silica-alumina ratio for the entrapped complex is around 2.39, which is found to be the same for the metal exchanged zeolites. So dealumination was not occurred in the encapsulated complexes. This proves that the zeolite framework is unaltered even after encapsulation. The metal content of the encapsulated complex is less compared to the corresponding metal exchanged zeolites, which suggests that a portion of the metal that remain uncomplexed is re-exchanged with the Na^+ ion. Some uncomplexed metal ions still remain in the zeolite cage after back exchange, the encapsulated complexes, may shield and thus prevent the free metal from leaching during the back exchange process. The carbon percentage of the zeolite encapsulated complexes gives only a qualitative idea about the entrapment of the complex inside the zeolite cavity. The carbon percentage values indicate an approximate ligand to metal ratio of 2:1.

Table 4.1
Analytical data of encapsulated complexes

Sample	%Si	%Al	%Na	%Metal	%C
YCoICSCZ	24.23	10.21	7.0	0.56	2.64
YNiICSCZ	24.35	10.23	7.1	0.59	2.87
YCuICSCZ	24.35	10.11	6.9	0.83	2.79

4.3.2 SEM analysis

Effectiveness of the soxhlet extraction in removing the surface adsorbed species is checked by SEM analysis. The SEM of CuICSCZ, before and after

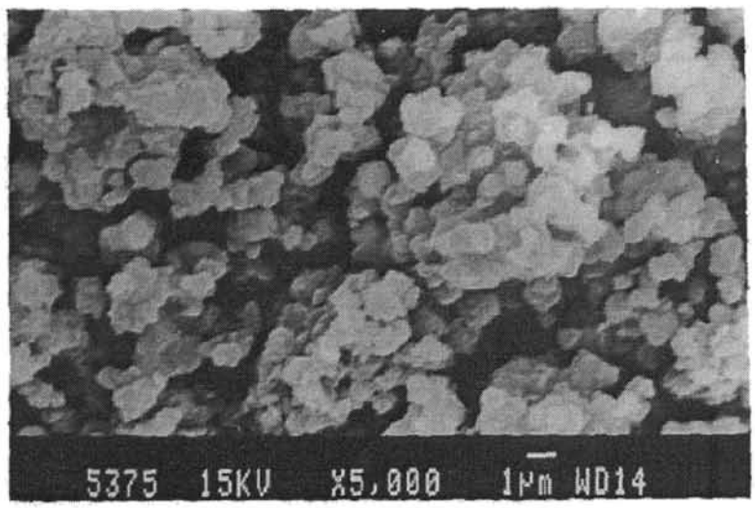

(i)

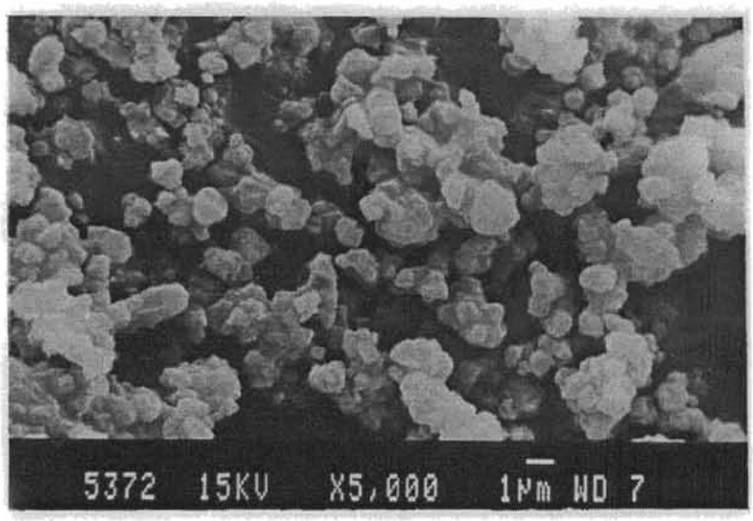

(ii)

Figure 4.2 Scanning Electron Micrograph of YCuISCZ
(i) before (ii) after soxhlet extraction

Soxhlet extraction is given in Figure 4.2. The surface of the zeolite encapsulated complex after soxhlet extraction is almost clean. The figures reveal that the morphology of the parent NaY has been retained in the encapsulated complex.

4.3.3 X-ray diffraction analysis

Powder XRD patterns of the encapsulated ICSCZ complexes of Co(II), Ni(II) and Cu(II) are given in Figure 4. 3. These patterns are similar to those for the corresponding metal exchanged zeolites and the parent zeolite, indicating that the crystallinity of the parent zeolite is well maintained even after the encapsulation. Therefore the zeolite framework structure was not altered during the encapsulation of the complexes within the supercages. More over the changes in intensities of the characteristics peaks of zeolite Y in the order $I_{331} > I_{311} > I_{220}$, is an ample proof of the cation redistribution that occurred following complex formation within the zeolite supercages[49].

4.3.4 Surface area and pore volume

Surface area and pore volume analyses of the samples determined by BET method are presented in Table 4.2. A drastic decrease in surface area and pore volume was observed in the case of zeolite encapsulated complexes. Since the XRD pattern shows that the crystalline nature of zeolite is intact, the decrease in surfaces area is a clear indication of blocking of pores due to encapsulation[82,37].

Table 4. 2
Surface area and pore volume data of the zeolite encapsulated complexes

Metal ion	Surface area (m^2/gm)		Pore volume (cc/g)	
	MY	Complex Y	MY	Complex Y
Co	640	515	0.26	0.21
Ni	635	510	0.25	0.20
Cu	640	480	0.24	0.18

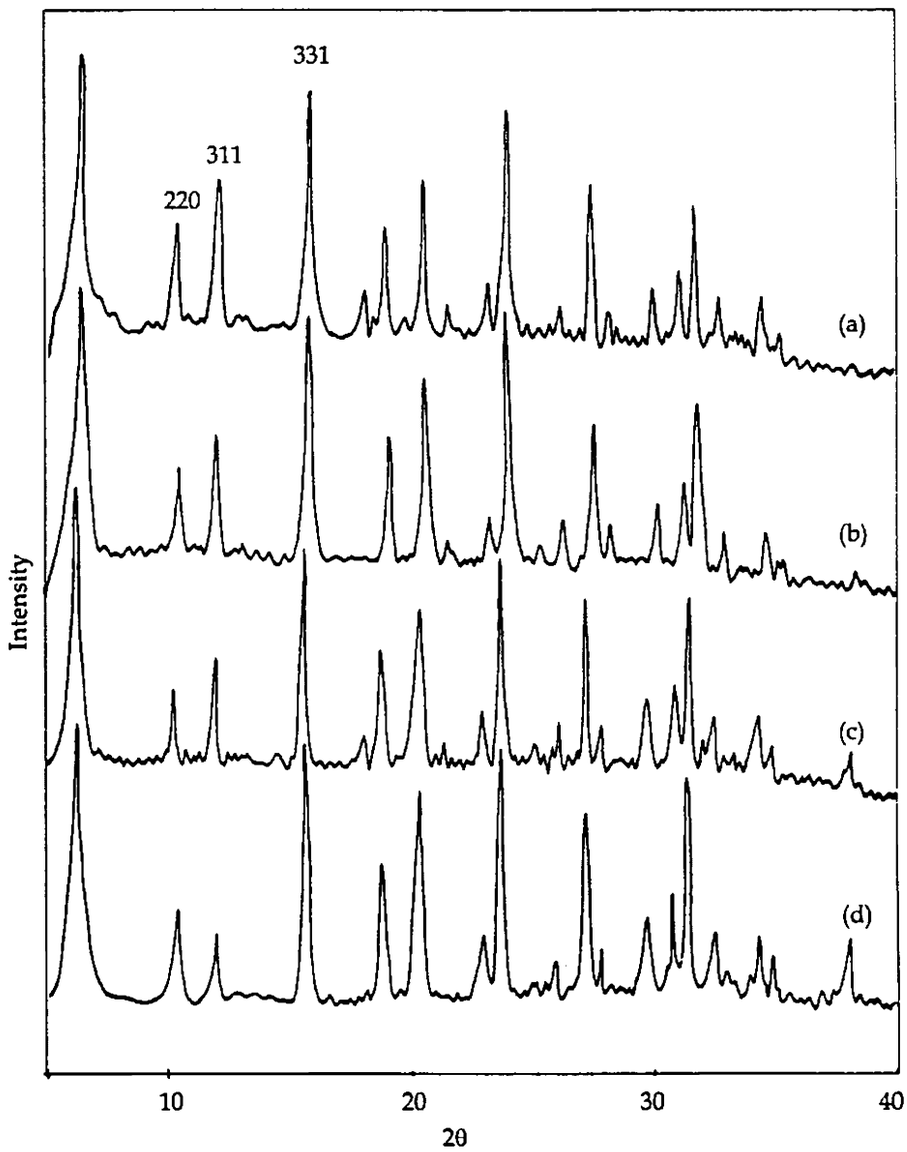

Figure 4.3 XRD Patterns of (a) YCoICSCZ (b) YNiICSCZ (c) YCuICSCZ (d) CuY

4.3.5 FTIR spectra

The infrared spectrum of the ligand is given in Figure 4.4. A strong band at ~3190 cm^{-1} of the ligand is attributed to the secondary N-H stretching. The band at 1590 cm^{-1} of the ligand is due to the C=N stretching and the peak at 1650 cm^{-1} can be attributed to the C=O stretching band. There is a medium band at 990 cm^{-1} in the spectrum corresponding to νN - N. The spectral data of the ligand and the encapsulated complexes are given in Table 4.3

Table 4.3
IR Spectral data of MY, ICSCZ and zeolite complexes

MY	ICSCZ	YCoICSCZ	YNiICSCZ	YCuICSCZ
575		577	580	579
790		792	792	791
	990			
1020		1024	1024	1025
	1116			
	1437	1437	1437	1437
	1504	1506	1505	1505
	1592	1562	1575	1555
	1620			
1644		1645	1645	1644
	1652	1624	1631	1637
	3180			
3464		3450	3450	3451

The infrared spectra of zeolite encapsulated cobalt, nickel and copper complexes of the ligand indole-3-carboxaldehyde semicarbazone (ICSCZ) are given in Figure 4.4a. The band at 1650 cm^{-1} of the ligand was shifted to 1624 cm^{-1} in the case of cobalt complex (YCoICSCZ), to 1631 cm^{-1} in the nickel complex (YNiICSCZ) and to 1637 cm^{-1} in the case of copper complex (YCuICSCZ). This

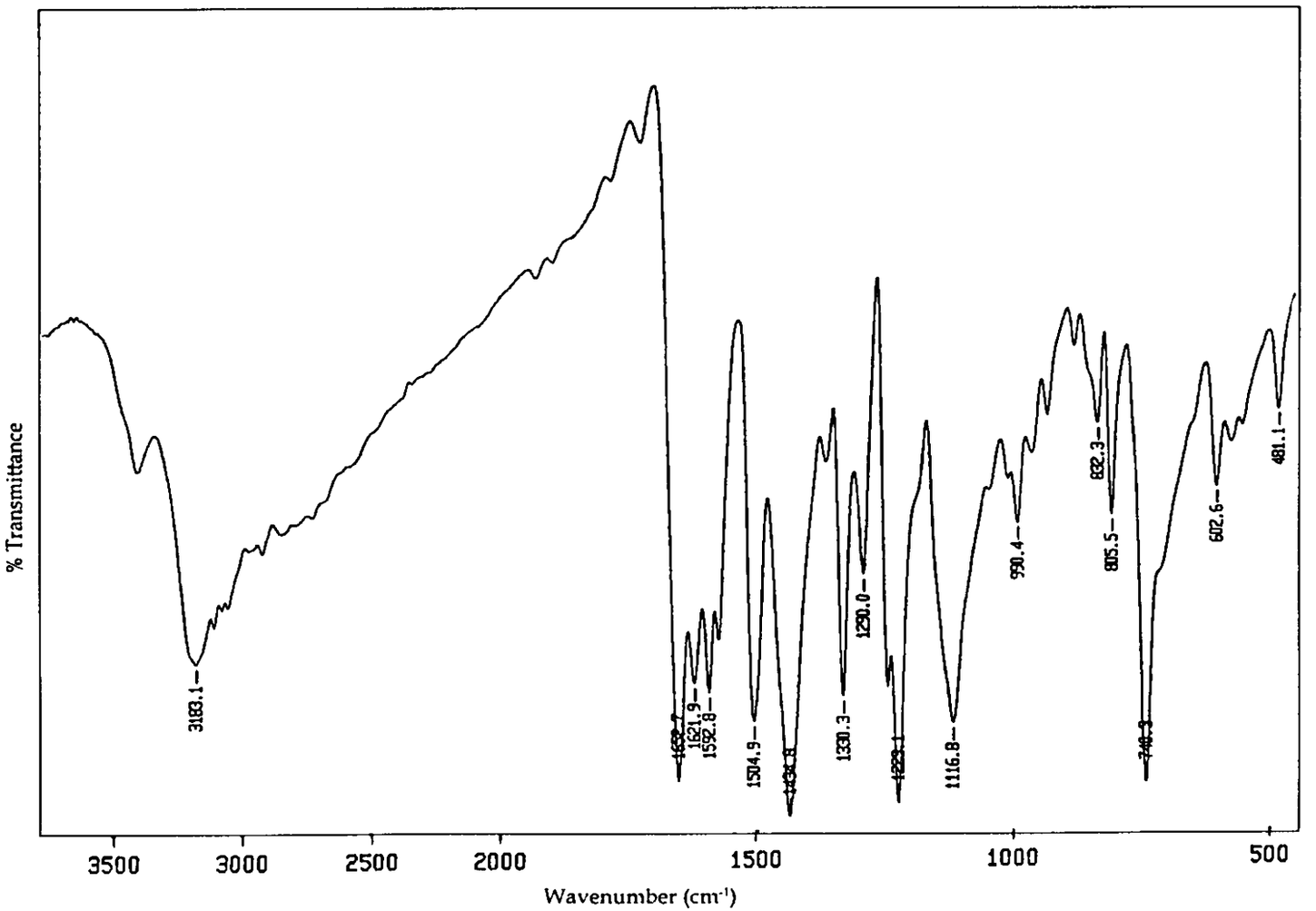

Figure 4.4 FTIR Spectrum of ICSCZ

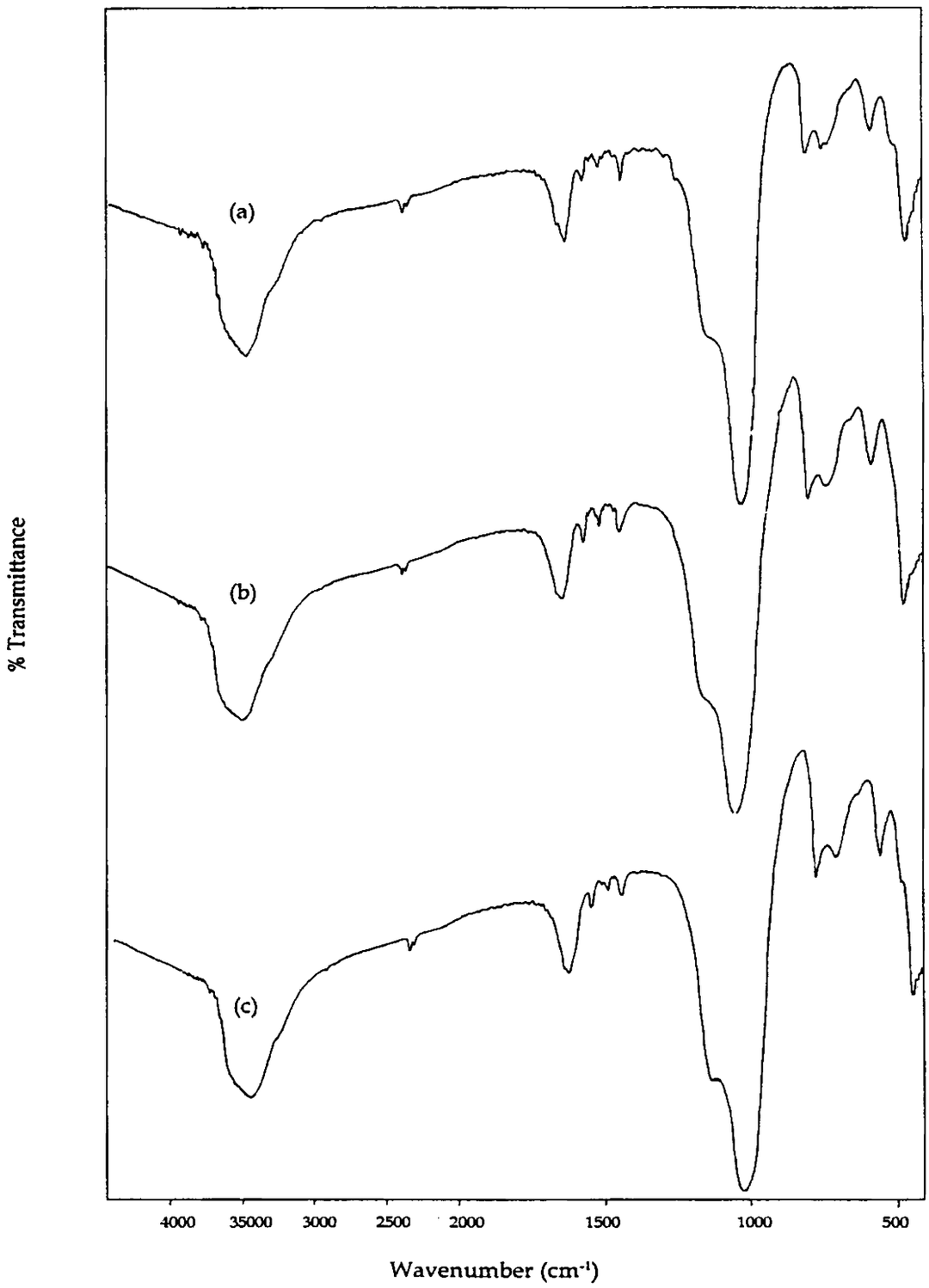

Figure 4.4a FTIR Spectra of (a) YCoICSCZ (b) YNiICSCZ (c) YCuICSCZ

shift in frequency towards low energy region indicates the coordination of oxygen of C=O group. Shifting of the peak at 1590 cm^{-1} of the ligand to lower frequencies was also observed in the case of the complexes, indicating that the unsaturated nitrogen of the azomethine of the ligand, ICSCZ, is coordinated to the metal atom. Some other peaks of the ligand are also observed showing the presence of complexes inside the zeolite cages.

4.3.6 TG analysis

TG/DTG curves were recorded for the encapsulated ICSCZ complexes in an inert atmosphere, and are given in Figure 4.5 and 4.5a and the results are summarized in Table 4.4. There are two main stages of decomposition. The first stage corresponds to the removal of coordinated water molecules. The decomposition of the encapsulated complexes might be happening after this stage. In the case of YCuICSCZ complex, the second stage is not predominant. This can be attributed to the simultaneous removal of water and decomposition of the encapsulated complex.

Table 4.4

TG/DTG Data

Sample	Weight loss-Stage I			Weight loss-Stage II		
	Temp range(^{0}C)	Peak temp (^{0}C)	% Mass loss	Temp range(^{0}C)	Peak temp (^{0}C)	% Mass loss
YCoICSCZ	80-170	130	6.8	475-600	530	12.2
YNiICSCZ	90-190	120	9.7	390-600	510	16.4
YCuICSCZ	60-160	99	8.8	390-575	477	13.5

4.3.7 Electronic spectra

Diffuse reflectance spectra of the complexes were recorded. The electronic transitions and their tentative assignments were given in Table 4.5. The electronic spectra of the complexes are given in Figure 4.6.

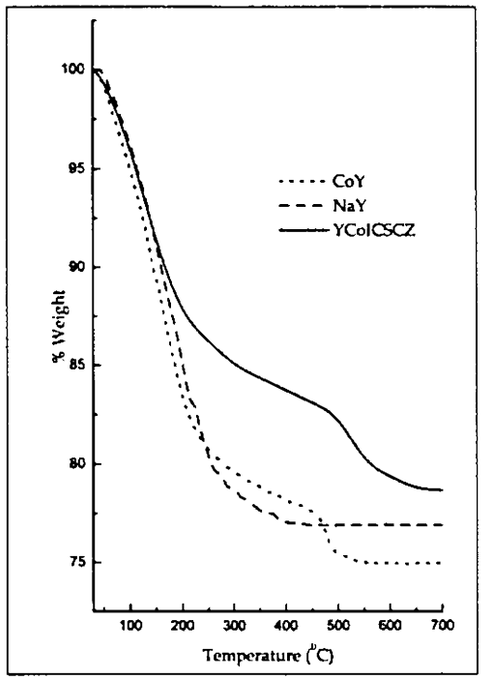

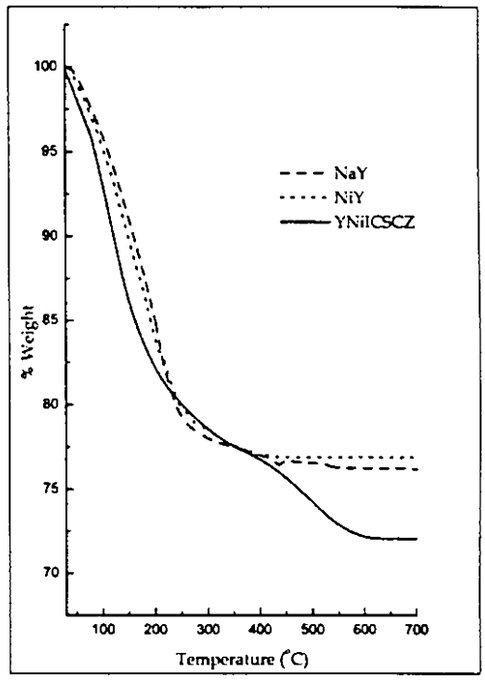

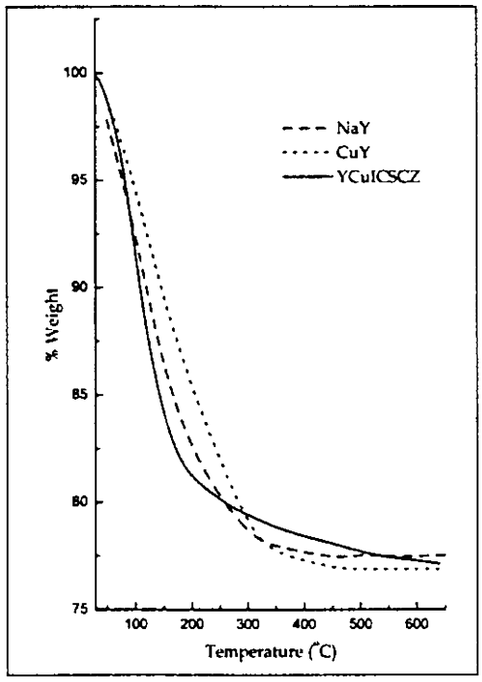

Figure 4.5

TG patterns of NaY, MY and
zeolite encapsulated ICSCZ complexes

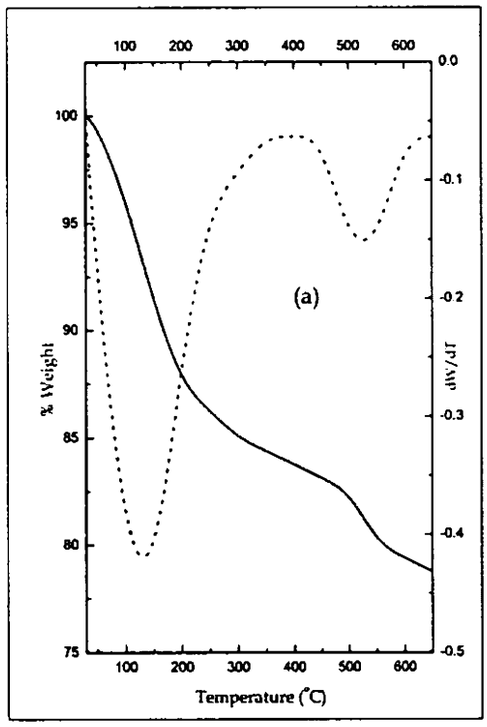

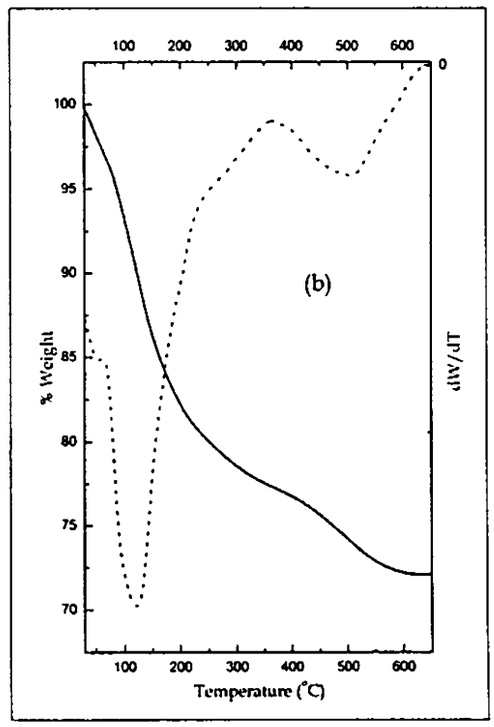

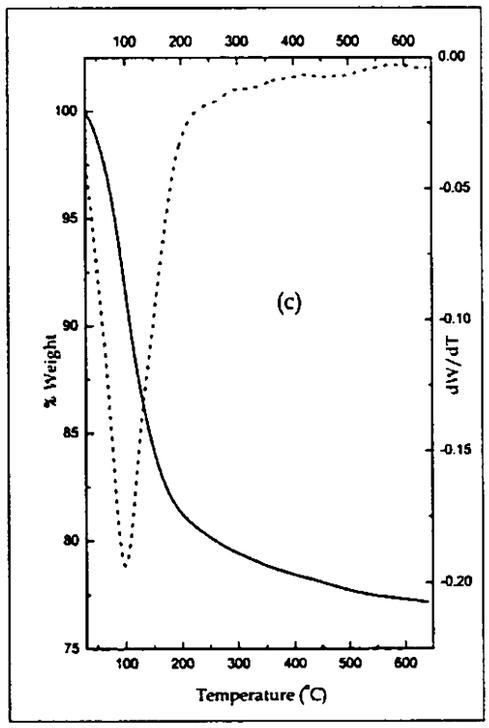

Figure 4.5a

TG/DTG patterns of (a) YCoICSCZ
(b) YNiICSCZ (c) YCuICSCZ

The spectrum of the octahedral cobalt(II) complex usually consists of a band in the near infrared, which may be assigned as ν_1; $^4T_{2g}(F) \leftarrow {}^4T_{1g}(F)$ and another in the visible region, ν_3; $^4T_{1g}(P) \leftarrow {}^4T_{1g}(F)$ often with a shoulder on the low energy side. The transition ν_2; $^4A_{2g}(F) \leftarrow {}^4T_{1g}(F)$, being an essentially two electron transition, is expected to be weak, and hence appears as a shoulder. The ν_2 band which is usually absent may appear in the spectra due to spin orbit coupling or distortions from the regular octahedral geometry[200]. $^4T_{1g}(P)$ state will spilt to $^4E_g(P)$ and $^4B_{1g}$[209]. The observed transitions in 22625, 21050 and 19760 cm^{-1} is in agreement with the assignments $^4A_{2g} \leftarrow {}^4T_{1g}$, $^4E_g(P) \leftarrow {}^4T_{1g}$ and $^4B_{1g} \leftarrow {}^4T_{1g}$ respectively for a tetragonally distorted octahedron.

Table 4. 5
Electronic spectral data

Sample	Absorption Max.		Tentative assignments
	(cm^{-1})	(nm)	
YCoICSCZ	19760	505	$^4B_{1g} \leftarrow {}^4T_{1g}$
	21050	475	$^4E_g(P) \leftarrow {}^4T_{1g}$
	22625	440	$^4A_{2g} \leftarrow {}^4T_{1g}$
	29250	340	Charge transfer
NiICSCZ	11830	845	$^3T_{2g} \leftarrow {}^3A_{2g}$
	13010	770	$^1E_g \leftarrow {}^3A_{2g}$
	17970	555	$^3T_{1g}(F) \leftarrow {}^3A_{2g}$
	28140	355	$^3T_{1g}(P) \leftarrow {}^3A_{2g}$
	33160	300	Charge transfer
YCuICSCZ	13755	730	d - d transition
	29410	340	Charge transfer
	32600	305	Intraligand transition

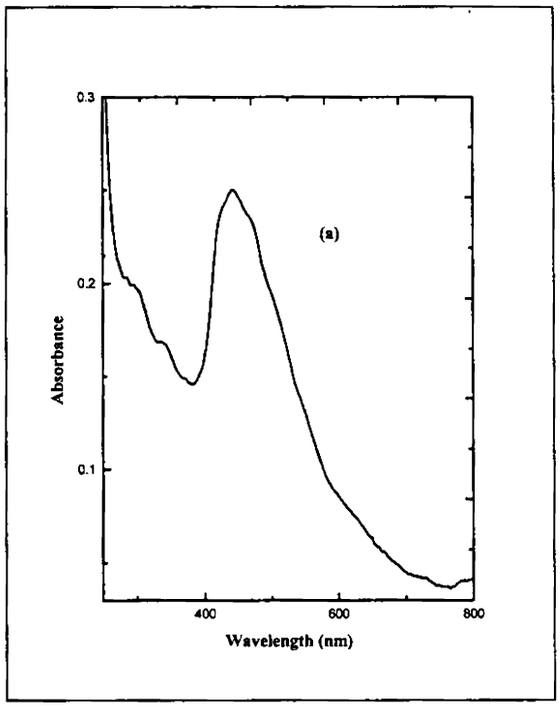

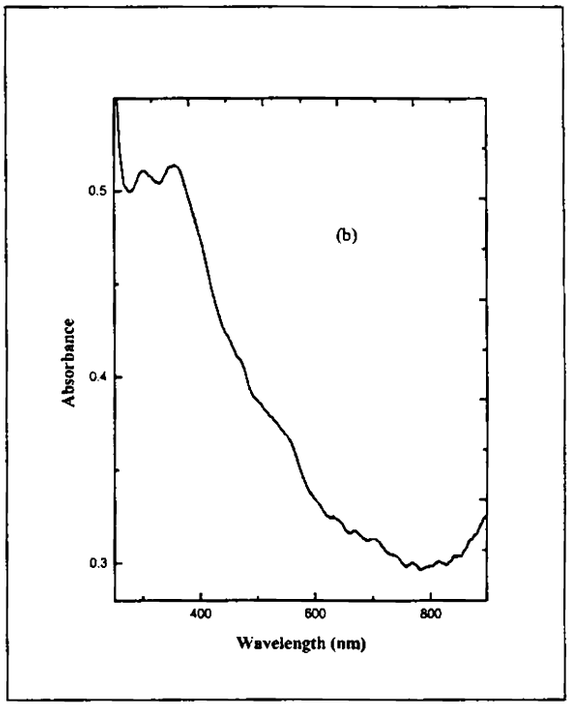

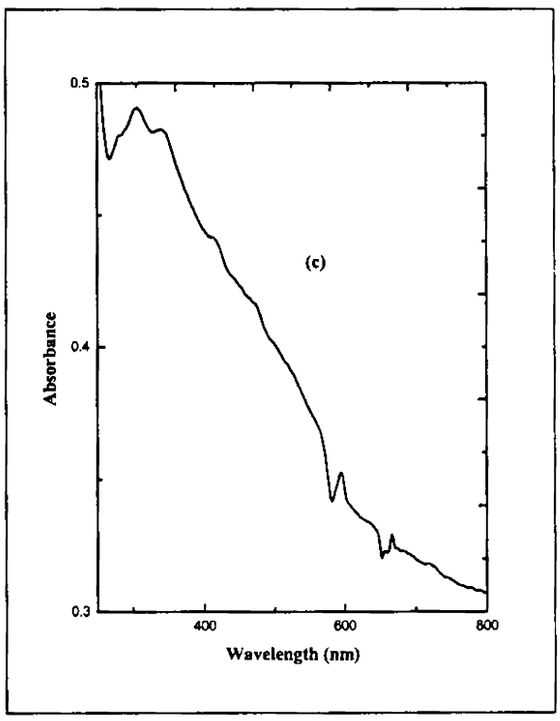

Figure 4.6

Electronic spectra of

(a) YCoICSCZ

(b) YNiICSCZ

(c) YCuICSCZ

The analysis of the spectra of the nickel(II) complex reveals an octahedral geometry for the metal ion. Bands at 28140, 17970, 13010 and 11820 cm^{-1} could be attributed to the $^3T_{1g}(P) \leftarrow {}^3A_{2g}$, $^3T_{1g}(F) \leftarrow {}^3A_{2g}$, $^1E_g \leftarrow {}^3A_{2g}$ and $^3T_{2g} \leftarrow {}^3A_{2g}$ transitions respectively.

Spectral bands are observed at 29410 and 13755 cm^{-1} of the copper complex. Since the electronic transitions alone are not effective in deriving the structural properties of copper complexes, conclusive structural information of the complex could not be obtained from the electronic spectra.

4.3.8 Magnetic measurements

Magnetic properties provide a complimentary means of distinguishing stereochemistry. The T ground term of octahedral cobalt(II) ion is expected to give rise to a temperature-dependent orbital contribution to the magnetic moment. In the case of high spin octahedral cobalt(II) complex (d^7 ion) a large orbital contribution to the magnetic moment is expected because of the three fold orbital degeneracy of the $^4T_{1g}$ ground state. Mixing of a singlet excited state lowers the moment but generally values ranging from 4.7 to 5.2 BM are expected[200,210]. A magnetic moment value of 5.3 BM was observed for the YCoICSCZ, suggesting an octahedral structure for the complex.

Table 4. 6
Magnetic moment data of the encapsulated ICSCZ complexes

Complexes	Magnetic moment (BM)	Unit Cell
YCoICSCZ	5.30	$Na_{53.20}Co_{1.40}(AlO_2)_{56}(SiO_2)_{136}nH_2O$
YNiICSCZ	3.21	$Na_{53.22}Ni_{1.38}(AlO_2)_{56}(SiO_2)_{136}nH_2O$
YCuICSCZ	1.89	$Na_{52.10}Cu_{1.95}(AlO_2)_{56}(SiO_2)_{136}nH_2O$

The spin only magnetic moment for nickel (II) is 2.83 BM. For tetrahedral nickel complexes the magnetic moment value lies between 3.2-4.1BM and for octahedral complex the magnetic moment value is between 2.9-3.3 BM. YNiICSCZ

complex exhibit a magnetic moment value of 3.2 BM indicating an octahedral geometry. The zeolite encapsulated copper complex of ICSCZ shows a magnetic moment of value of 1.89BM. No definite conclusion about the geometry of the copper(II) complex can be arrived from this value

4.3.9 EPR spectra

The EPR spectrum of YCuICSCZ was recorded at liquid nitrogen temperature and is given in Figure 4.7 and the observed spin Hamiltonian parameters are given in Table 4.7. The copper hyperfine features were well resolved in the parallel regions, which suggests that the molecules encapsulated in Zeolite-Y are isolated and located in the supercages[64]. The higher $g_{\parallel}$ observed for the copper complex may be due to the effect of oxygen donor atoms. This increased value also may be due to the distortion caused by the ligand and the zeolite frame work. The $g_{\parallel}$ value of 2.4 and $g_{\parallel}/A_{\parallel}$ ratio of 141 cm suggests that the complex has a geometry of flattened tetrahedra[205]. The α^2 value for this complex is 0.82, which indicates the large ionic nature of the metal-ligand bond.

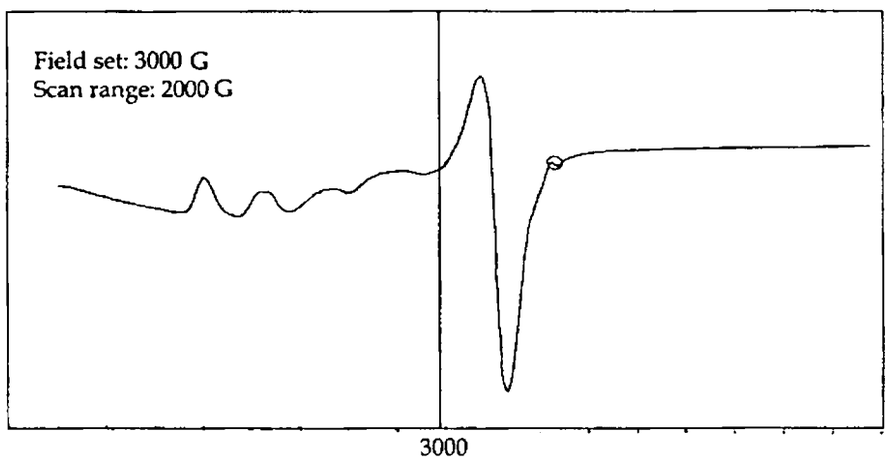

Figure 4.7 EPR spectrum of YCuICSCZ

Table 4.7
EPR Spectral data of YCuICSCZ

EPR parameter	YCuICSCZ
$g_{\|\|}$	2.40
$A_{\|\|}$	$170x10^{-4}$ cm^{-1}
$g_{\|\|}/A_{\|\|}$	141 cm
$g_{\perp}$	2.06
α^2	0.82

The YCoICSCZ complex was found to be EPR active. However the spectrum is very broad at LNT, which indicates that cobalt(II) is in the high spin state. Any further conclusion regarding the structure could not be arrived from the spectrum.

ZEOLITE ENCAPSULATED METAL COMPLEXES OF INDOLE-3-CARBOXALIDENE-3-AMINO-1,2,4-TRIAZOLE

5.1 Introduction

Aromatic nitrogen heterocyclices represent an important class of compounds which can act as ligands towards metal ions[211]. Triazoles are five-membered heterocyclic ligands containing three nitrogen donor atoms in its structure. They find wide applications in agriculture and industry[212,213], especially in photographic process, corrosion control and dye industry. 5-Amino-1,2,4-triazole is known to be a precursor of additives used in photography and for products with known anti corrosion properties[214,215]. 3-Amino-1,2,4-triazole is used in the synthesis of diazahemicyanine dyes[216].

Triazoles are versatile ligands and are known to form mononuclear, binuclear, trinuclear, pentanuclear or polynuclear complexes[217-219], and also complexes with chain or layer type structures depending on the nature of chelation of these ligands with the metal ion. It was therefore considered interesting to synthesise and characterize some zeolite encapsulated complexes of Schiff base derived from 1,2,4-triazole. This chapter deals with studies on zeolite encapsulated cobalt(II), nickel(II) and copper(II) complexes of the Schiff base, indole-3-carboxalidene-3-amino-1,2,4-triazole (Figure 5.1), formed by the condensation of indole-3-carboxalidehyde and 3-amino-1,2,4-triazole.

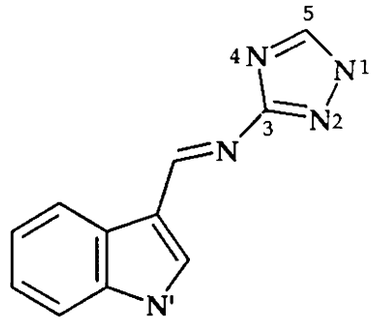

Figure 5.1 Structure of indole-3-carboxalidene-3-amino-1,2,4-triazole

5.2 Experimental

5.2.1 Materials

Details regarding the materials used, preparation of metal exchanged zeolites, and synthesis and purification of the ligand are given in Chapter 2.

5.2.2 Synthesis of zeolite encapsulated complexes of indole-3-carboxalidene-3-amino-1,2,4-triazole (ICAT)

The metal exchanged zeolite (5g) and excess of ICAT ligand (1.95g) were mixed well. This mixture was taken in a closed ampoule and was then heated at 100^{0}C for 16h to effect complexation. The resulting material was soxhlet extracted with ethanol to remove unreacted ligand and surface complexes. The soxhlet extraction was continued till the solution becomes colourless. The material was then stirred with 1.0 M sodium chloride solution to re-exchange the uncomplexed metal ions and was finally dried at 120^{0}C.

5.2.3 Analytical method

The details regarding various analytical and characterization techniques employed are given in Chapter 2.

5.3 Results and discussion

5.3.1 Chemical analysis

The analytical data of the zeolite encapsulated complexes are given in Table 5.1. The Si/Al ratio of 2.38-2.40 was same as that of the metal exchanged zeolites. So the probability of de-alumination can be ruled out. The presence of carbon is an indication of the presence of organic component in the zeolite cavities. The carbon percentage also indicate that the metal to ligand ratio in the complex is 1:2.

Table 5.1
Analytical data of encapsulated complexes

Sample	%Si	%Al	%Na	%Metal	%C
YCoICAT	24.40	10.20	7.2	0.85	3.34
YNiICAT	24.35	10.23	7.2	0.87	4.37
YCuICAT	24.35	10.14	6.8	1.98	7 .40

5.3.2 SEM analysis

As a representative case, SEM of YCuICAT before and after Soxhlet extraction was taken and the micrographs are presented in Figure 5.2. It is clear from the micrographs that the surface of the zeolite encapsulated copper complex after soxhlet extraction is more clean than that of the crude sample.

5.3.3 X-Ray diffraction analysis

XRD patterns of CuY and the encapsulated metal complexes of ICAT are given in Figure 5.3. It is clear from the XRD that the zeolite framework structure was not altered because of the encapsulation of the complexes within the supercages. The change in the peak intensity order of the 331, 311 and 220 reflections $I_{331} > I_{311} > I_{220}$ with respect to the intensity order of metal exchanged

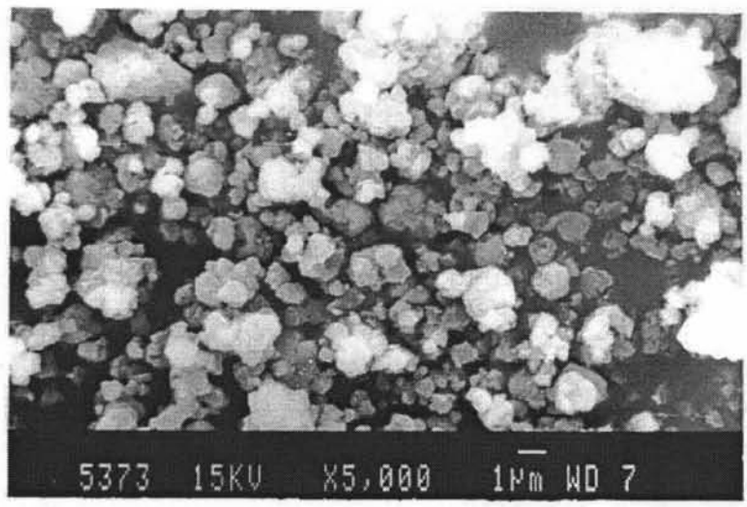

(i)

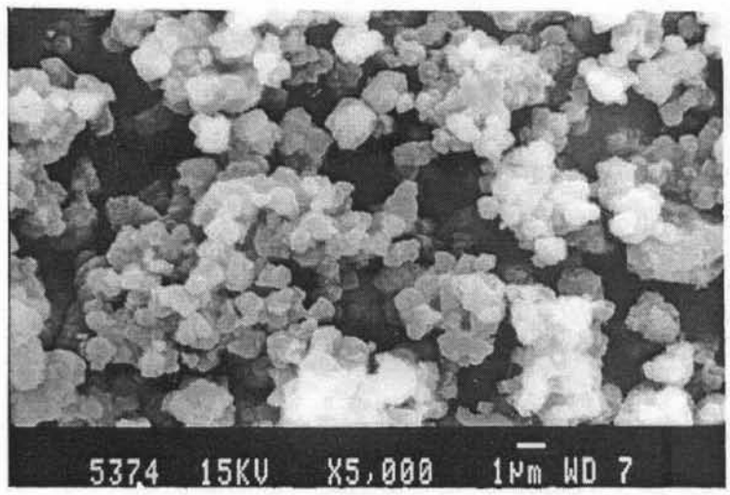

(ii)

Figure 5.2 Scanning Electron Micrograph of YCuICAT
(i) before and (ii) after soxhlet extraction

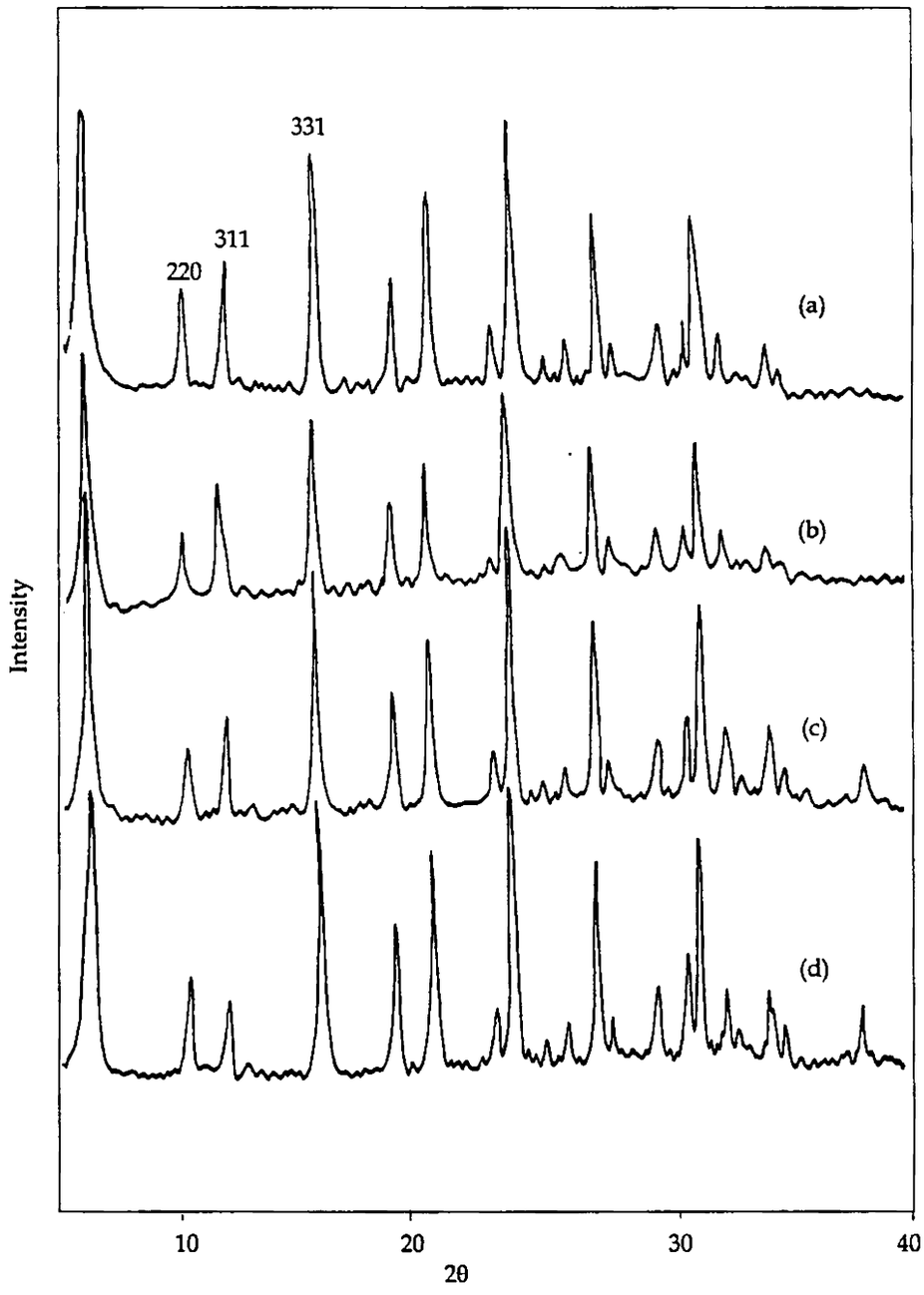

Figure 5.3 XRD Patterns of (a) YCoICAT (b) YNiICAT (c) YCuICAT (d) CuY

zeolite-Y (where it is in the order $I_{331} > I_{220} > I_{311}$) indicates cation redistribution during the complex formation within the zeolite supercages[49].

5.3.4 Surface area and pore volume

The surface area and pore volume of the zeolite encapsulated complexes were found to be decreasing drastically (Table 5. 2). The decrease can be attributed either to the loss of crystallinity of the zeolite or to the pore blocking. The X-ray patterns conclusively prove that there is no loss in crystalline nature of zeolite even after the encapsulation. So the decrease in surface area and pore volume can be attributed to the filling of the pore due to encapsulation.

Table 5. 2
Surface area and pore volume data of the zeolite encapsulated complexes

Metal ion	Surface area (m^2/gm)		Pore volume (cc/g)	
	MY	Complex Y	MY	Complex Y
Co	640	510	0.26	0.21
Ni	635	490	0.25	0.19
Cu	640	440	0.24	0.17

5.3.5 FTIR spectra

The IR spectrum of the ligand ICAT and the zeolite encapsulated complexes of cobalt, copper and nickel are given in Figure 5.4 and 5.4a respectively. The medium bands observed for the ligand in the region 3300-3200 cm^{-1} can be assigned to ν(N-H) modes[220]. The band observed at 1635 cm^{-1} in the spectrum of the ligand is due to ν(C=N) of the azomethine group. The ligand exhibit two more bands due to the ν(C=N) of the triazole ring, which appears at 1575 and 1520 cm^{-1} corresponds to the N1 and N4 of the triazole ring respectively[221].

The encapsulated complexes of the ligand ICAT exhibit a shift in the ν(C=N) of azomethine nitrogen. The peak at 1635 cm^{-1} of the ligand is shifted to 1620 cm^{-1} in the case of cobalt and nickel complexes where as the peak is shifted to 1622 cm^{-1} in the case of copper complex suggesting coordination of azomethine nitrogen to the metal. This band is seen to appear as shoulder band on the strong zeolite peak at 1645 cm^{-1}. Another peak at 1520 cm^{-1} of the ligand is found to be shifted to 1495 cm^{-1} for cobalt, 1500 cm^{-1} for nickel and 1507 cm^{-1} for cobalt complexes. This shows that the N4 of the triazole ring is also coordinated to the metal.

Table 5.3
IR Spectral data of MY, ICAT and zeolite complexes

MY	ICAT	YCoICAT	YNiICAT	YCuICAT
575		577	578	577
	638			
	788			
790		792	790	790
	1004			
1020		1022	1021	1020
	1125			
	1242			
	1333		1332	1330
	1442	1433	1432	1442
	1575	1576	1574	1577
	1520	1495	1500	1507
	1635	1620	1620	1622
1644		1639	1640	1647
	2930			
	3167			
3464		3453	3451	3450

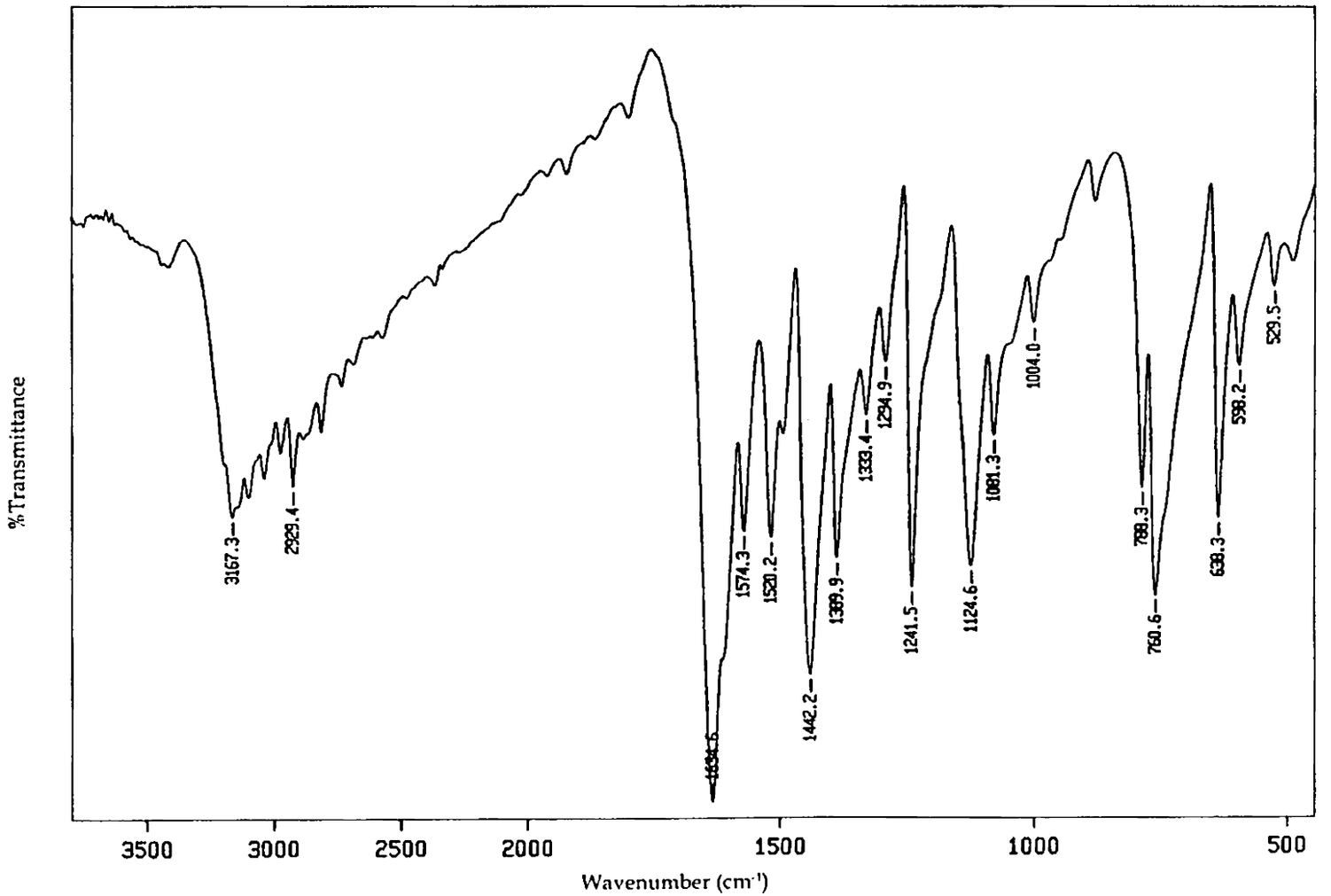

Figure 5.4 FTIR Spectrum of ICAT

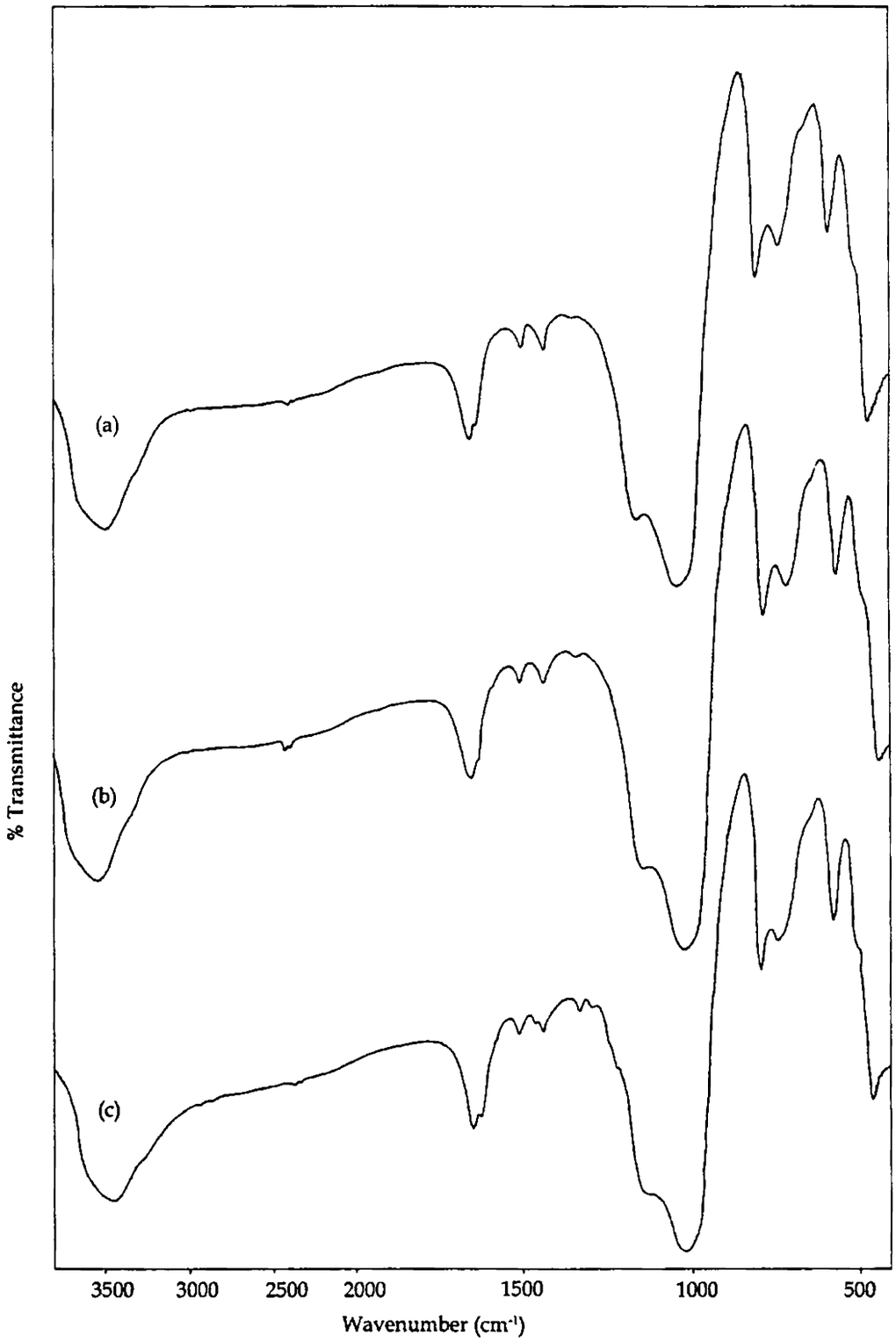

Figure 5.4a FTIR Spectra of (a) YCoICAT (b) YNiICAT (c) YCuICAT

5.3.6 TG analysis

TG/DTG data for the zeolite encapsulated complexes of ICAT are given in Table 5.4 and the TG and DTG are given in Figure 5.5 and 5.5a. All the complexes exhibit two stages of decomposition. The first stage is due to the loss of water molecule, and the second stage is due to the decomposition of encapsulated species. The much broader temperature range of the 2nd stage decomposition shows the difficulty in the combustion of the organic part, which is consequence of encapsulation of the complex[64].

Table 5.4

TG/DTG Data

Sample	Weight loss-Stage I			Weight loss-Stage II		
	Temp range(°C)	Peak temp (°C)	% Mass loss	Temp range(°C)	Peak temp (°C)	% Mass loss
YCoICAT	75-200	104	10.00	560-700	670	16.1
YNiICAT	70-200	106	10.10	545-700	640	15.5
YCuICAT	80-210	140	7.75	530-690	600	11.1

5.3.7 Electronic spectra

Electronic spectra of the zeolite complexes in the diffuse reflectance mode were taken and are presented in Figure 5.6 and the spectral data are given in Table 5.5

The analysis of the spectrum of the cobalt(II) complex reveals an octahedral geometry for the metal ion. Bands at 21360, 17610 and 11430 cm^{-1} could be attributed to the $^4T_{1g}(P) \leftarrow {}^4T_{1g}(F)$, $^4A_{2g}(F) \leftarrow {}^4T_{1g}(F)$ and $^4T_{2g}(F) \leftarrow {}^4T_{1g}(F)$ respectively.

The absorption maxima in the case of YNiICAT were at 24290, 17570 and 11415 cm^{-1}. These transitions are in agreement with those expected for an octahedral geometry.

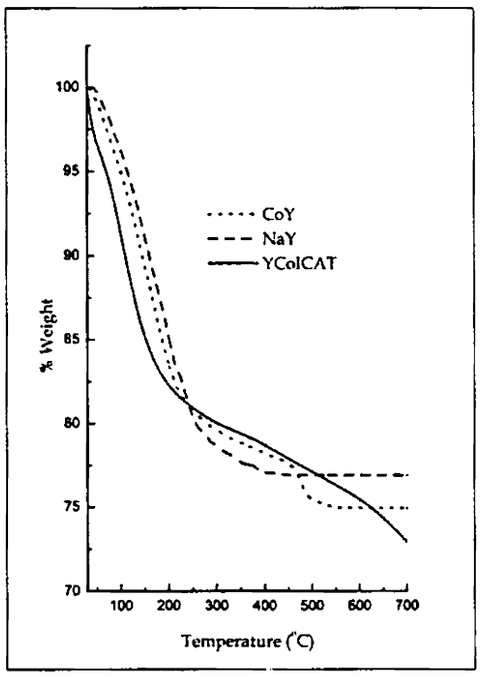

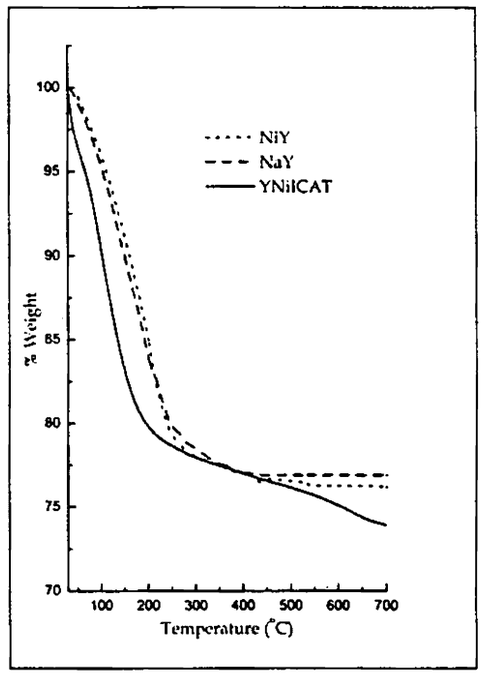

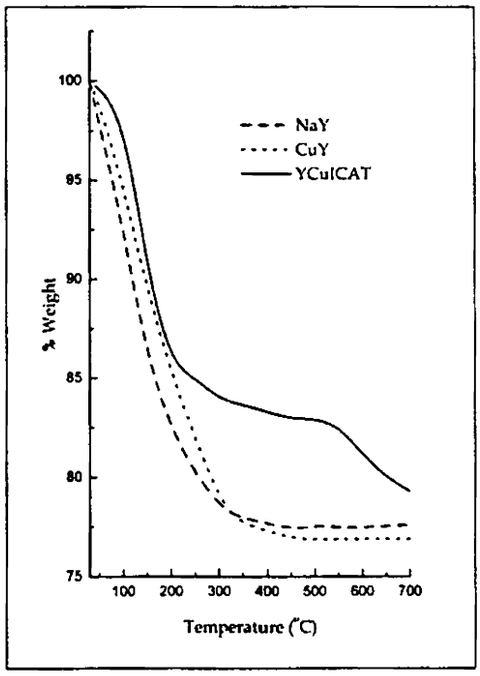

Figure 5.5

TG Patterns of MY, NaY and encapsulated complexes of ICAT

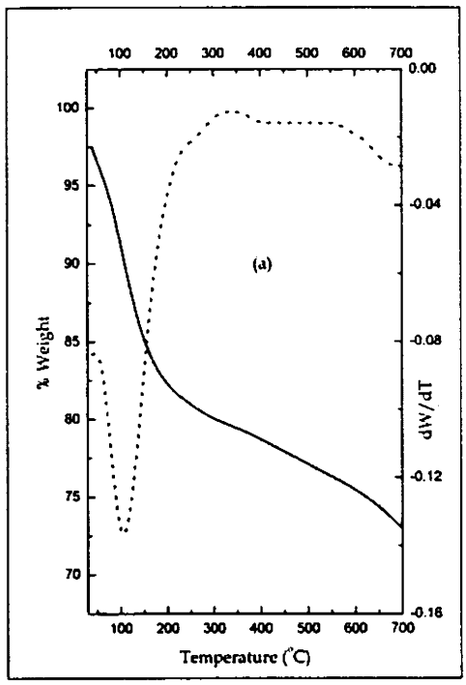

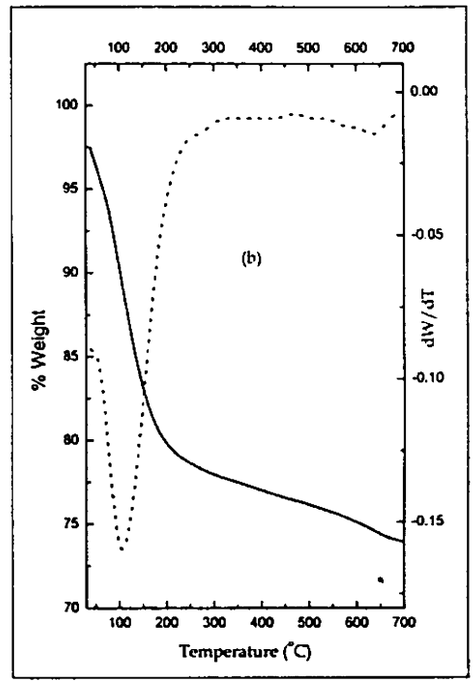

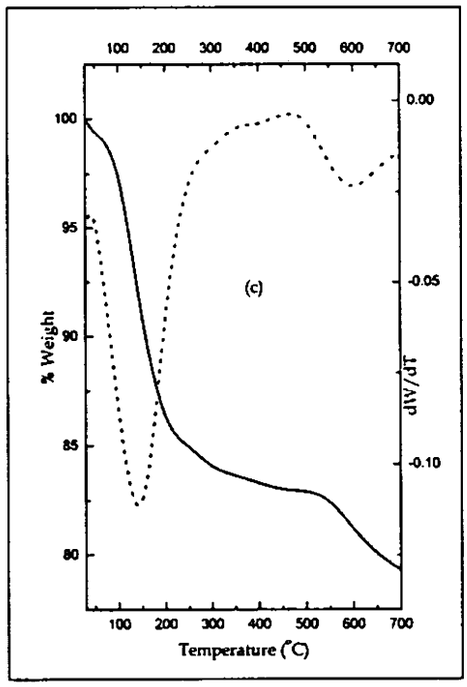

Figure 5.5a

TG/DTG patterns of
(a)YCoICAT (b) YNiICAT (c) YCuICAT

YCuICAT exhibit transitions at 21550, 17700 and 13330 cm^{-1}. These transitions can be assigned to $^2E \leftarrow {}^2B_2$ $^2B_1 \leftarrow {}^2B_2$ $^2A_1 \leftarrow {}^2B_2$, the transitions of pseudotetrahedral geometry. Tetrahedral copper(II) complex is invariably distorted to a near square planar geometry.

Table 5.5
Electronic spectral data

Sample	Absorbance Max.		Tentative assignments
	cm^{-1}	nm	
YCoICAT	11430	875	$^4T_{2g}(F) \leftarrow {}^4T_{1g}(F)$
	17610	570	$^4A_{2g}(F) \leftarrow {}^4T_{1g}(F)$
	21360	470	$^4T_{1g}(P) \leftarrow {}^4T_{1g}(F)$
	28670	350	Charge transfer
YNiICAT	11415	875	$^3T_{2g} \leftarrow {}^3A_{2g}$
	17570	570	$^3T_{1g}(F) \leftarrow {}^3A_{2g}$
	24290	410	$^3T_{1g}(P) \leftarrow {}^3A_{2g}$
YCuICAT	13330	750	$^2E \leftarrow {}^2B_2$
	17700	565	$^2B_1 \leftarrow {}^2B_2$
	21550	465	$^2A_1 \leftarrow {}^2B_2$
	28735	350	Charge transfer

5.3.8 Magnetic measurements

Magnetic moments of the complexes were calculated and the values along with the unit cell formula are presented in Table 5.6. The magnetic moment values of 4.9 BM and 3.2 BM were obtained for the cobalt and nickel complexes respectively, suggesting an octahedral geometry for the complexes. A magnetic moment value of 1.9 BM for the copper complex indicates square planar or flattened tetrahedral structure[200,210].

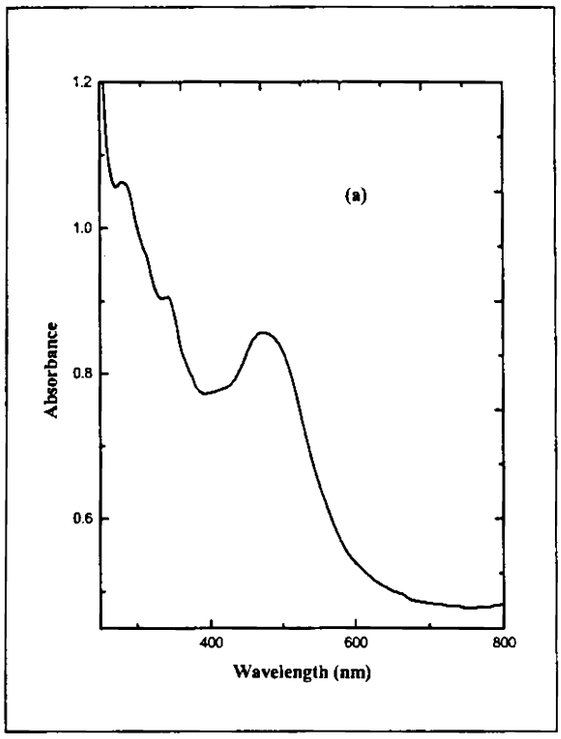

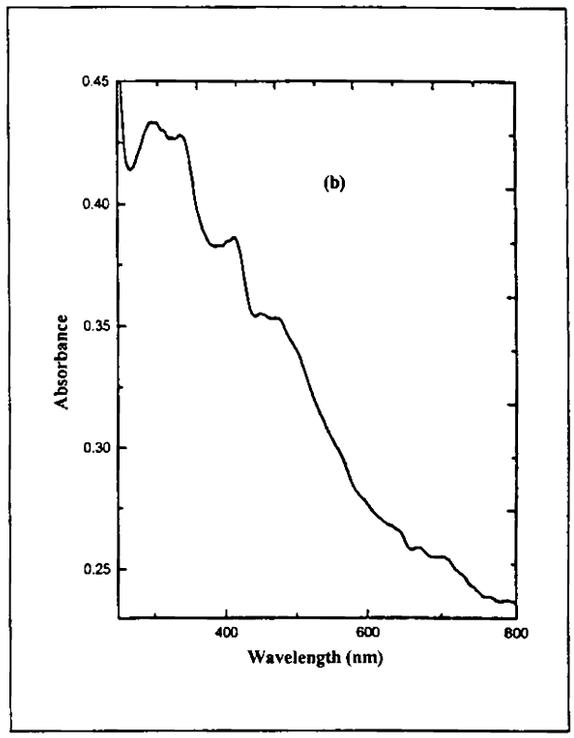

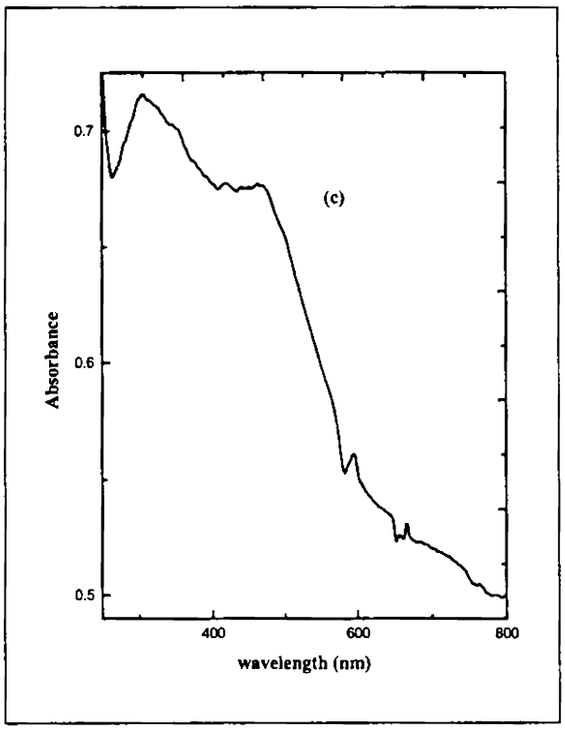

Figure 5.6

Electronic spectra of

(a) YCoICAT

(b) YNiICAT

(c) YCuICAT

Table 5.6
Magnetic moment data of the encapsulated ICAT complexes

Complexes	Magnetic moment (BM)	Unit Cell
YCoICAT	4.9	$Na_{51.75}Co_{2.13}(AlO_2)_{56}(SiO_2)_{136}nH_2O$
YNiICAT	3.2	$Na_{51.19}Ni_{2.40}(AlO_2)_{56}(SiO_2)_{136}nH_2O$
YCuICAT	1.9	$Na_{46.70}Cu_{4.64}(AlO_2)_{56}(SiO_2)_{136}nH_2O$

5.3.9 EPR spectra

EPR spectra of the complexes were recorded at liquid nitrogen temperature. The spectrum of YCoICAT was found to be very broad suggesting high spin octahedral nature of the complex. The EPR spectrum of YCuICAT is given in Figure 5.7. The hyperfine splitting is observed, which suggests coordination of nitrogen to the metal ion. High $g_{\parallel}/A_{\parallel}$ value was obtained for YCuICAT . Such higher values are reported[222-224] in the case of copper(II) complexes with flattened tetrahedral structures. For example $g_{\parallel}/A_{\parallel}$ value is 152 cm for the copper(II) complex of dipiperidylthiouramdisulphide, 154 cm for zinc dialkyl dithiophosphinate and 157 cm for bis(*N-tert*-butyl salicylaldiminato) copper(II) complex. All these complexes have flattened tetrahedral structures. Therefore, YCuICAT might also have a similar structure. Conclusion arrived from electronic spectral results are also in agreement with this observation.

Table 5.7
EPR Spectral data of YCuICAT

EPR Parameter	YCuICAT
$g_{\parallel}$	2.46
$A_{\parallel}$	$164x10^{-4}$ cm^{-1}
$g_{\parallel}/A_{\parallel}$	150 cm
$g_{\perp}$	2.09
α^2	0.99

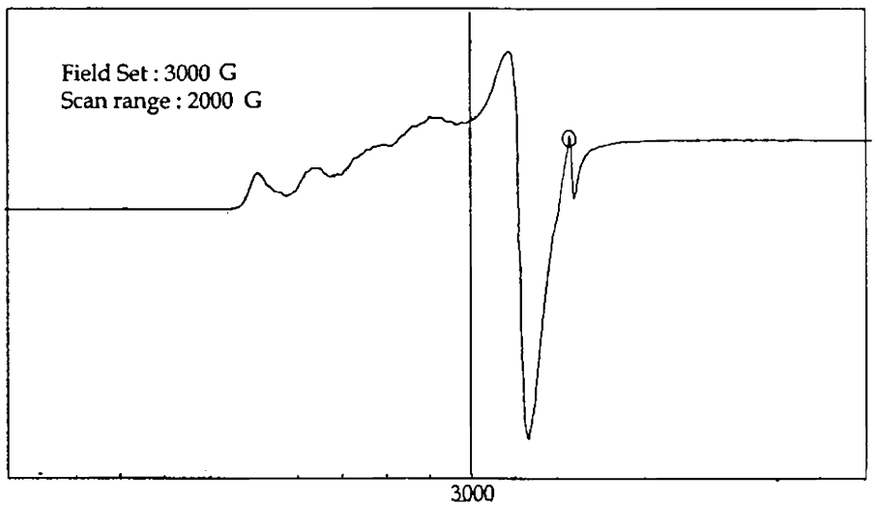

Figure 5.7 EPR spectrum of YCuICAT

ZEOLITE ENCAPSULATED METAL COMPLEXES OF *N,N'-bis* (4-HYDROXY-3-METHOXYBENZALIDENE) -*O*-PHENYLENEDIAMINE

6.1 Introduction

Vanillin (4-hydroxy-3-methoxybenzaldehyde) is a pleasant smelling aromatic compound, which is the principal flavoring constituent in vanilla beans. As a primary substitute for natural vanilla, vanillin is widely used as an ingredient in food and animal feeds. It serves as a food flavoring, a pharmaceutical intermediate and as a fragrance in perfumes and odour-masking products. A large number of complexes of Schiff bases derived from vanillin was reported[225-231]. However, reports on zeolite encapsulated complexes of Schiff bases derived from vanillin are scanty. It was thought worthwhile to study the changes in the structure and properties of such complexes on encapsulation. We have synthesized and characterized zeolite encapsulated cobalt(II), nickel(II) and copper(II) complexes of the Schiff base derived from the condensation of vanillin and *o*-phenylenediamine (Figure 6.1). The details of these studies are presented in this chapter.

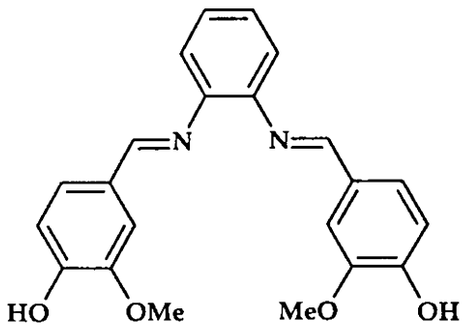

Figure 6.1 Structure of N,N'-*bis* (4-hydroxy-3-methoxybenzalidene)-*o*-phenylenediamine (VOPD)

6.2 Experimental

6.2.1 Materials

The procedural details regarding the preparation of metal exchanged zeolite are given in Chapter 2. The metal exchanged zeolites are used for preparation of encapsulated metal complexes.

6.2.2 Synthesis of zeolite encapsulated complexes of *N,N'*-bis (4-hydroxy-3-methoxybenzalidene)-*o*-phenylenediamine (VOPD)

Zeolite encapsulated complexes of the Schiff base *N,N'*-bis (4-hydroxy-3-methoxybenzalidene)-*o*-phenylenediamine (VOPD), were prepared by making use of intrazeolite synthesis by complexation method. The metal exchanged zeolite (5g) was mixed with excess of VOPD ligand (1.75g), and was heated at 160°C in a closed ampoule for 16 h for complexation. After complexation the material was Soxhlet extracted with chloroform and then with ethanol to remove the free ligand and the complexes formed on the surfaces of zeolite. The zeolite encapsulated complexes thus purified by soxhlet extraction was then stirred with 1.0M sodium chloride solution to re-exchange the uncomplexed metal ion. The complexes were finally dried at 120°C and kept over anhydrous calcium chloride in a desiccator.

6.2.3 Analytical method

Details regarding the various analytical and characterization techniques used are given in Chapter 2.

6.3 Results and discussion

6.3.1 Chemical analysis

The analytical data of the zeolite encapsulated complexes are given in Table 6.1. The possibility of loss in crystallinity of the zeolite Y due to dealumination can be ruled out, as the Si/Al ratio of 2.37-2.40 for the complex was same as that of the metal exchanged zeolites. The percentage carbon indicate a ligand to metal ratio of 1:1 for the complexes.

Table 6.1
Analytical data of encapsulated complexes

Sample	%Si	%Al	%Na	%Metal	%C
YCoVOPD	24.31	10.22	7.0	0.79	3.20
YNiVOPD	24.60	10.25	7.1	0.59	2.55
YCuVOPD	24.23	10.11	6.9	1.21	5.01

6.3.2 SEM analysis

The scanning electron microscope of YCuVOPD complexes were taken before and after soxhlet extraction and are given in Figure 6.2. From the micrographs it can be seen that soxhlet extraction removed all the surface adsorbed complexes. The average particle size of 1 μm is maintained even after the encapsulation.

6.3.3 X-ray diffraction analysis

XRD patterns of CuY, YCuVOPD, YNiVOPD and YCuVOPD are given in Figure 6.3. These patterns are very much identical to that of CuY. This confirms that the framework structure remains intact during the synthesis of the complexes within the supercages. The changes in the peak intensities of the 331, 311, and 220, reflections reveal the cation redistribution that take place during the complex formation within the zeolite cavities[49].

6.3.4 Surface area and pore volume

Surface area and pore volume of the zeolite encapsulated complexes were determined using nitrogen adsorption at liquid nitrogen temperature. The surface area and pore volume were found to be decreased (Table 6.2). This decrease can be attributed to the pore blocking of zeolite due to encapsulation.

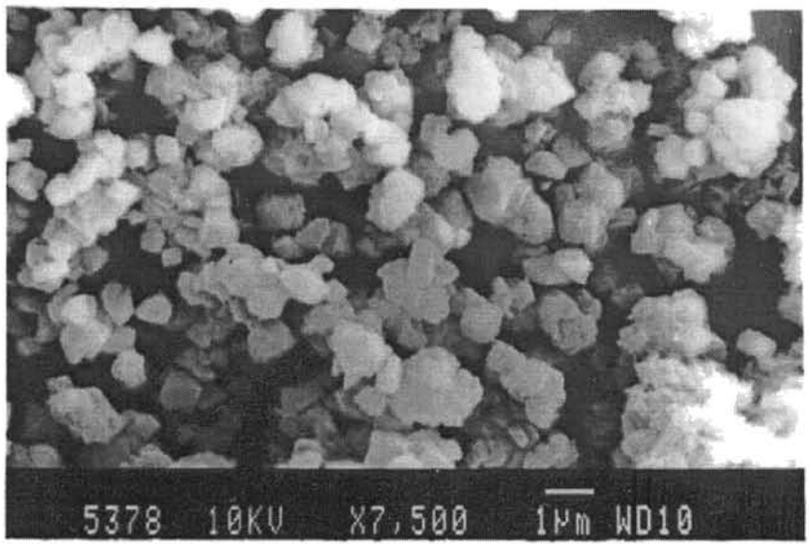

(i)

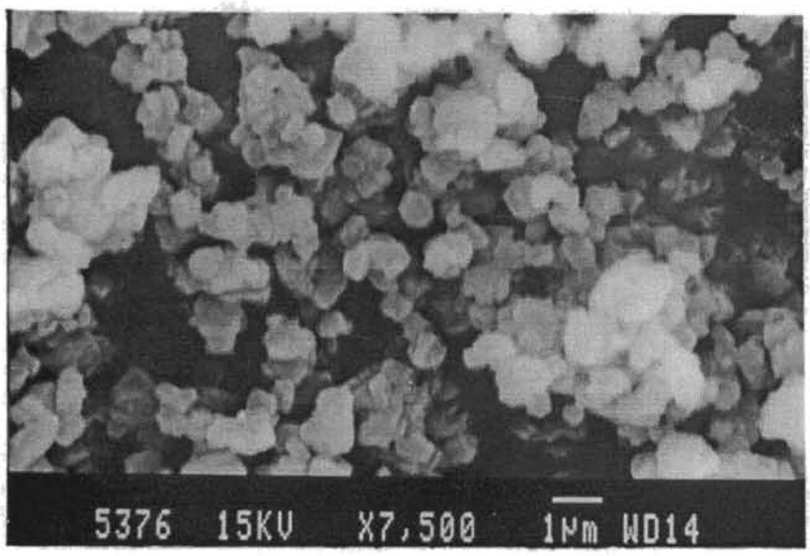

(ii)

Figure 6.2 Scanning Electron Micrograph of VOPD
(i) before and (ii) after soxhlet extraction

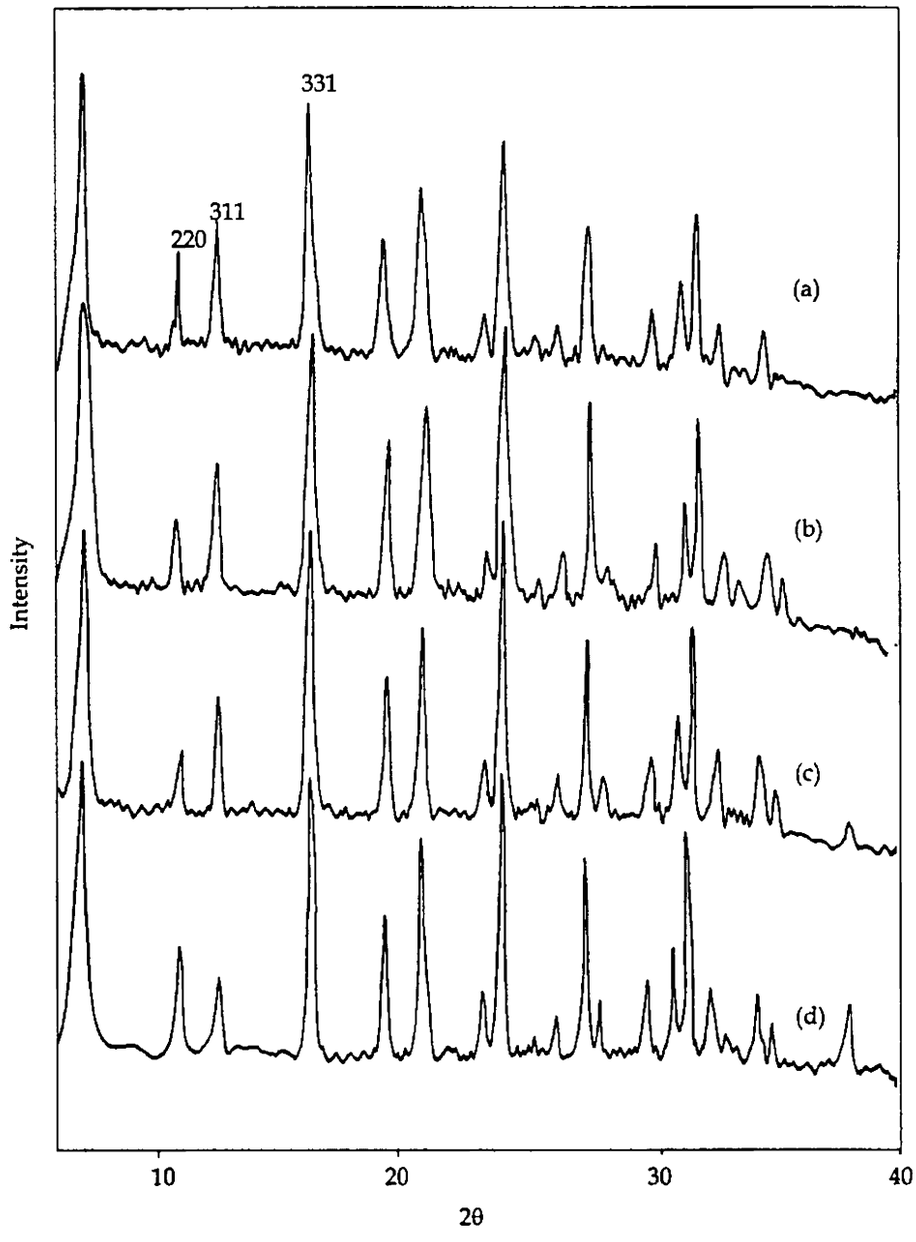

Figure 6.3 XRD Patterns of (a) YCoVOPD (b) YNiVOPD (c) YCuVOPD (d) CuY

Table 6.2
Surface area and pore volume data of the zeolite encapsulated complexes

Metal ion	Surface area (m^2/gm)		Pore volume (cc/g)	
	MY	Complex Y	MY	Complex Y
Co	640	450	0.26	0.20
Ni	635	460	0.25	0.21
Cu	640	420	0.24	0.18

6.3.5 FTIR spectra

FTIR Spectra of the ligand VOPD and the zeolite encapsulated cobalt, nickel and copper complexes of VOPD are given in Figure 6.4 and 6.4a respectively. The broad band between 3300-3390 cm^{-1} can be assigned to the -O-H stretching of the ligand[232]. The azomethine stretching vibration is seen at 1600 cm^{-1}. The peak at 1035 cm^{-1} can be attributed to νC-N of the ligand.

In the spectra of zeolite encapsulated complexes, the peak at 1600 cm^{-1} due to azomethine nitrogen of the ligand is found to be shifted to 1513 cm^{-1} in the case of YCoVOPD and 1518 cm^{-1} in the case of nickel(II) and copper(II) complexes that the coordination is taking place through the azomethine nitrogen. The peak due to νC-N is not visible in the zeolite encapsulated VOPD complexes since they are obscured by the broad zeolite band around 1000 cm^{-1}. Some other peaks of the ligand can be seen in the zeolite encapsulated complexes in the region where the peaks due to zeolite are absent. This can be considered as an indication of the complexes inside the zeolite cavities.

Table 6.3
IR Spectral data of MY, VOPD and zeolite complexes

MY	VOPD	YCoVOPD	YNiVOPD	YCuVOPD
	553			
575		573	574	578
	586			
	645			
	735	725	728	725
790		788	793	787
	815			
	868			
	910			
1020		1018	1020	1020
	1035			
	1125			
	1270	1272	1270	1274
	1370	1368	1367	
	1395	1394		1394
	1435			
	1457	1453	1462	1460
	1495	1500	1500	
	1560	1513	1518	1518
1640		1635	1635	1637
	1876			
	1920			
	2995	2993	2994	2994
	3380			
3464		3470	3468	3465

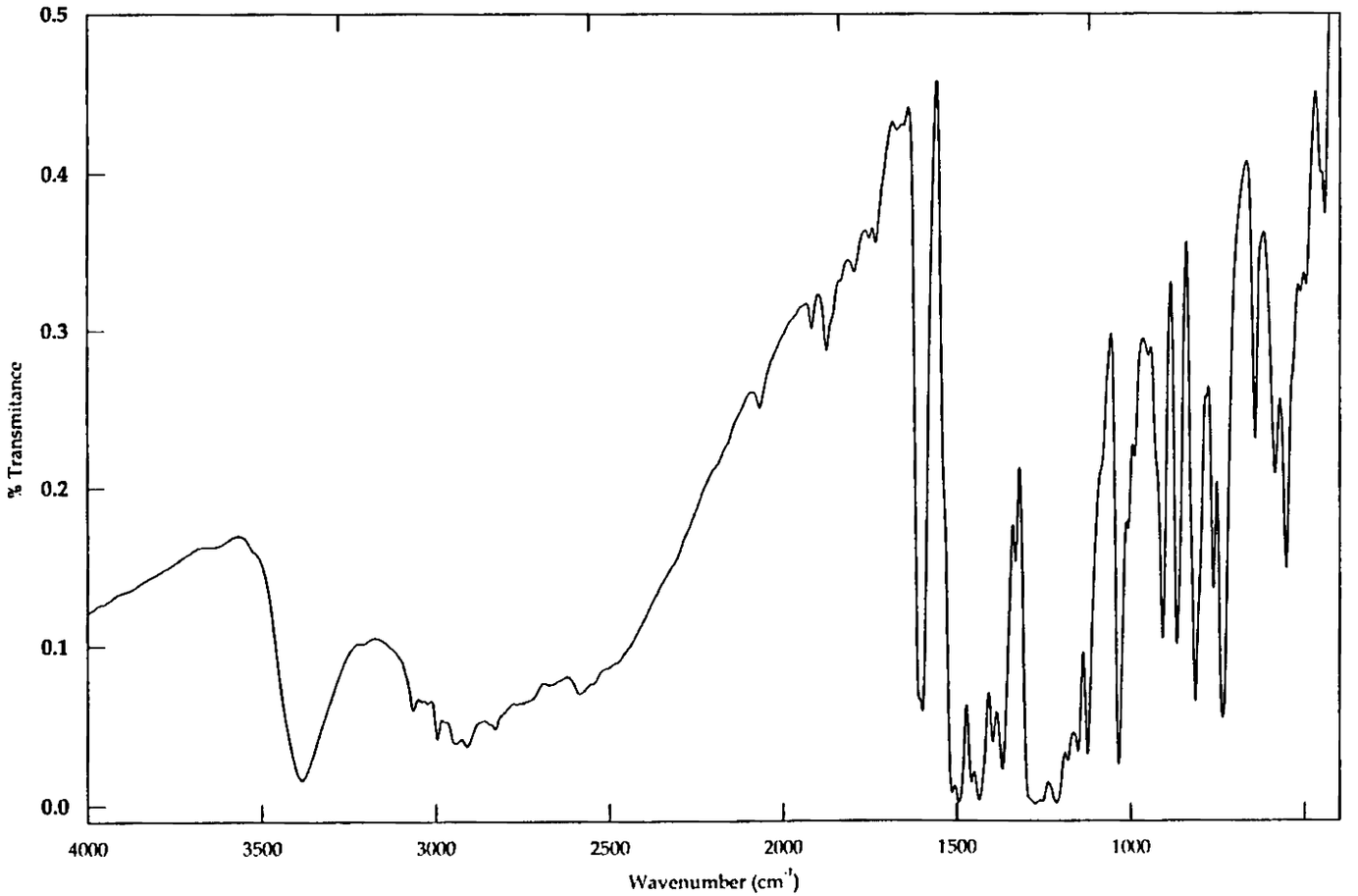

Figure 6.4 FTIR of VOPD

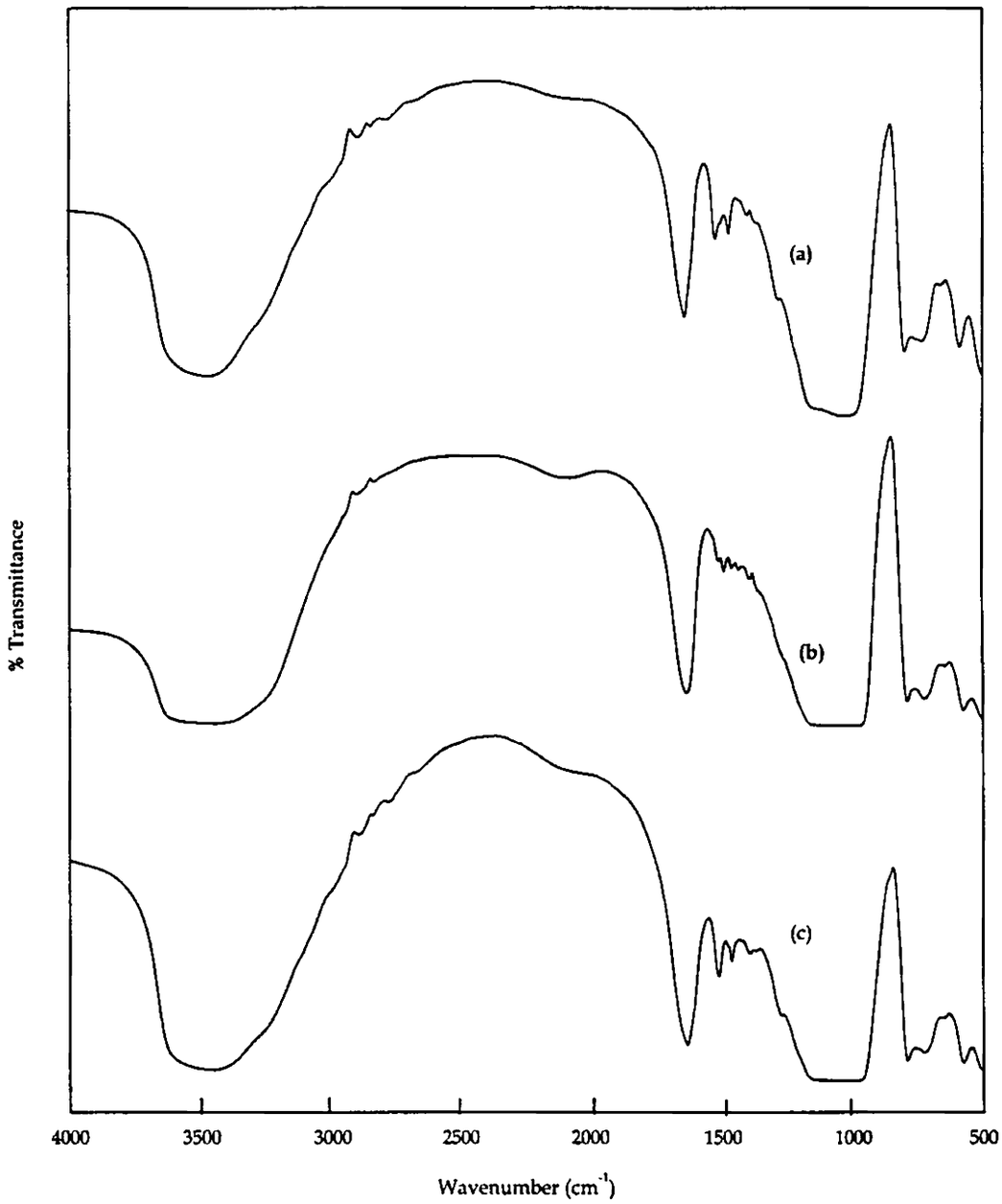

Figure 6.4a FTIR spectra of (a)YCoVOPD (b) YNiVOPD (c) YCuVOPD

6.3.6 TG analysis

TG/DTG curves of zeolite encapsulated VOPD complexes are shown in Figure 6.5 and 6.5a respectively. The removal of free moisture from zeolite samples was seen as the first stage of weight loss in TG curves. The decomposition of encapsulated complexes is clearly visible in second stage decomposition in the case of Ni(II) and Cu(II) complexes. However, this weight loss is not well defined for the cobalt complex. The TG/DTG data is tabulated in Table 6.4.

Table 6.4

TG/DTG data

Sample	Weight loss:Stage I			Weight loss:Stage II		
	Temp range(^{0}C)	Peak temp (^{0}C)	% Mass loss	Temp range(^{0}C)	Peak temp (^{0}C)	% Mass loss
YCoVOPD	55-170	95	8.0			
YNiVOPD	55-170	91	5.6	480-630	545	12.8
YCuVOPD	60-165	91	5.5	355-525	410	12.5

6.3.7 Electronic spectra

Electronic spectra of the zeolite complexes in the diffuse reflectance mode were taken and are given in Figure 6.6 and the absorbance and tentative assignments are given in Table 6.5. The interpretation of these data gives an idea of the structure of the metal complexes.

The cobalt complex, YCoVOPD, exhibits bands at 11755 cm^{-1}, 17460 cm^{-1} and 22820 cm^{-1}, which can be assigned to $^4T_{2g}(F) \leftarrow ^4T_{1g}(F)$, $^4A_{2g}(F) \leftarrow ^4T_{1g}(F)$, $^4T_{1g}(P) \leftarrow ^4T_{1g}(F)$ transitions respectively. These transitions indicate an octahedral geometry around cobalt(II) ion. The intense band observed at 31065 cm^{-1} can be assigned to charge transfer transitions.

The Ni(II) complex, YNiVOPD, exhibits bands at 13515 cm^{-1}, 21415 cm^{-1} and 29850 cm^{-1}. These bands can be assigned to the transitions $^3T_{2g} \leftarrow ^3A_{2g}(F)$,

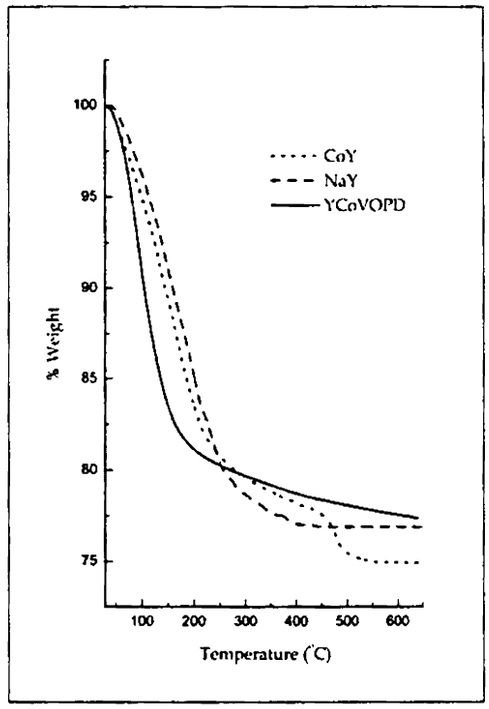

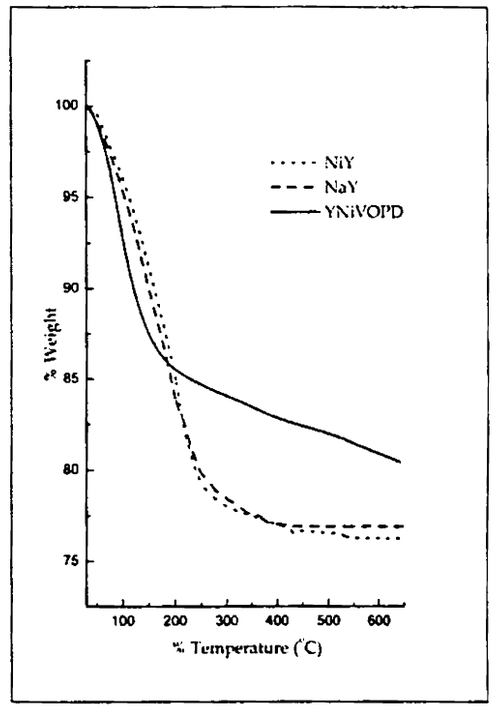

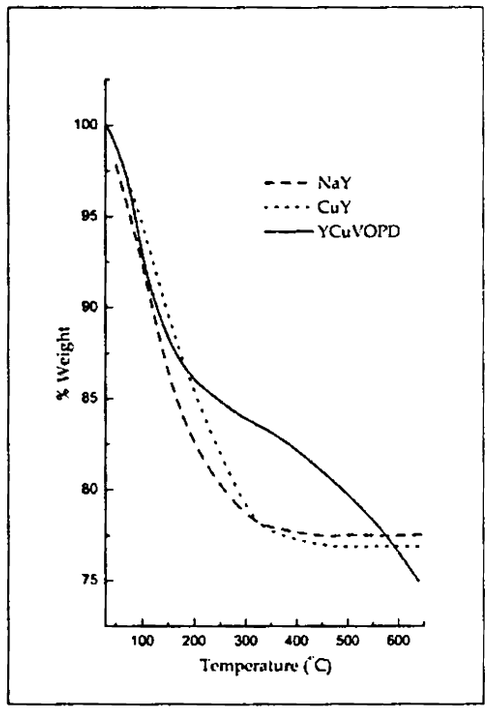

Figure 6.5

TG plots of MY, NaY and encapsulated complexed of VOPD

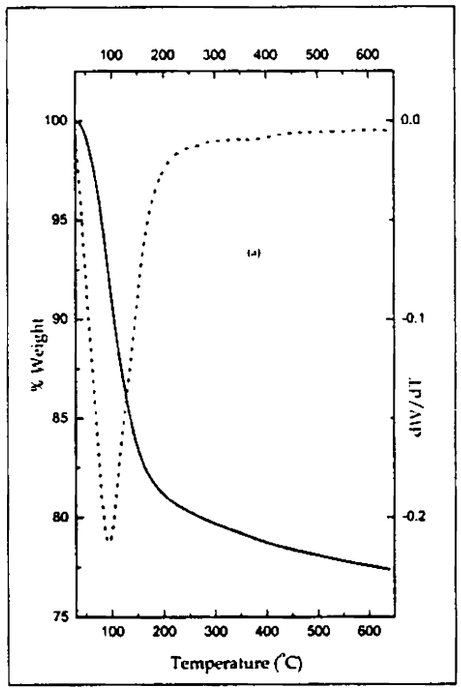

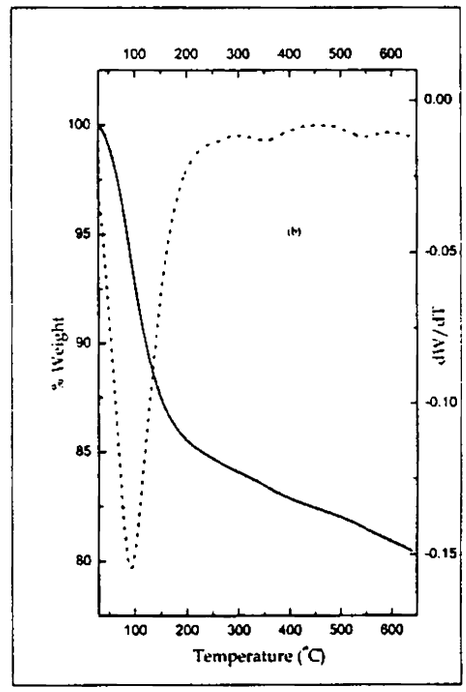

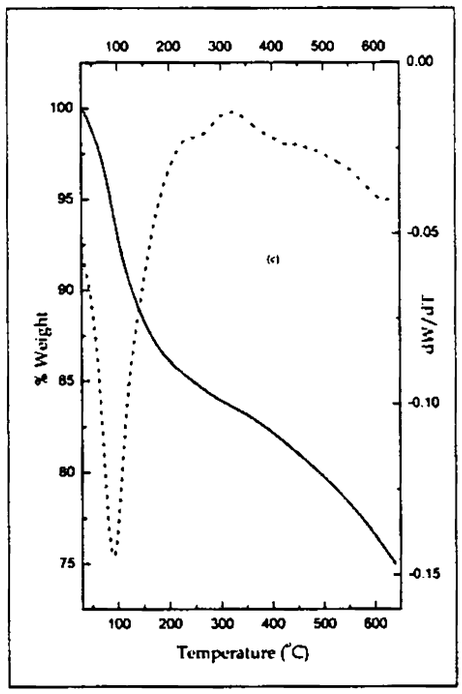

Figure 6.5a

TG/DTG Plots of
(a)YCoVOPD (b) YNiVOPD (c) YCuVOPD

$^3T_{1g}(F) \leftarrow ^3A_{2g}(F)$ and $^3T_{1g}(P) \leftarrow ^3A_{2g}(F)$ respectively, which are in accordance with a Ni(II) complex having an octahedral geometry[201].

Bands are observed at 14970 cm^{-1} and 12500 cm^{-1} for the copper(II) complex, YCuVOPD. The values and positions of the bands point to a somewhat distorted octahedral geometry[201].

Table 6.5
Electronic spectral data

Sample	Absorbance Max.		Tentative assignments
	cm^{-1}	Nm	
YCoVOPD	11755	850	$^4T_{2g}(F) \leftarrow ^4T_{1g}(F)$
	17460	570	$^4A_{2g}(F) \leftarrow ^4T_{1g}(F)$
	22820	440	$^4T_{1g}(P) \leftarrow ^4T_{1g}(F)$
	31065	320	Charge transfer
YNiVOPD	13515	740	$^3T_{2g} \leftarrow ^3A_{2g}$
	21415	465	$^3T_{1g}(F) \leftarrow ^3A_{2g}$
	29850	335	$^3T_{1g}(P) \leftarrow ^3A_{2g}$
YCuVOPD	14970	670	d-d transition
	22675	440	Charge transfer
	29585	340	Intraligand transition

6.3.8 Magnetic measurements

Room temperature magnetic moments of VOPD complexes are given in Table 6.6. Magnetic moment value of 4.80 BM observed for YCoVOPD agrees with that of octahedral Co(II) complexes. The nickel(II) complex, YNiVOPD exhibits a magnetic moment of 3.18 indicating an octahedral geometry for the complex.

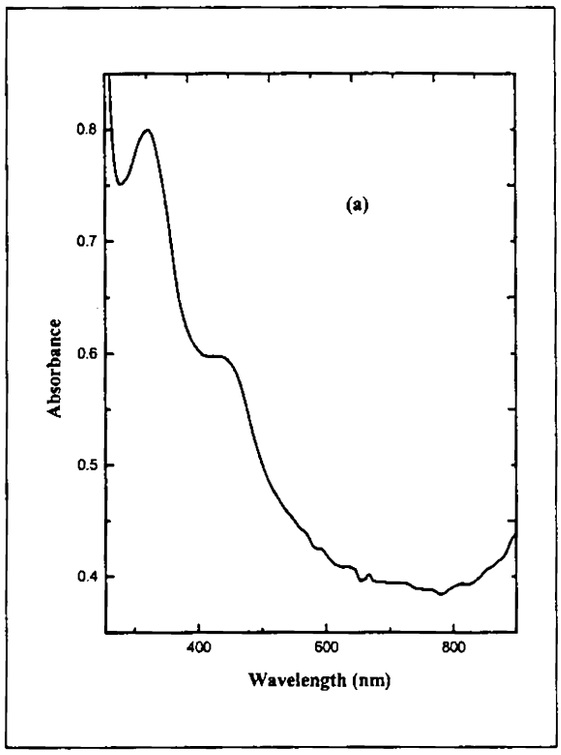

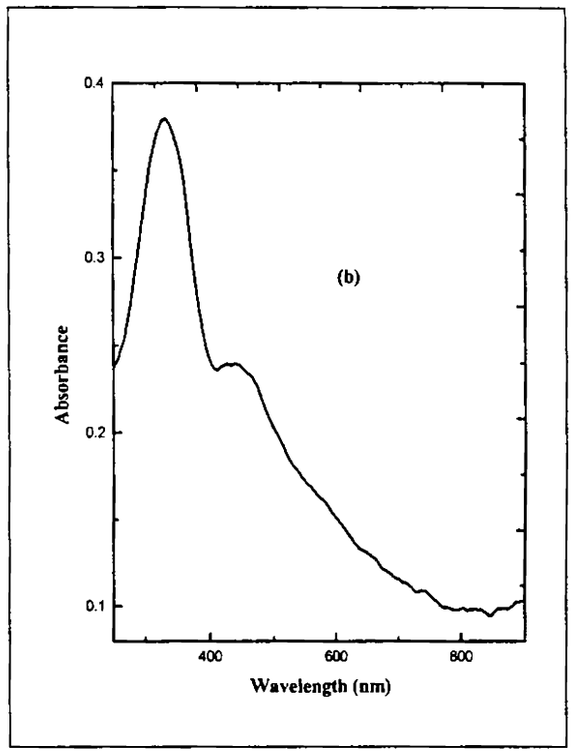

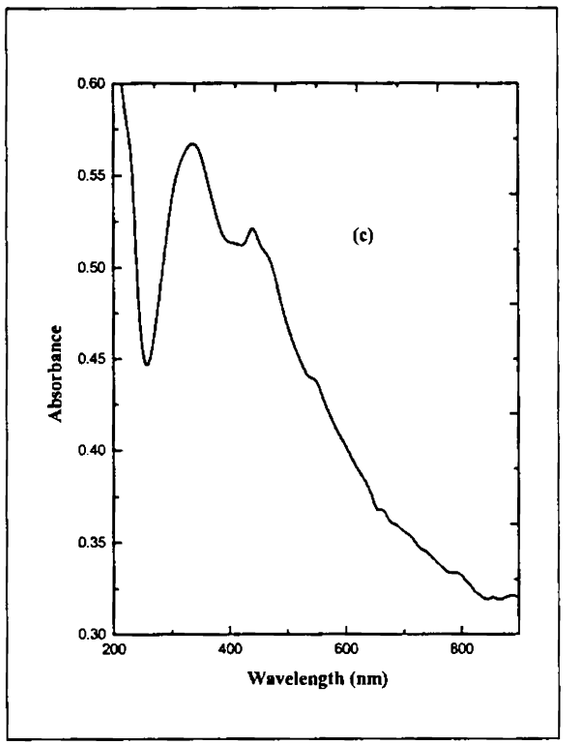

Figure 6.6

Electronic spectra of

(a) YCoVOPD

(b) YNiVOPD

(c) YCuVOPD

Magnetic moment of 1.82 BM was observed for the encapsulated copper(II) complex[200,210].

Table 6.6
Magnetic moment data of the encapsulated VOPD complexes

Complexes	Magnetic moment (BM)	Unit Cell
YCoVOPD	4.80	$Na_{52.03}Co_{2.00}(AlO_2)_{56}(SiO_2)_{136}nH_2O$
YNiVOPD	3.18	$Na_{53.03}Ni_{1.48}(AlO_2)_{56}(SiO_2)_{136}nH_2O$
YCuVOPD	1.82	$Na_{50.03}Cu_{2.85}(AlO_2)_{56}(SiO_2)_{136}nH_2O$

6.3.9 EPR spectra

The EPR spectrum of YCuVOPD recorded at liquid nitrogen temperature is given in Figure 6.7. The ratio of $g_{\parallel}/A_{\parallel}$ increases markedly on the introduction of tetrahedral distortion to the chromophore. For the complex with tetrahedral distortion $[Cu(ta)_4]^{2+}$ (*ta* = *thioacetamide*) the $g_{\parallel}/A_{\parallel}$ is 247 cm and for Cu^{2+} doped into the tetramethylthiouram disulphide lattice the $g_{\parallel}/A_{\parallel}$ is 247 cm[233]. The high $g_{\parallel}/A_{\parallel}$ value of 223 cm observed for YCuVOPD suggest a tetrahedrally distorted square planar sturucture.

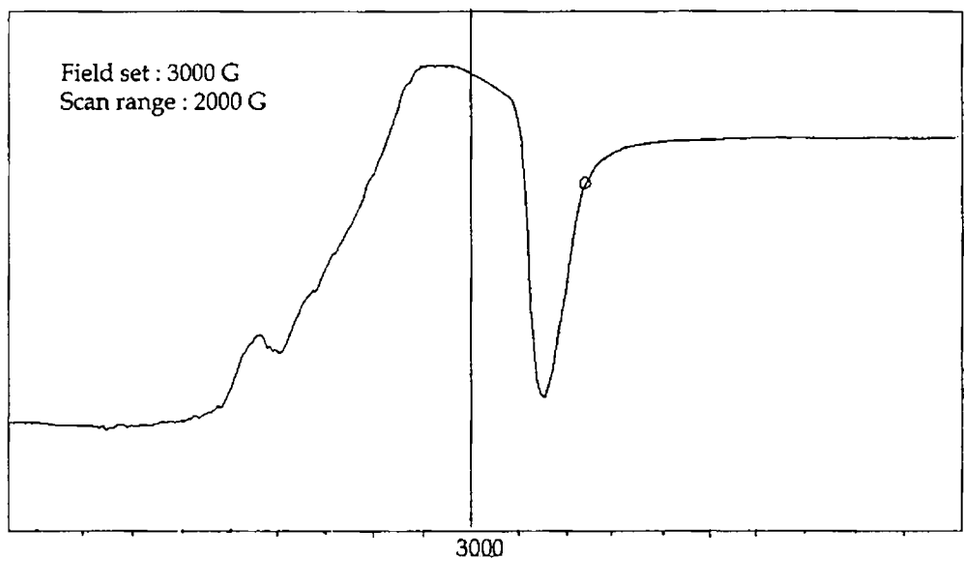

Figure 3.7 EPR spectrum of YCuVOPD

Table 6.7
EPR spectral data of YCuVOPD

EPR Parameter	YCuVOPD
$g_{\parallel}$	2.40
$A_{\parallel}$	107×10^{-4} cm^{-1}
$g_{\parallel}/A_{\parallel}$	223 cm
$g_{\perp}$	2.09
α^2	0.77

The cobalt complex shows a broad EPR pattern suggesting a high spin octahedral structure for the complex.

ZEOLITE ENCAPSULATED METAL COMPLEXES OF CURCUMIN

7.1 Introduction

Curcumin, (1,7-*bis*(4-hydroxy-3-methyoxyphenyl)-1,6-heptadiene-3,5-dione) is the main active ingredient found in the food spice turmeric, an everyday spice in India that has been used for centuries. Curcumin (Figure 7.1) give turmeric, its distinctive, mild flavor and yellow colour. Curcumin exhibits a variety of biological and photochemical activity, including phototoxicity to bacteria[234]. Curcuminoids were demonstrated to be cytotoxic against human ovarian cancer OVCAR-3 cells[235]. It was reported to be a free radical scavenger[236], and also shows anti-oxidant and anti-inflammatory properties[237]. Now Researchers are trying to use curcumin against HIV and Alzheimer's disease[238,239]. Transition metal complexes of curcumin with the metals, copper(II) and nickel(II) were studied by Hartung *et. al.*[240]. There are no reports of zeolite encapsulated curcumin complexes. This chapter deals with the synthesis and characterization of Y zeolite encapsulated complexes of copper and nickel using curcumin as the ligand.

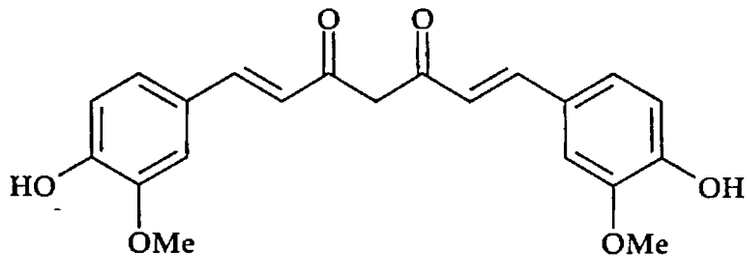

Figure 7.1 Structure of curcumin (Cur)

7.2 Experimental

7.2.1 Materials

The details regarding the preparation of metal exchanged zeolite is given in Chapter 2.

7.2.2 Synthesis of zeolite encapsulated complexes of curcumin (Cur)

Zeolite encapsulated complexes of curcumin (Cur) was prepared by making use of intrazeolite synthesis by complexation method. The metal exchanged zeolite (5g) mixed with excess of curcumin ligand (3.5g), was heated at 150^{0}C in a closed ampoule for 16 h for complexation. After complexation the material was soxhlet extracted with chloroform and then with methanol to remove the free ligand and the complexes formed on the surface of zeolite. The zeolite encapsulated complex thus purified by soxhlet extraction was then stirred with 1.0M sodium chloride solution to re-exchange the uncomplexed metal ion and was finally dried at 120^{0}C.

7.2.3 Analytical methods

Details regarding the various analytical and characterization techniques used are given in Chapter 2.

7.3 Results and discussion

Zeolite encapsulated curcumin complexes of copper(II) and nickel(II) were synthesized. Attempts to synthesize the cobalt(II) complex were unsuccessful. The red coloured compound formed by heating the mixture of CoY and curcumin at 150^{0}C, was found to leach out of the zeolite cage during soxhlet extraction with chloroform. Probably the labile nature of the cobalt(II) complexes might be the reason for the instability of the encapsulated complex.

7.3.1 Chemical analysis

The analytical data of zeolite encapsulated curcumin complexes are presented in Table 7.1. The analytical data reveal that Si/Al ratio of metal exchanged zeolite (~2.40) remains unchanged in the zeolite encapsulated

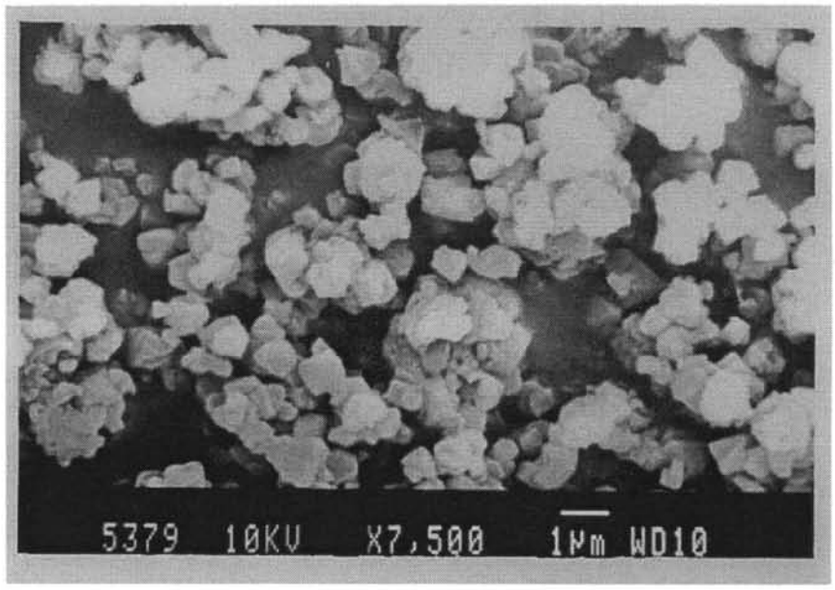

(i)

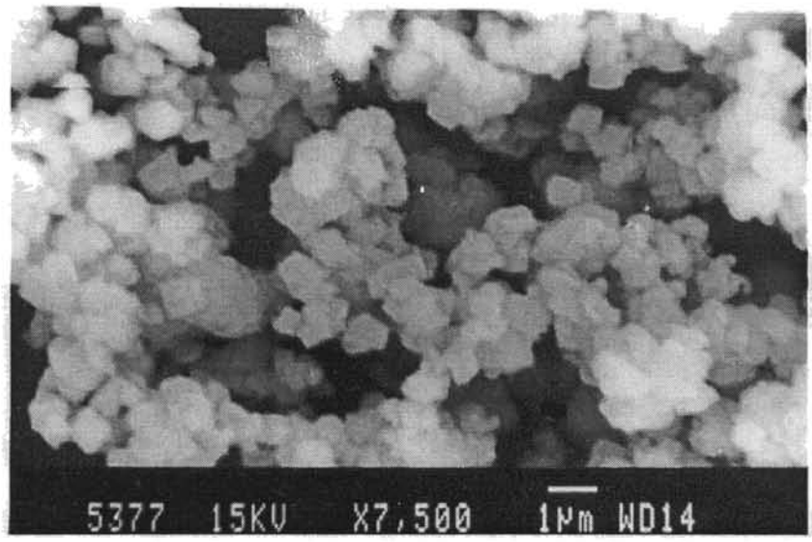

(ii)

Figure 7.2 Scanning Electron Micgrographs of YCuCur
(i) before (ii) after soxhlet extraction

complexes indicating the capability of zeolite structure to withstand encapsulation conditions. Percentage of carbon indicates ligand to metal ratio of 2:1 for the encapsulated complex.

Table 7.1
Analytical data of encapsulated complexes

Sample	%Si	%Al	%Na	%Metal	%C
YNiCur	24.24	10.13	6.65	1.22	8.60
YCuCur	24.38	10.15	6.80	0.75	5.64

7.3.2 SEM analysis

The scanning electron micrograph of YCuCur complex before and after purification is given in Figure 7.2. It can be seen that the surface is clean and the surface adsorbed species is removed as a result of soxhlet extraction. The morphology of the parent NaY is seen to be retained for the zeolite encapsulated complex.

7.3.3 X-ray diffraction analysis

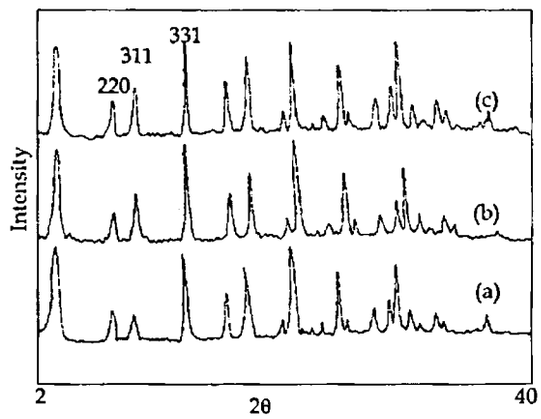

Figure 7.3 XRD Patterns of (a) CuY, (b) YNiCur (c) YCuCur

XRD Patterns of CuY, YCNiCur and YCuCur are given in Figure 7.3. These patterns are very much identical to those of metal exchanged zeolite which implies that the framework structure remains uncollapsed during the synthesis. Moreover the changes in characteristic peak intensities after encapsulation confirm the cation redistribution due to encapsulation of complex in the zeolite cavities[49].

7.3.4 Surface area and pore volume

Surface area and pore volume data are given in Table 7.2. These values are lower than those of the corresponding metal exchanged zeolite. The decrease can be attributed to the effect of the encapsulation of complexes in the pores.

Table 7.2
Surface area and pore volume data of the zeolite encapsulated complexes

Metal ion	Surface area (m^2/gm)		Pore volume (cc/g)	
	MY	Complex Y	MY	Complex Y
Ni	635	450	0.25	0.1890
Cu	640	385	0.24	0.1850

7.3.5 FTIR spectra

IR spectrum of curcumin and its zeolite encapsulated complexes of copper and nickel are given in Figure 7.4. β-Diketones usually exist as mixture of tautomeric keto and enol forms. The enolic form does not show the normal absorption of conjugated ketones. Instead, a broad band appears in the 1640-1580 cm^{-1} region[232]. The keto form and small amount of unbonded enolic form of the compound may be responsible for the two bands observed at 1629 cm^{-1} and 1600 cm^{-1}. The broad band at 3400 cm^{-1} can be assigned to the enolic -O - H stretching absorption.

In complexes, usually the bands due to -C=O stretching should be shifted to lower frequencies during complexation. But the shift in frequency could not be clearly seen in the spectra of zeolite complexes as this band is masked by the

zeolite bands. The peak at 1600 cm^{-1} is found to be shifted to 1558 cm^{-1} in the case of nickel complexes and in the case of the copper complex this band is shifted to 1575 cm^{-1} suggesting coordination of C=O group in both the complexes. The bands in the region 1400 to 1500 cm^{-1} is due to the curcumin ligand. The presence of these bands reveal complex formation inside the zeolite cages. The spectral details are summarized in Table 7.3.

Table 7.3
IR spectral data of MY, Cur and zeolite complexes

MY	Cur	YNiCur	YCuCur
	572		
575		579	580
	719	724	724
790		791	791
	812		
	857		
	962		
1020		1030	1030
	1027		
	1155		
	1206		
	1234	1230	1232
	1280		
	1430		1425
	1460		1461
	1510	1510	1510
	1600	1558	1575
	1629		
1640		1638	1637
	3415		
3464		3450	3450

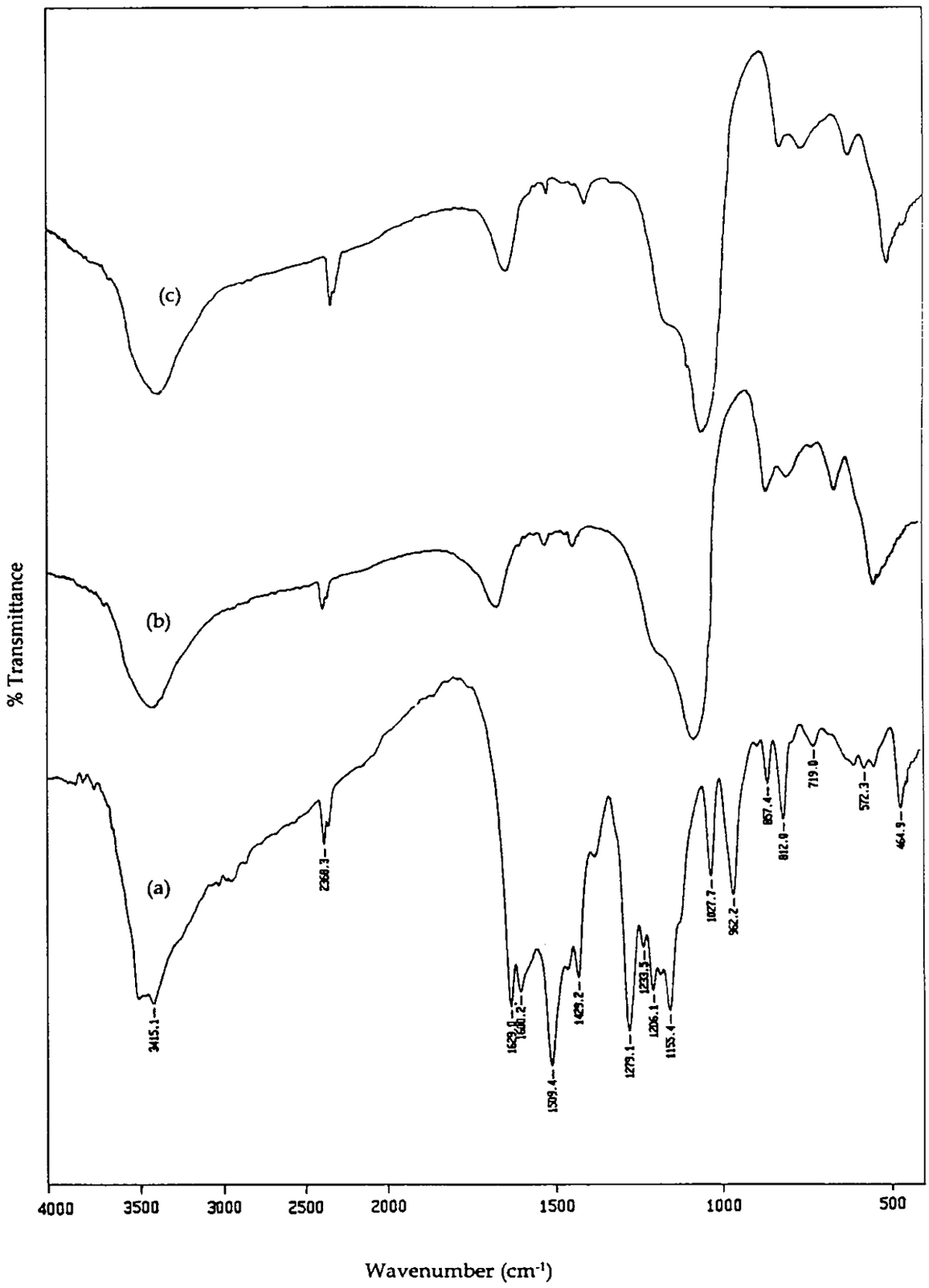

Figure 7.4 FTIR spectra of (a) Curcumin (b) YCuCur (c) YNiCur

7.3.6 TG analysis

The TG/DTG curves of zeolite encapsulated curcumin complexes are shown in the Figure 7.5a. The TG data are tabulated in Table 7.4. The weight loss in the first stage of decomposition is due to the removal of free moisture from zeolite samples. The decomposition of the complex is seen to take place in two stages in the case of copper complex. The DTG peaks of second and third stage are very broad. In the nickel complex the third stage decomposition is not clear. TG curves of curcumin complexes are compared with those of corresponding metal exchanged zeolite in Figure 7.5. The difference in the TG pattern of the curcumin complex could be taken as an evidence for the encapsulation of curcumin complex.

Table 7.4
TG/DTG Data

Sample	Weight loss-stage I			Weight loss-stage II			Weight loss-stage III		
	Temp range (^{0}C)	Peak temp (^{0}C)	% Mass loss	Temp range (^{0}C)	Peak temp (^{0}C)	% Mass loss	Temp range (^{0}C)	Peak temp (^{0}C)	% Mass loss
YCuCur	60-180	90	6.0	200-320	263	11.0	305-540	480	3.3
YNiCur	60-170	100	8.4	230-300	280	12.3			

7.3.7 Electronic spectra

Electronic spectra of the zeolite complexes in the diffuse reflectance mode were taken and are given in Figure 7.6 and the absorbance and tentative assignments are given in Table 7.5. The interpretation of these data gives an idea of the structure of the metal complexes.

The spectrum of YNiCur shows transitions at 12320 cm^{-1}, 14880 cm^{-1} and 24335 cm^{-1}. These absorption bands agree with those reported for octahedral complexes of Ni(II) ion. The water molecule in zeolite lattice or oxide ions of the

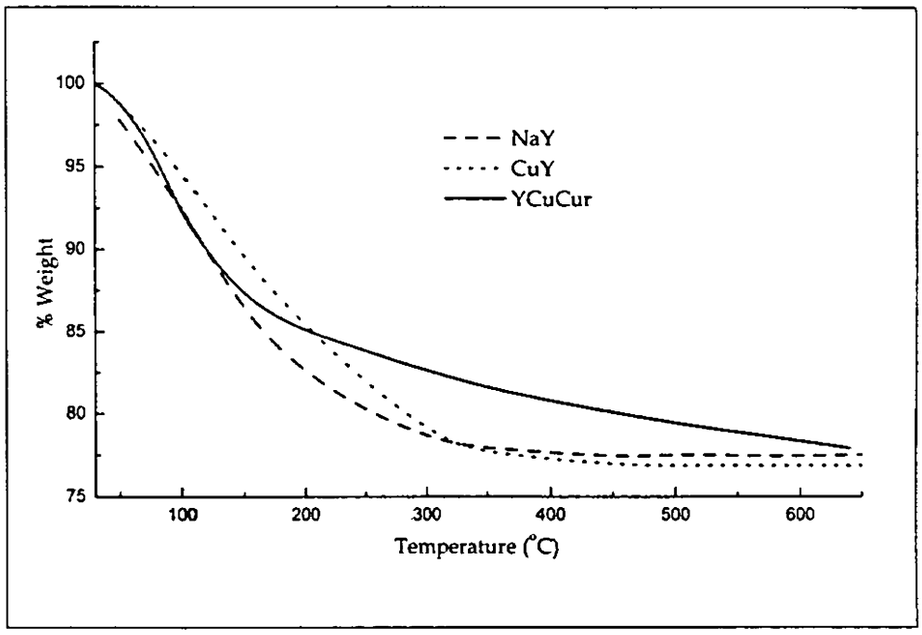

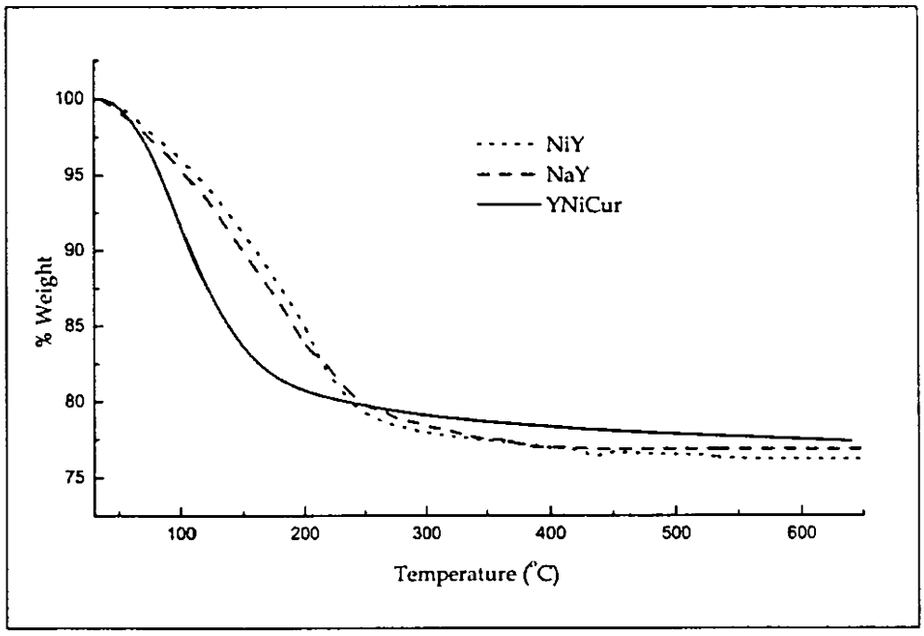

Figure 7.5 TG Plots of MY, NaY and encapsulated complexes of Curcumin

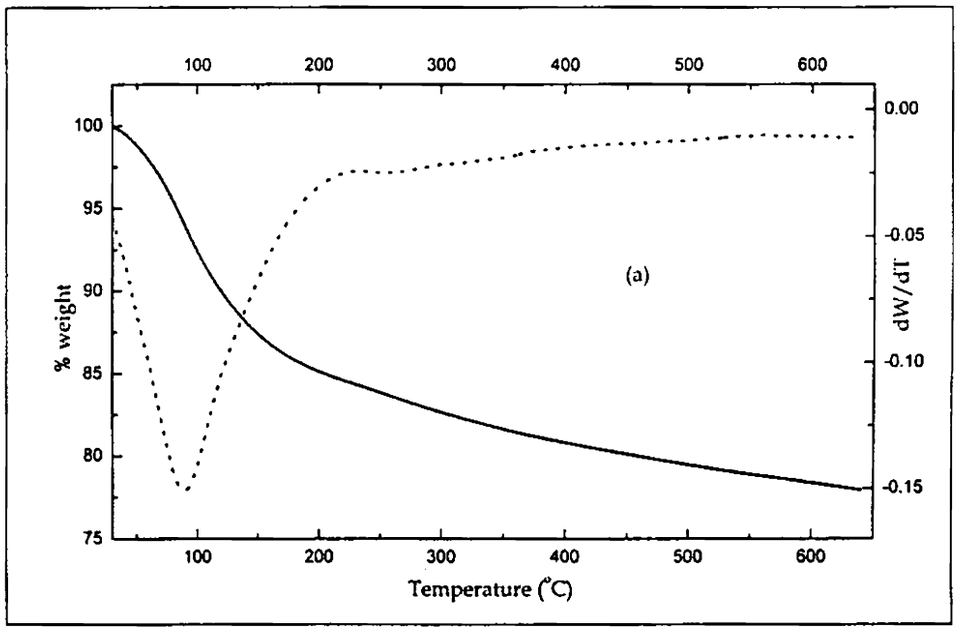

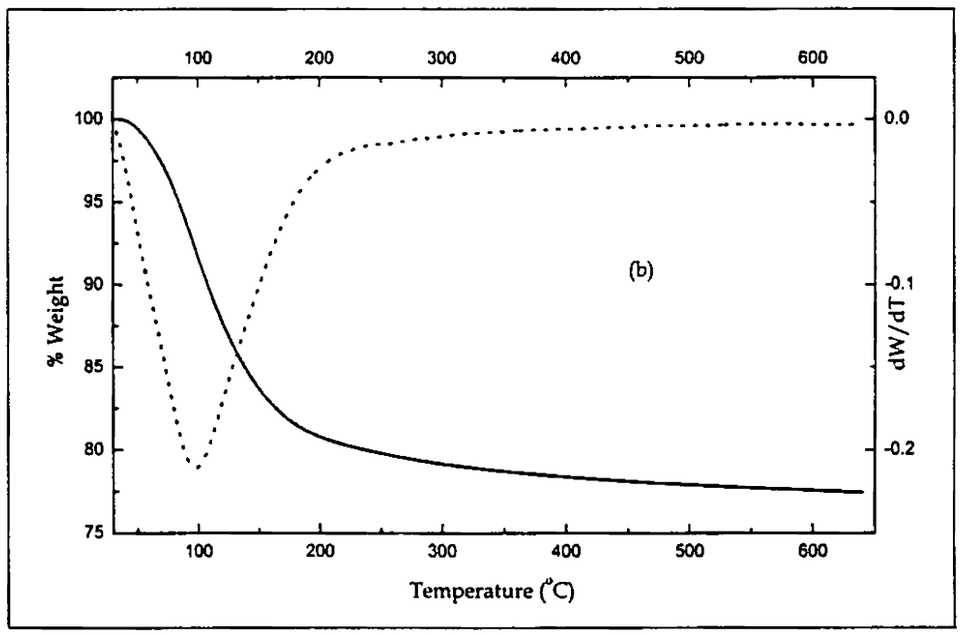

Figure 7.5a TG/DTG Plots of (a) YCuCur (b) YNiCur

framework are likely to involve in achieving the octahedral geometry of nickel(II) ion[200].

The copper complex, YCuCur exhibits bands at 17700 cm^{-1}, characteristic of a four-coordinated geometry with planar arrangements of ligands[201].

Table 7. 5
Electronic spectral data

Sample	Absorbance Max.		Tentative assignments
	cm^{-1}	Nm	
YNiCur	12320	810	$^3T_{2g} \leftarrow {}^3A_{2g}(F)$
	14880	670	$^3T_{1g}(F) \leftarrow {}^3A_{2g}(F)$
	24335	410	$^3T_{1g}(P) \leftarrow {}^3A_{2g}(F)$
	33485	300	Intraligand transition
YCuCur	17700	565	d-d transition
	31055	320	Intraligand transition

7.3.8 Magnetic measurements

Room temperature magnetic moments of curcumin complexes are given in Table 7.6. YNiCur has exhibited a magnetic moment of 3.2 BM indicating an octahedral geometry for the encapsulated complex. Magnetic moment of 1.89 BM was observed for YCuCur complex[210,200]. The value indicates a square planar or distorted octahedral structure for the complex.

Table 7.6

Magnetic moment data of the encapsulated Cur complexes

Complexes	Magnetic moment (BM)	Unit Cell
YNiCur	3.20	$Na_{49.80}Ni_{3.10}(AlO_2)_{56}(SiO_2)_{136}nH_2O$
YCuCur	1.89	$Na_{52.48}Cu_{1.76}(AlO_2)_{56}(SiO_2)_{136}nH_2O$

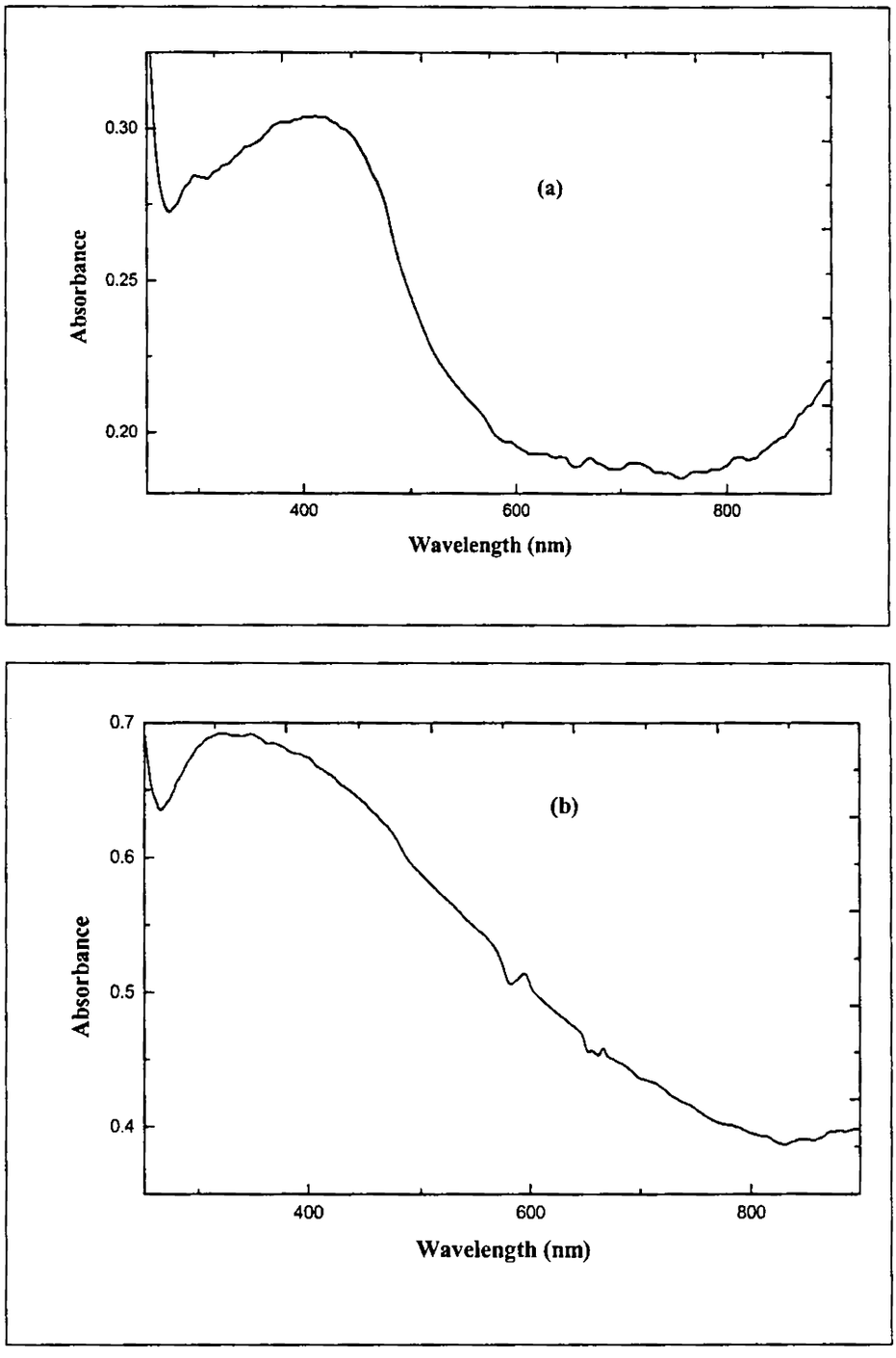

Figure 7.6 Electronic spectra of (a) YNiCur and (b) YCuCur

7.3.9 EPR spectra

The EPR spectrum of YCuCur was recorded at liquid nitrogen temperature. The spectrum is presented in Figure 7.7. The $g_{\parallel}/A_{\parallel}$ of 104 cm obtained for the complex suggests a square planar geometry for the encapsulated complex[205]. The value of in-plane covalence parameter (α^2) is 0.87, which indicates the large ionic nature of metal-ligand bond.

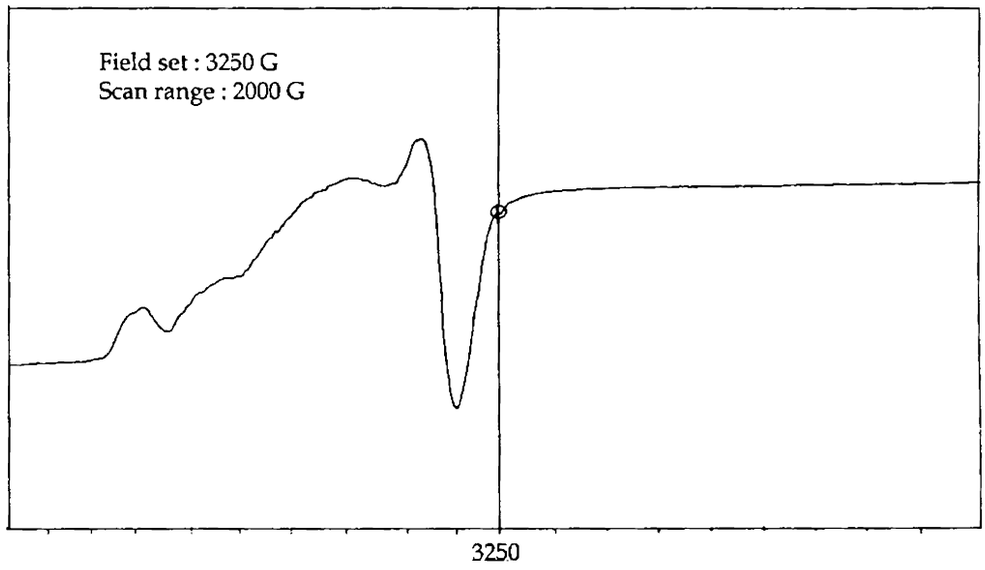

Figure 7.7 EPR spectrum of YCuCur

Table 7.7
EPR spectral data of YCuCur

EPR parameter	YCuCur
$g_{\parallel}$	2.3
$A_{\parallel}$	180×10^{-4} cm^{-1}
$g_{\parallel}/A_{\parallel}$	104 cm
$g_{\perp}$	2.08
α^2	0.87

ZEOLITE ENCAPSULATED METAL COMPLEXES: CATALYSTS FOR CYCLOHEXANOL OXIDATION

8.1 Introduction

The oxidation of alcohols to aldehdyes and ketones is a fundamental reaction in organic synthesis, and numerous oxidizing reagents are available to affect this key transformation. In most instances the reagents used are stoichiometric amounts and are very often toxic. For example, chromium oxidants are used in vast amounts for this purpose in both the laboratory and industry. With the ever-growing environmental and economic concerns, the development of new catalytic processes for alcohol oxidation is becoming increasingly important. Oxidation of cyclohexanol to hexanone is an industrially important reaction. Cyclohexanone is the major feed stock for the production of ε-caprolactum or adipic acid[241]. Even though a mixture of cyclohexanone and cyclohexanol is acceptable for nylon production, cyclohexanone is desirable as the sole oxidation product in a variety of fine chemical synthesis[242,243].

Homogeneous catalysts such as metal complexes are generally very efficient for catalytic wet peroxidation reactions. But their recovery from the treated effluent is rather difficult and requires additional separation step, which induces an increase in the treatment cost. All these drawbacks can be overcome by using heterogeneous catalysts.

Zeolite encapsulated metal complexes offer several advantages in catalytic reactions due to their ruggedness, protection against deactivation by dimer and cluster formation during catalysis and the ease of separation from the reaction

products[83]. Application of such complexes as catalysts have been reported in reactions like vapour phase carbonylation of methanol, or aromatic compounds and hydroformylation reaction using zeolite encapsulated Rh/Ir mono and polynuclear carbonyl compounds[244-246]. The cyclohexanol oxidation with H_2O_2 using Cu(Salen)Y has been studied and a conversion of 50% with 90% selectivity was reported[83].

Tert-butyl hydroperoxide (TBHP) is an environment friendly and cheap oxidant and an industrially more appropriate oxygen source[247]. With this oxidant much higher turn-over values are obtained. In this chapter, our studies on the application of zeolite encapsulated complexes as catalysts for oxidation of cyclohexanol using TBHP are presented.

8.2 Materials

The details for all the materials used for catalytic studies are given in Chapter 2.

8.3 Procedure for catalytic reactions

The required amount of the substrate and oxidant in a suitable solvent was kept in a round bottom flask, fitted with water condenser. The whole set up was taken in an oil bath and stirred magnetically. After the experiment, the flask was cooled, the catalyst was separated by filtration and the reactant was analyzed with GC to estimate the conversion.

The oxidation of cyclohexanol with 70% TBHP as the oxidant and toluene as the solvent at 70^{0}C in the presence of the complexes was carried out. The product formed *viz.* cyclohexanone was analyzed using a carbowax column.

8.4 Screening studies

Zeolite encapsulated cobalt, nickel and copper complexes of the Schiff bases, QOPD, ICSCZ, ICAT, VOPD and the copper and nickel complexes of curcumin were evaluated for their activity for the oxidation of cyclohexanol. The

reactions were carried out in toluene at 70°C, keeping the cycohexanol to TBHP ratio as 1.0. The percentage conversion of cyclohexanol was noted after 4h. of reaction. The reaction conditions and the conversion data are presented in Table 8.1. Further, the percentage conversion are represented graphically in Figure 8.1

Table 8.1
Results of screening studies.

Metal	% Conversion				
	Cur	ICAT	VOPD	ICSCZ	QOPD
Cobalt	-	1.0	1.5	2.5	2.0
Nickel	0.05	1.5	2.0	2.0	3.0
Copper	11.5	10.0	13.5	14.0	16.0

Reaction conditions:

Catalyst wt - 20mg
Temperature - 70°C
Solvent - Toluene
Oxidant/substrate - 1
Duration - 4h

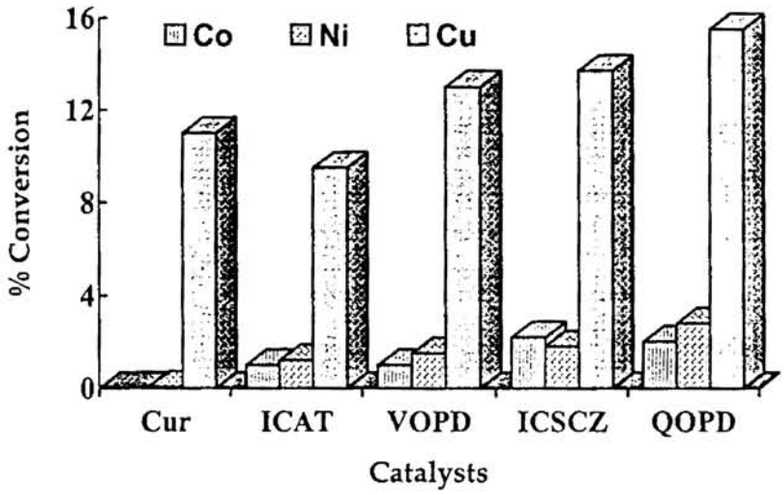

Figure 8.1 Screening study using all the zeolite encapsulated complexes for the oxidation of cyclohexanol using *tert*-butylhydroperoxide

The screening studies indicated that the copper complexes were most active. So further studies were confined to copper complexes only. The selectivity towards cyclohexanone was >98%.

8.5 Blank run

A blank run was carried out at 70°C. The conditions used for the blank run were same as that of the screening studies. But no catalyst was used for this purpose. No conversion was observed even after 4 h. of reaction.

8.6 Effect of various parameters on catalysis

The effects of following parameters on the oxidation of cyclohexanol were carried out.

1. Temperature
2. Oxidant to substrate ratio
3. Amount of catalyst
4. Solvent

8.6.1 Temperature dependence

The influence of temperatures on the percentage conversion was studied by carrying out the reaction at three different temperatures 50°C, 70°C and 90°C. The results of the studies are presented in the Figure 8.2

For all the complexes the conversion was found to increase with temperature. Moreover there was no change in selectivity at higher temperatures. The maximum conversion was found to be at 90°C. However the temperatures higher than 90°C were not tried, as the oxidant may decompose at higher temperatures. Therefore, 90°C was chosen as the temperature for all the further studies. The zeolite encapsulated copper complexes of curcumin did not show much increase in activity. Moreover it was found to decompose at that reaction condition. So further studies were not carried out with the curcumin complex.

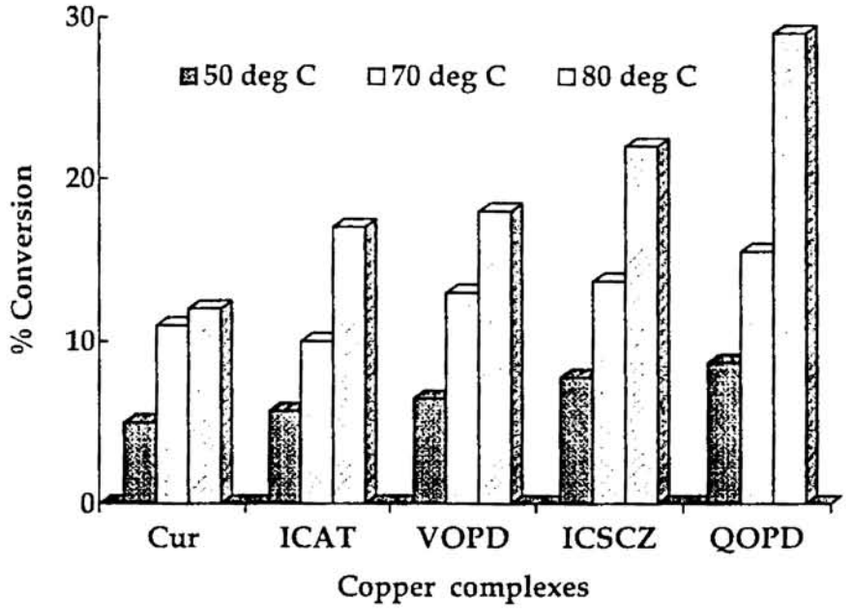

Figure 8.2 Effect of temperature on the copper complexes for cyclohexanol oxdiation

Reaction conditions:

Catalyst wt – 20mg
Solvent – Toluene
Oxidant/substrate – 1
Duration – 4h

8.6.2 Effect of oxidant to substrate ratio

The results of studies involving the variation of oxidant to substrate ratio are given graphically in Figure 8.2.

The conversion was found to increase substantially when the oxidant/substrate ratio was increased from 1 to 2. However, there was no significant increase in the conversion when the ratio was increased from 2 to 3. Therefore the ratio 2 was taken as the optimum conditions for the reactions.

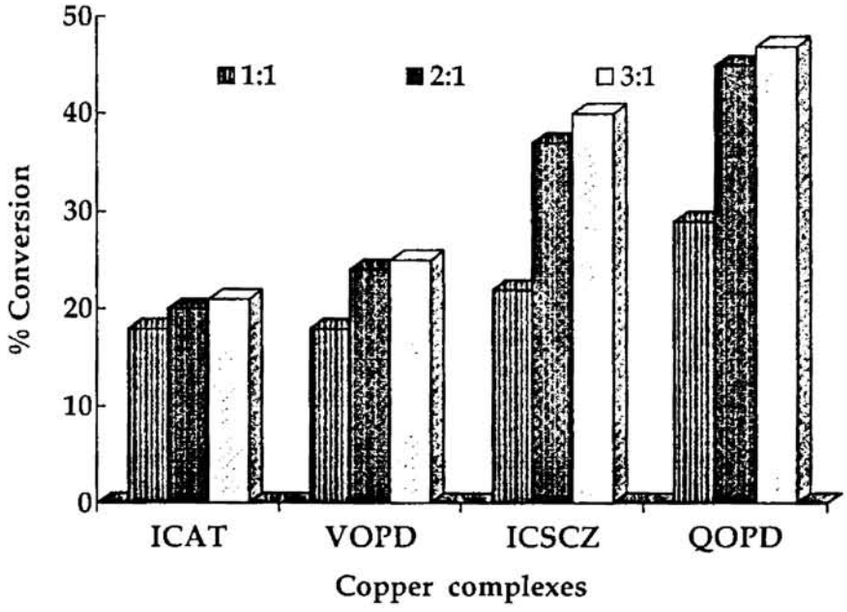

Figure 8.3 Effect of oxidant/substrate ratio on activity

Reaction conditions:

Catalyst wt - 20mg
Solvent - Toluene
Temperature - 90°C
Duration - 4h

8.6.3 Amount of catalyst

The data and the conversion of cyclohexanol on varying the amount of catalysts are presented in Table 8.2

It can be seen that eventhough the catalyst amount was increased from 20 mg to 60 mg, there was not much increase in conversion for zeolite encapsulated complexes. This will be very clear when the turn over number (TON) of the catalyst is taken into account (Table 8.4.). In the case of YCuQOPD complexes the TON, is 181.5 when 20 mg of the catalyst was taken. The TON was found to be 113.4 when 40 mg of the catalyst was taken and it was further low when 60 mg of

the catalyst was taken. In this case TON is only 81.0. A similar trend was observed in all the cases.

Table 8.2
Effect of amount of catalyst on percentage conversion of cyclohexanol oxidation

Sample	% Conversion when the amount of catalyst is		
	20mg	40mg	60mg
YCuICAT	20.0	22.0	23.5
YCuVOPD	25.0	30.0	33.0
YCuICSCZ	40.0	48.0	51.0
YCuQOPD	48.0	60.0	64.5

Reaction conditions:

Oxidant/substrate - 2:1
Solvent - Toluene
Temperature - 90°C
Duration - 4h

8.6.4 Variation of solvent

The cyclohexanol oxidation using the YCuQOPD complex was carried out using different solvents like alcohol, water, toluene and chlorobenzene. The results obtained are given in the Figure 8.4. Cholorobenzene was found to be the best solvent with a higher conversion percentage. Toluene and water were found to give more or less same percentage conversion, whereas alcohol was found to give least conversion among these solvents.

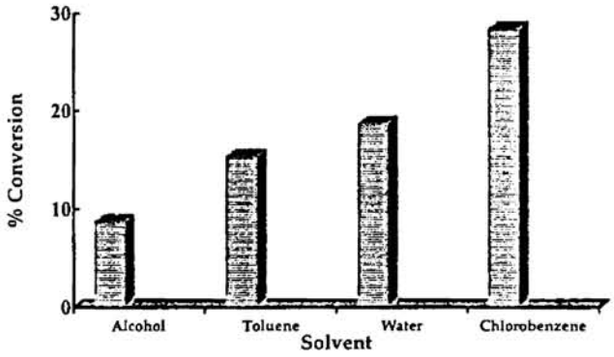

Reaction conditions:

Oxidant/substrate - 2:1
Catalyst weight - 20mg
Temperature -70°C
Duration - 4h

Figure 8.4 Effect of solvent variation on oxidation of cyclohexanol using YCuQOPD as the catalyst.

8.7 Recycling studies

Recycling was carried out twice for the zeolite encapsulated copper complexes. All the copper complexes except the YCuCur could retain their activity. This shows that the zeolite encapsulated complexes were stable and can be recycled. The details of the recycling studies are given in Table 8.3

Table 8.3
Results of recycling studies

Sample	% conversion at		
	Fresh sample	1st recycle	2nd recycle
YCuICAT	20	18	17
YCuVOPD	24	22	22
YCuICSCZ	37	35	33
YCuQOPD	45	42	42

Reaction conditions:

Oxidant/substrate - 2:1
Catalyst weight - 20mg
Temperature -90°C
Duration - 4h

8.8 Discussion

All the results regarding the catalytic activity is summarized in Table 8.4

Table 8.4
Catalytic evaluation data*

Complex	Oxidant/ substrate	Catalyst weight (mg)	Temp.	% Conversion	TON
YCuQOPD	1	20	50	8.7	32.9
	1	20	70	15.3	57.8
	1	20	90	29.0	109.6
	2	20	90	45.0	170.2
	3	20	90	48.0	181.5
	2	40	90	60.0	113.4
	2	60	90	64.5	81.0
YCuICSCZ	1	20	50	7.8	74.6
	1	20	70	13.7	131.1
	1	20	90	22.0	210.0
	2	20	90	37.0	354.0
	3	20	90	40.0	382.0
	2	40	90	48.0	229.0
	2	60	90	51.0	162.7
YCuVOPD	1	20	50	6.5	34.19
	1	20	70	13.0	68.40
	1	20	90	18.0	94.69
	2	20	90	24.0	126.26
	3	20	90	25.0	131.52
	2	40	90	30.0	78.91
	2	60	90	33.0	57.87
YCuICAT	1	20	50	5.7	22.8
	1	20	70	10.0	40.1
	1	20	90	18.0	72.2
	2	20	90	20.0	80.2
	3	20	90	21.0	84.24
	2	40	90	22.0	44.2
	2	60	90	23.5	31.42
CuY	2	20	90	7.5	22.0

Solvent used: Toluene

From the turn over number (moles converted per mole of copper ions per hour) it can be concluded that the optimum conditions for the reactions is.

Amount of catalyst		20mg
Oxidant/substrate		2:1
Temperature	:	90^0C
Duration		4h.

The optimum oxidant/substrate ratio was found to be 2 for the oxidation of cyclohexanol over copper complexes using *tert*-butylhydroperoxide as the oxidant. An excess of oxidant is required because of its parallel decomposition which is independent of the oxidation of organic substrate. The oxygen gas liberated may partially involve in the oxidation reaction by interacting with the active site of the catalyst.

It was reported that the two competitive reactions i.e., the selective oxidation of cyclohexanol with *t*-BHP(I) and the decomposition of TBHP(II) are both influenced by the different reaction modes[57]. The decomposition reaction is second order in the peroxide concentration and is therefore strongly dependent on the variation in concentration of the peroxide, whereas the selective oxidation is first order in both the cyclohexanol and peroxide and consequently less dependent on the variation in peroxide concentration.

The activity of the zeolite encapsulated copper complexes was found to be in the order: YCuQOPD > YCuICSCZ > YCuVOPD > YCuICAT. The variation in activity can be explained on the basis of structural properties of the complexes. The square planar geometry and distorted octahedral structures of these complexes may account for their higher activity. The oxidation reaction may involve the coordination of oxygen atom at the vacant sites of metal atoms in the complex to form a binuclear oxo-complex. This intermediate transfers the coordinated oxygen atom to the substrate to obtain the product. Thus the availability of the vacant sites in the square planar/flattened tetrahedral copper

complexes may facilitate the coordination of oxygen atom, thereby facilitating higher activity for these complexes.

The low activity of the cobalt and nickel complexes may be due to the octahedral nature of the complex. These structures do not have vacant coordination sites and may prevent the coordination of the oxygen atom.

$CoMo/Al_2O_3$ CATALYSTS PREPARED USING PYRROLIDINE-*N*-CARBODITHIOATE COMPLEXES – CATALYTIC ACITIVITY FOR HYDRODESULPHURIZATION OF DIESEL

9.1 Introduction

Over 80 million barrels of petroleum are processed every day in refineries around the world to meet the requirements for liquid transportation fuels such as gasoline, diesel fuel and jet fuel. Despite the advances made in improving fuel economy of automobiles and trucks, worldwide consumption of transportation fuels has continued to grow and is expected to remain strong well into this millennium.

For a number of years, the oil and auto industry have worked in a cooperative effort called the Auto-Oil Air Quality Research Program to understand the relationships between fuel composition and vehicle emissions. The intent of this effort is to make cost-effective improvements to transportation vehicles and fuels to minimize the adverse impacts on the environment resulting from the combustion of fossil fuels. Regulatory changes being enacted over the next 10 years will require dramatic changes in fuel composition. Both gasoline and diesel fuel will likely to be required to have ultra-low sulphur content.

It is now widely recognized that sulphur dioxide pollution of the atmosphere can no longer be tolerated. Thus widespread attention has been given to remove sulphur from the fuels that we now burn. Solutions of this problem are quite simple for natural gas; at the opposite extreme, for the case of coal, the problem has not yet been solved.

The desulphurization of petroleum and petroleum fractions is almost universally accomplished by the catalytic reaction of hydrogen with sulphur compounds in the charge stock to produce hydrogen sulphide, which is readily separable from the oil. Such hydrodesulphurization operations are in widespread use in the petroleum refining industry.

Environmentally driven regulations are requiring significant improvement in the quality of diesel and gasoline in many parts of the world. Reducing the concentration of organic sulphur species in gasoline has been recognized as one way of reducing emissions. The regulatory norms put forward by India and Europe are given below (Table 9.1)

Table 9.1
Regulatory out look

Standards	Sulphur, % max	
	2000 spec.	Target 2005 spec.
Indian	0.200	0.050
European	0.035	0.005

Hydrotreating process involves the removal of sulphur, nitrogen, oxygen and metals from oil fraction by reduction treatment using supported metal sulfide catalysts. The process is of great importance because air polluting emissions of sulphur and nitrogen oxides, which contribute to acid rain will be diminished. Furthermore, catalysts which are used for the processing of oil products, cannot tolerate sulphur and metals. Hydrotreating is the largest application of industrial catalysis on the basis of the amount of material processed per year[248].

The origin of hydrotreating catalysts goes back to the 1920s when German researchers developed metal sulphide catalysts to liquefy coal, but it was not before the 1970s that the structure of these catalysts and the mechanism of their catalytic action were comprehended.

A detailed understanding of the individual sulphur compounds in a feed and their reactivity is important to satisfy the increased environmental demands for further reduction of sulphur levels in many refinery products. Some typical sulphur compounds found in petroleum fractions are given below.

Thiols, Sulphides and disulphides	R—SH, R—S—R, R—S—S—R'
Benzothiophenes	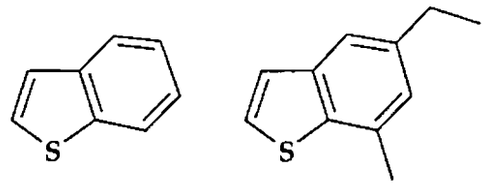
Dibenzothiophenes	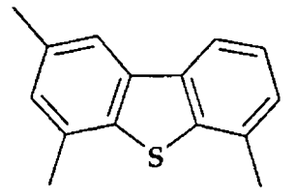

Hydrodesulphurization reactivity depends critically on the molecular size and the structure of the sulphur-containing compound. Thus the following order in rates has been reported[249]for desulphurization reactions: thiophene > benzothiophene > dibenzothiophene. For higher analogues of dibenzothiophene, e.g., benzonaphthothiophene, hydrogenation of one of the aromatic rings accompanies hydrodesulphurization reaction. Hydrogenated analogues are more easily desulphurized than the thiophenic compounds[250].

The most common combinations of active elements in hydrotreating catalysts are CoMo, NiMo or NiW supported on alumina/silica/alumina silicate. The concentration by weight of the metals is usually 1-4% for Co and Ni, 8-16% for Mo and 12-25% for W. Typical support materials are alumina, silica-alumina, silica, zeolites, kieselguhur and magnesia, with surface areas in the 100-300 m^2/g range. The choice of the catalyst type varies according to the application and

desired activity/selectivity. CoMo catalysts are excellent HDS catalyst but are somewhat less active for HDN and hydrogenation of aromatics. As a result, the CoMo catalysts give relatively low hydrogen consumption. Consequently NiMo catalysts are often preferred for treating unsaturated feeds. Of the three combinations mentioned above, NiW catalysts have the highest activity for aromatic hydrogenation at low hydrogen sulfide partial pressures[251], but their use has been limited due to the higher cost.

One of the more important and intriguing questions posed is the role which cobalt plays in catalysis over molybdena catalysts. Its promoting effect is unquestioned in HDS reactions and is responsible for the commercial success of these catalysts. According to some of the more important theories regarding the role of cobalt the cobalt ions increase the monolayer Mo area[252], increase the rate of Mo reduction[253,254], increase hydrogen mobility[255], prevent deactivation[256] and prevent MoS_2 crystallization[257].

The hydrodesulphurization activity was measured under continuous flow conditions at 400^{0}C and atmospheric pressure for Mo and Co containing catalyst supported on different materials (γ-and η-Al_2O_3 and SiO_2) and on materials using different methods of preparation[258]. The result showed that all supports having a high specific surface area are suitable in HDS preparation. Alumina is to be preferred because it inhibits the formation of $CoMoO_4$, and thus exerts a beneficial influence on catalyst preparation. The main function of the support is to stabilize a high degree of dispersion of the actual active component MoS_2. In addition the carrier may facilitate hydrogenation and isomerization reactions.

Hydrotreating catalysts are industrially prepared by pore volume impregnation of γ-Al_2O_3 with an aqueous solution of $(NH_4)_6Mo_7O_{24}$, $Co(NO_3)_2$ or $Ni(NO_3)_2$ and phosphate, followed by drying and calcinations, or by co-impregnation of all three inorganic materials followed by drying and calcinations. Phosphate is added as phosphoric acid or ammonium phosphate to enhance the solubility of the molybdate by the formation of phosphomolybdate complex[259]

The activity of the hydrodesulphurization catalysts mainly depends on the dispersion of the active component, which in turn depends on the method of preparation and nature of the support. The catalysts are generally prepared by impregnation of the alumina support using aqueous solutions, which contain ammonium molybdate and nitrates of cobalt or nickel, followed by calcination in air at higher temperatures (~500°C)[260]. The calcined oxide precursors are then converted into active sulphided state. However, the conversion of the oxidic phase into the sulphidic phase is not complete in the case of conventional methods of preparation. Thus there is a continuing interest for developing new preparation techniques to overcome these difficulties.

Rao *et. al.*, reported the precipitation from homogeneous solution (PFHS) method[261] for the development of better controlled catalysts with respect to crystallite size, surface area, pore structure, uniform composition and high dispersion of metal. Chelating agents such as 1,2-cyclohexanediamine-*N,N,N',N'*-tetraacetic acid, ethylenediaminetetraacetic acid, nitrilotriacetic acid etc., added in impregnation stage was also found to be effective in achieving high metal dispersion and activity[262,263]. It was therefore though interesting to prepare these catalysts making use of metal complexes as precursors of molybdenum and cobalt.

We have synthesised hydrodesulphurization catalysts using the cobalt and molybdenum complexes of pyrrolidine-*N*-carbodithioate as precursors. The catalysts prepared through this molecular designed dispersion (MDD) method have been characterized using various physicochemical techniques. Hydrodesulphurization activities of the catalysts were carried out and compared with that of the catalyst prepared through conventional method. The results of these studies are presented in this chapter.

9.2 Experimental

9.2.1 Materials

Details regarding various physicochemical methods used in the present study are given in Chapter 2.

9.2.2 Molecular Designed Dispersion (MDD) method

The details about molecular designed dispersion method[168] is given in Chapter 1. MDD method consists of two steps: In the first step, a neutral transition metal complex is anchored to the surface of a high surface area support. In a consecutive step, the adsorbed complex is decomposed in an oxygen containing atmosphere at elevated temperature, yielding the supported transition metal oxide catalyst. Here molybdenum and cobalt pyrrolidine-*N*-carbodithioate complexes were used for the above said purpose.

9.2.3 Preparation of pyrrolidine-*N*-carbodithioate complexes

Details regarding the preparation of pyrrolidine-N-carbodithioate ligand are given in Chapter 2.

a) Molybdenum complex

A solution of ammonium molybdate (9.0 g) in distilled water (100mL) was stirred vigorously using a magnetic stirrer. A solution of sodium pyrrolidine-*N*-carbodithioate (14.69 gm) in water (50mL) was added dropwise. Stirring was continued for 15 min. even after the completion of addition. The red coloured dioxo complex was filtered, washed with water and then with methanol and dried in vacuum over anhydrous calcium chloride[264].

b) Cobalt complex

A solution of cobaltous sulphate (14.0 g) in distilled water (100mL) was stirred vigorously using a magnetic stirrer, and to this a solution of sodium pyrrolidine-*N*-carbodithioate (14.69 gm) in water (50mL) was added dropwise. Stirring is continued for 15 min. after the addition is complete. The green coloured complex is filtered, washed with water and then with methanol and dried in vacuum over anhydrous calcium chloride[265].

9.2.4 Preparation of the catalyst

Seven hydrodesulphurization catalysts were prepared of which first three catalysts were prepared according to the conventional method. The last four samples were prepared according to the molecular designed dispersion method.

9.2.4.1 Catalysts prepared by conventional method

γ-Al_2O_3 extrusions were processed to catalysts by changing the sequence of addition of cobalt and molybdenum during the impregnation as follows:

Catalyst A: Cobalt loading followed by molybdenum loading.

Catalyst B: Molybdenum loading followed by cobalt loading.

Catalyst C: Cobalt and molybdenum loaded together.

All the impregnations were carried out by wet impregnation technique from excess solution. Cobalt nitrate and ammoniacal solution of molybdic acid was used as the precursor compounds for loading cobalt and molybdenum. After each impregnation, calcinations was carried out at 500°C. This calcination temperature has been reported to give optimal HDS activity[266]. This temperature is high enough to ensure full decomposition of the metal salts used in the impregnation but is sufficiently low to prevent unwanted solid state reactions.

9.2.4.2 Catalysts prepared through MDD method

γ-Al_2O_3 extrusions (50 gm), with 5% MoO_3 (incorporated during the mixmulling stage) were dipped in a solution of $MoO_2(Pydtc)_2$ (20 gm) in dichloromethane and kept for one week at room temperature. After one week period, the solution was found to be colourless suggesting complete and selective adsorption of the complex on the carrier. The extrusions were filtered, washed with the solvent and dried at 120°C for 2h. Thus prepared sample was used as the support for further preparations. This support was divided into four portions and the following preparations were carried out.

Catalyst D: $MoO_2(PyDtc)_2/\gamma$-Al_2O_3 was calcined at 500°C for 2h at a heating rate of 10°C/min., cooled, dipped in a solution of cobalt acetate in ethanol by pore filling method, filtered and dried at 500°C for 2h.

Catalyst E: $MoO_2(PyDtc)_2/\gamma$-Al_2O_3 was dipped in cobalt acetate solution in ethanol by pore filling method, filtered, dried and then calcined at 500°C for 2h.

Catalyst F: $MoO_2(PyDtc)_2/\gamma$-Al_2O_3 was calcined at 500°C for 2h at a heating rate of 10°C/min., cooled, dipped in a solution of cobalt pyrrolidine-*N*-

carbodithioate complex in chloroform by pore filling method, filtered and dried at 500°C for 2h.

Catalyst G: $MoO_2(PyDtc)_2/\gamma\text{-}Al_2O_3$ was dipped in cobalt pyrrolidine-*N*-carbodithioate complex in chloroform by pore filling method, filtered and dried at 500°C for 2h.

9.3 Results and discussion

9.3.1 Physicochemical measurements

Chemical analysis shows the presence of cobalt and molybdenum and further confirms the successful impregnation of metals on the support. Surface area of the alumina extrusions used for the catalyst's preparation is $245m^2/g$ and was found to be decreased after impregnation. Analytical data is given in Table 9.2.

Table 9.2
Analytical, surface area and pore volume data

Catalysts	% MoO_3	%CoO	Surface area (m^2/gm)	Pore volume ml/gm
$\gamma\text{-}Al_2O_3$	-	-	245	0.51
Catalyst A	18.0	4.5	200	0.35
Catalyst B	19.8	4.8	202	0.44
Catalyst C	20.0	4.9	203	0.44
Catalyst D	17.2	3.9	219	0.45
Catalyst E	17.3	4.0	214	0.44
Catalyst F	17.8	1.7	214	0.45
Catalyst G	18.0	1.8	216	0.43

The analytical data reveal that the percentage molybdenum content was as expected in all the cases. Thus the selective adsorption of $MoO_2(Pydtc)_2$ is as effective as that of pore filling method. The cobalt loading was also as

expected.; but in the case of last two samples, it was low. In those cases $Co(Pydtc)_2$ was used as a precursor for the metal source. The solubility of $Co(Pydtc)_2$ was poor, and selective adsorption was negligible. So pore filling method with multiple impregnations was carried out. Even then the cobalt loading was found to be low in comparison with that of cobalt acetate solution.

Surface area of the catalyst was found to be decreased upon impregnation of CoMo and calcinations. This is because of the pore blocking and surface smoothing by the deposition of the metal oxide on the support. The percentage drop in surface area of catalysts prepared through MDD method was smaller than that of the catalysts prepared through the conventional method. This implies that compared to the conventional method of preparation the new preparation technique was beneficial as the large metal oxide agglomerates are converted to small metal oxide particles on the support. This is further confirmed by Raman spectroscopy. The percentage drop in surface area is presented graphically in Figure 9.1.

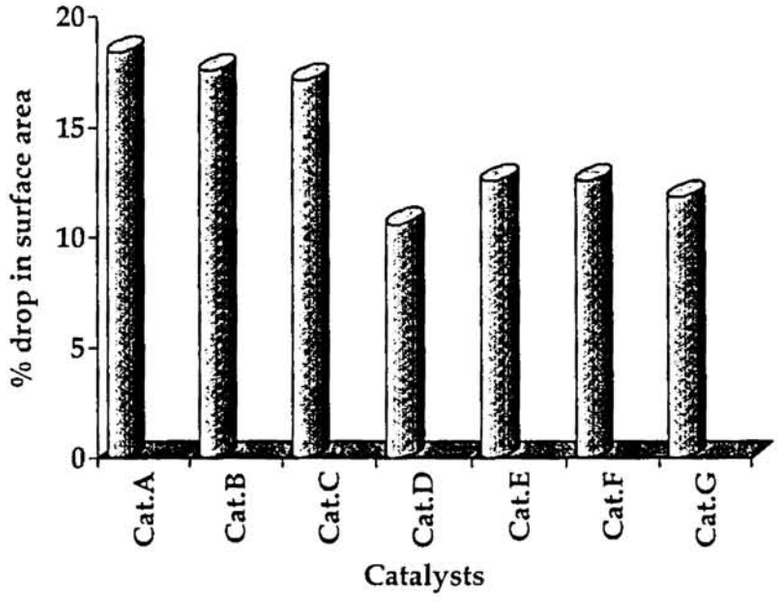

Figure 9.1
% Drop in surface area

9.3.2 Oxygen chemisorption

Adsorption studies of various probe molecules, like O_2, H_2S, NO and CO have provided information on the type of surface sites and the dispersion of the species present in hydrotreating catalysts. Oxygen has shown some promise as a selective probe for the active sites in hydrotreating catalysts, and many studies have been carried using oxygen chemisorption[267-269]. Good correlation between HDS activity and the total oxygen adsorption are typically observed for unpromoted sulphided molybdenum catalysts. Such correlation was also suggested to exist for promoted catalysts[270-272]. The low temperature oxygen chemisroption of the samples were carried out. A dry ice acetone mixture was used to get the required temperature (-78^{0}C). The experimental procedure is given in Chapter 2. The oxygen chemisorption data are given in Table 9.3. About 25% increase in % metal dispersion was observed in the case of catalysts prepared though molecular designed dispersion method. This shows that the MDD method can produce catalysts, with a highly dispersed active phase.

Table 9.3
Oxygen chemisorption data

Samples	% Molybdenum dispersion
Catalyst A	18.0
Catalyst B	18.0
Catalyst C	19.0
Catalyst D	23.0
Catalyst E	22.0
Catalyst F	24.0
Catalyst G	23.0

9.3.3 Temperature programmed reduction (TPR)

Temperature programmed reduction is an effective tool to investigate the surface structure and the oxidation state of the samples. It was reported that the reducibility of a catalyst was closely related to the activity[273]. TPR experiments were performed to examine the effect of the method of preparation on the reducibility of the catalyst. The reaction conditions for TPR studies are as follows.

Catalyst weight		0.1gm
Carrier		2% hydrogen in argon
Flow rate		30ml/min.
Heating rate	:	10°C/min.

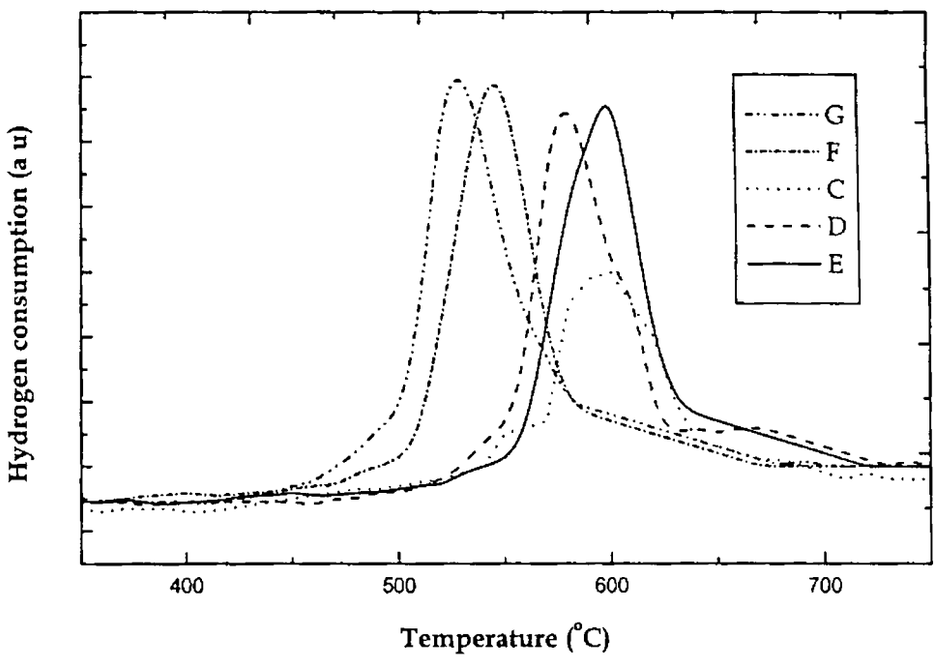

Figure 9.2 TPR profile of the catalysts

Normally there are two reduction temperature peaks for MoO_3. One at lower temperature, (between 500-600°C) and the other one at higher temperature (between 800-950°C). It was observed that the lower and higher temperature peaks are due to the reduction of MoO_3 to MoO_2 and MoO_2 to Mo respectively.

The present TPR study was limited to lower temperature range, as the activity of the catalyst is known to be related to the reduction of MoO_3 to MoO_2[274] Figure 9. 2 gives the TPR profile of the five samples (Catalyst C to Catalyst G). From the patterns it is clear that the catalysts prepared through MDD method consumes hydrogen remarkably than that of catalyst C. Moreover the reduction temperature of the samples F and G shows a shift towards lower temperature, (the reduction temperature is shifted from 600°C to 525-545°C). In these two samples $Co(Pydtc)_2$ was used as the metal precursor. So the cobalt complex further enhances the lowering of reduction temperature.

9.3.4 Raman spectra

Raman spectroscopy has probably been the greatest contributor to the rapid progress in the area of supported metal oxide catalysts characterization, because of its ability to discriminate between metal oxide structures and its *insitu* capabilities. The supports such as alumina and silica show no specific peaks in Raman spectroscopy. A number of studies on the assignment of Raman band positions have been reported for supported molybdena catalysts[275,276].

Ng and Gulari[277] have proposed that the bands at 956 cm^{-1} or at lower wave numbers of supported molybdena catalysts can be attributed to the terminal Mo=O bonds of isolated tetrahedral species and the bonds above 955 cm^{-1} are due to the polymeric octahedral species. A similar interpretation of Raman band shifts with increasing molybdenum oxide content have also been reported by Wang and Hall [278,279]. Brown et. al., confirmed that the Raman bands observed at 930-970 cm^{-1} are attributed to the octahderally coordinated polymolybdate species[280].

Raman spectra of the samples are given in Figure 9.3. Catalyst C, shows a peak at 980 cm^{-1}. This shift in the peak position can be attributed to high metal content and to polymeric octahedral species. In the case of catalysts prepared through MDD method, the peak intensity at 980 cm^{-1} was found to be decreased drastically. A new peak at 940 cm^{-1} was observed in catalyst F and G. and can be assigned to the symmetric Mo=O stretching of MoO_4^{2-} in tetrahedral

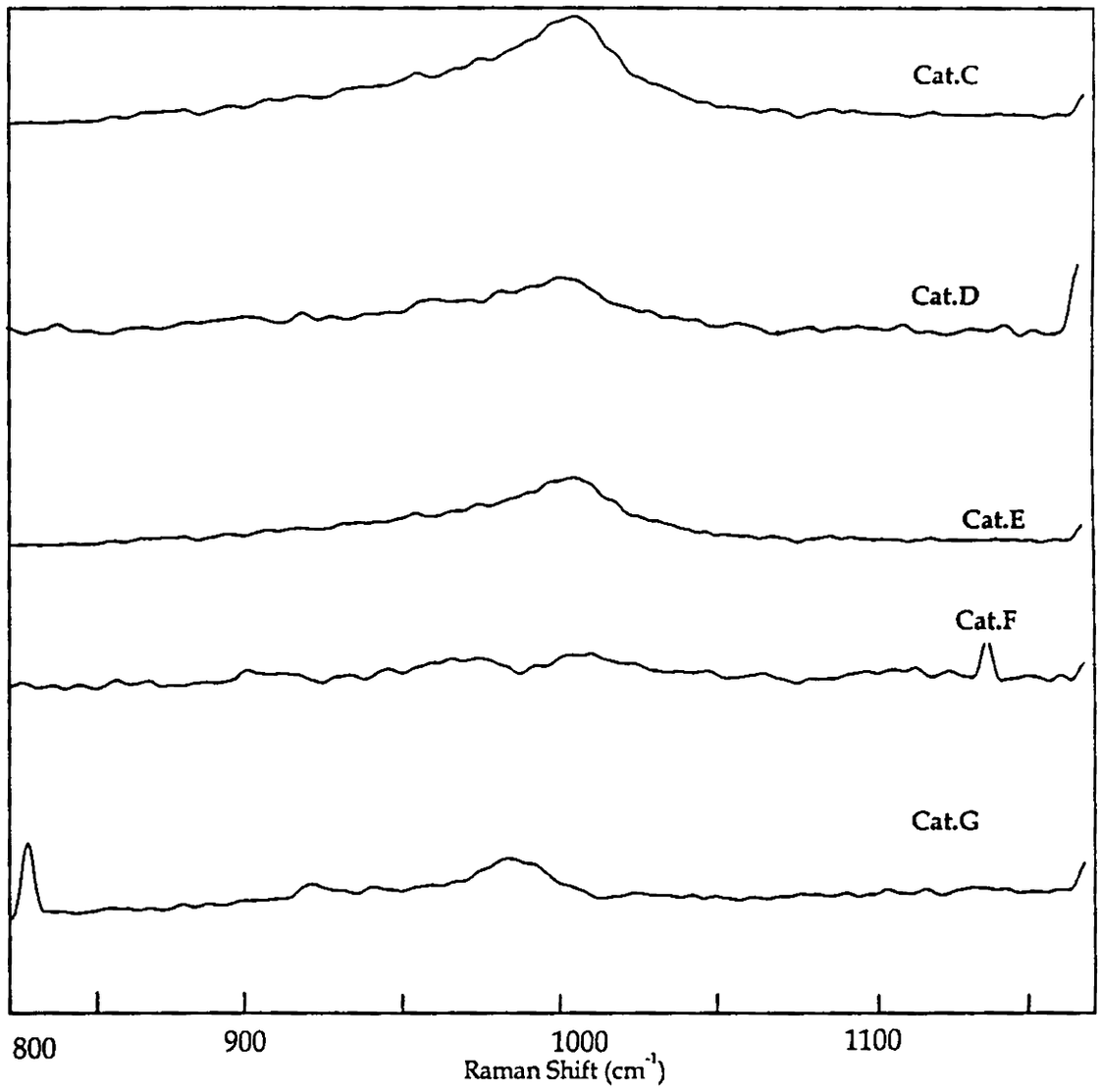

Figure 9.3
Laser Raman Spectra of Catalyst samples

coordination[281]. Therefore in the case of the MDD technique, the large polymeric octahedral $Mo_7O_{24}^{6-}$ clusters are not formed, instead smaller tetrahedral MoO_4^{2-} species are formed suggesting higher dispersion of molybdenum[282].

9.3.5 Hydrodesulphurization activity

9.3.5.1 Conversion of the precursor to the active phase

The conversion of the oxide precursor into the active sulfide form is an important step in the catalyst preparation. Sulphidation transforms the precursor into active sulphide phase. During the interaction of unsupported bulk MoO_3 with a H_2/H_2S mixture, the transformation of MoO_3 to MoS_2 is complete even at low temperature. In the case of supported catalysts the mechanism of sulphidation is complicated. Mascot[283] noticed, through a detailed study of rates and stoichiometry of sulphidation of Mo/Alumina catalyst, that in the range of 350-420^{0}C, the catalyst is not completely sulphided. If the catalyst is reduced before sulphiding, the sulphidation cannot be carried out to completion. In this case, the behaviour of the supported and unsupported catalysts is similar.

9.3.5.2 Catalytic activity evaluation

A reported procedure was followed for the catalytic activity evaluation of catalytic activity[284]. A bench-scale cocurrent down-flow trickle bed reactor supplied by CHEMITO was used in this study. A stainless steel tubular reactor of internal diameter 19mm, outer diameter 25mm and length 450 mm was used in this study. A schematic diagram for the set up for activity evaluation is given in Figure 9.4. The reactor was loaded with 10 gm of the catalyst extrudates mixed uniformly with carborandum (SiC). The reactor was monitored with three thermocouples. Straight run diesel supplied by Kochi Refineries was used for the activity evaluation. The details of the feed is given in Table 9.4

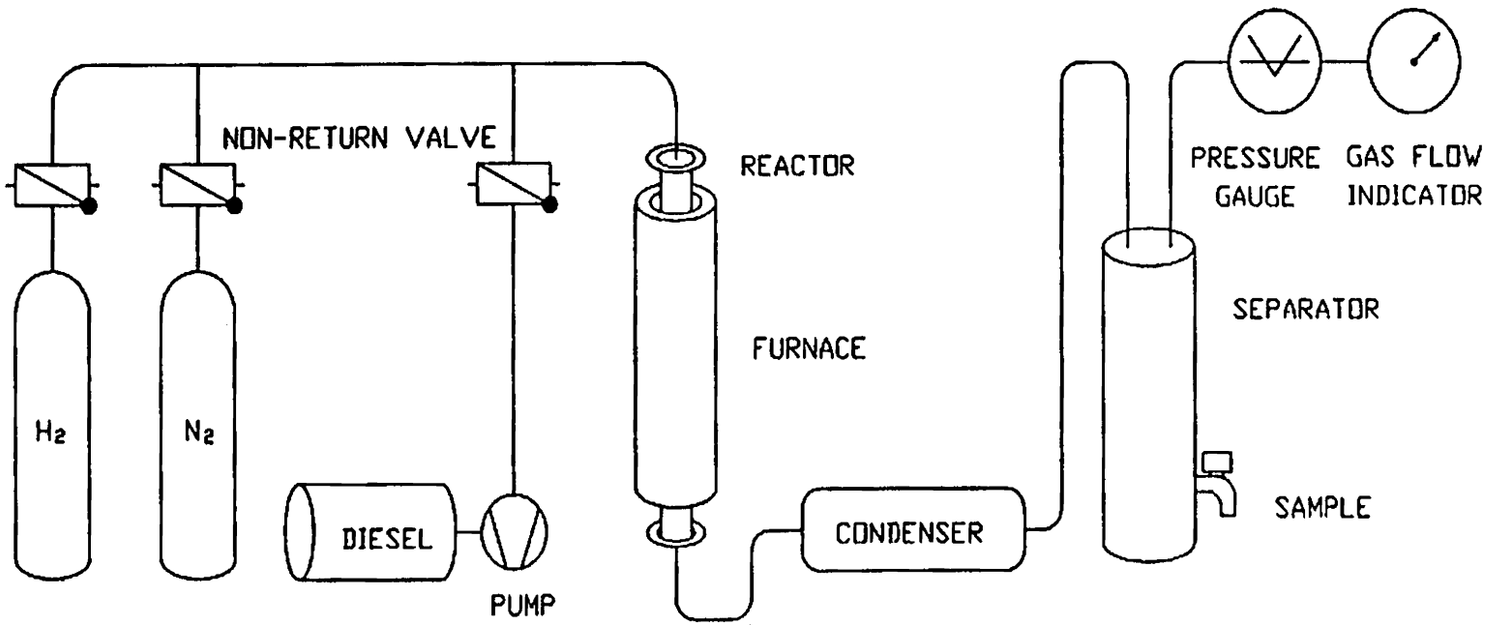

Figure 9.4 Set up for the HDS activity

Table 9.4
Feed properties

% Sulphur	1.105%
Initial Boiling point	242.6^{0}C
Final Boiling point	369.6^{0}C

At first the catalyst was dried with a nitrogen purge at 120^{0}C for 2h to remove the moisture present in the catalyst. And then it was sulphided using the feed diesel doped with 1% dimethyl disulphide (DMDS). The reaction condition for the presulfidation are as follows:

Catalyst weight		10gm
Feed	:	SR diesel doped with 1% DMDS
Pressure		30kg
H_2/Hydrocarbon	:	300
Liquid Hourly Space Velocity(LHSV)	:	$3h^{-1}$
Duration		8hrs

The temperature profile for the presulphidation is as follows:

The catalyst was heated from room temperature to 175^{0}C and kept for 2h and then increased to 250^{0}C and held for 4h; after that the temperature was increased to 300^{0}C and the sulphiding was continued for 8h.

The sulphided catalysts were then subjected to desulphurization activity using the SR diesel containing 1.105% sulphur. The reaction conditions for the activity evaluation are as follows:

Feed		SR diesel
Temperature	:	340^{0}C
Pressure	:	35kg
H_2/Hydrocarbon		300
Liquid Hourly Space Velocity(LHSV)	:	$3h^{-1}$
Duration	:	8hrs

After the activity evaluation samples were collected and the %sulphur was evaluated using X-Ray fluorescence spectroscopy. The results obtained are given in Table 9.5, and the percentage conversion is presented in Figure 9.5.

Table 9.5
Hydrodesulphurization activity data

Samples	% S in the outlet
Catalyst A	0.2750
Catalyst B	0.1375
Catalyst C	0.1175
Catalyst D	0.0690
Catalyst E	0.0875
Catalyst F	0.0625
Catalyst G	0.0665

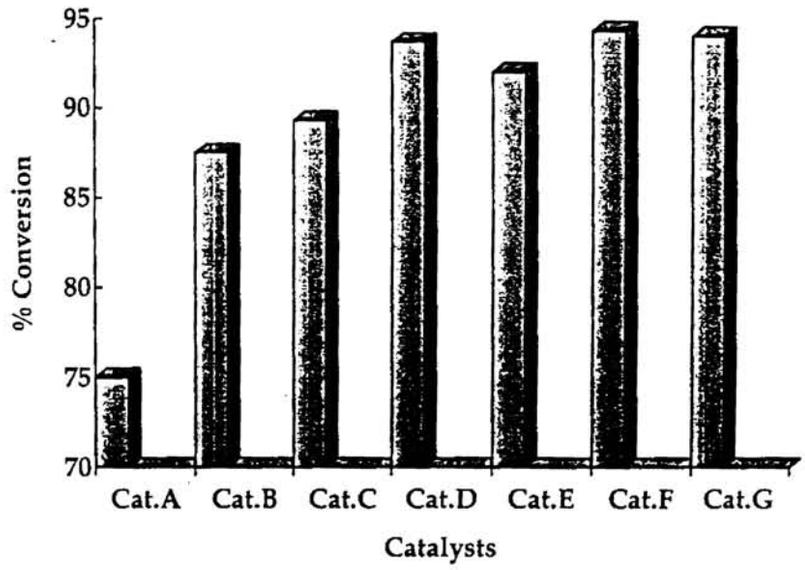

Figure 9.5 Hydrodesulphurization data

From the analysis of desulphurization data the activity of the samples are in the order Catalyst F > Catalyst G > Catalyst D > Catalyst F > Catalyst C > Catalyst B > Catalyst A. From these data it can be concluded that the method of preparation is having a commanding effect on the desulphurization activity. The catalysts prepared by molecular designed dispersion method show much better activity than those prepared using conventional method.

Among the catalysts prepared by conventional method Catalyst C shows much better activity followed by Catalyst B, while the performance of Catalyst A is very poor. The Catalyst A and Catalyst B are prepared by a two-stage impregnation method. In the case of Catalyst A, the carrier was dipped in a solution of cobalt nitrate followed by ammoniacal solution of molybdic acid and calcined at 500°C. In the case of Catalyst B, the carrier was dipped in an ammoniacal solution of molybdic acid followed by cobalt nitrate solution and calcined at 500°C. The catalyst C was prepared by a single stage impregnation, in this case, the carrier was dipped in an ammoniacal solution of molybdic acid, and cobalt nitrate solution followed by calcining at 500°C. From these it is concluded that the most active Co-Mo-S phase will be more available when cobalt and molybdenum are loaded together in the carrier during catalyst preparation (i.e., in the case of Catalyst C). Initial metal loading of cobalt can lead to the formation of cobalt aluminate and moreover, during sulfidation inactive Co_9S_8 will be formed to a greater extent. This could be the reason why Catalyst A is showing a lower activity.

All the catalysts developed by molecular designed dispersion method show more comparable activity. The catalysts F and G show slightly higher activity than the other two (Catalyst D and E). In these cases the cobalt was also impregnated as the dithiocarbamate complex. In these catalysts the molybdenum exhibited higher dispersion. The higher amount of active sites available enhances the catalytic activity. Studies also indicate that an enhancement in reducibility, dispersion and the decomposition of cluster complexes into smaller one happens in the case of molecular designed dispersion method. Simultaneous dipping is not

possible in this case since the molybdenum complex is having higher affinity towards the alumina than the cobalt complex as evidenced by the analytical data of the samples. It can be concluded that higher molybdenum dispersion, smaller molybdenum clusters, high reducibility of MoO_3 and lower reduction temperature can be achieved through molecular designed dispersion method involving the complexes and these properties are required for a better hydrodesulphurization activity.

REFERENCES

1. M. Sitting, *Combine Hydrocarbons and Oxygen for Profit, Chem. Process Rev.* No.11, Noyen Dev. Co., Park Ridge, New Jersey, **1968**
2. T. Dumas,W. Bulani, *Oxidation of Petrochemicals: Chemistry and Technology,* Appl. Sci. Publ., London, **1974**
3. J. E. Huheey, E. A. Keiter, R. L. Keiter, *Inorganic Chemistry - Principles of Structure and reactivity,* Harper Collins College Publishers, **1993**
4. J. Smidt, W. Hafner, R. Jira, J. Seedlneir, R. Sieber, R. Rulttinger, H. Kojer, *Angew. Chem.*, **1959**, 71, 176
5. T. L. Schull, J. C. Fettinger, D. A. Knight, *Inorg. Chem.*, **1996**, 35, 6717
6. F. A. Cotton, G. Wilkinsons, *Advanced Inorganic Chemistry,* 5th Edition, Wiley-Interscience, New York, **1988,** 1224
7. J. F. Roth, J. H. Graddock, A. Harshman, A. E. Paullk, *Chem. Tech.*, **1971**, 1, 600
8. J. Falbe, H. Bahrmann, *J. Chem. Edu.*, **1984**, 61, 961
9. K. S. Coleman, C. Y. Lorber and J. A. Osborn, *Eur. J. Inorg. Chem.*, **1998**, 1673
10. E. G. Samsel, K. Srinivasan, J. K. Kochi, *J. Am. Chem. Soc.*, **1985**, 107, 7606
11. R. A. Scheldon, J. A. Kochi, *Metal Catalyzed Oxidation of Organic Compounds;* Academic Press: New York, **1981**
12. R. A. Scheldon, *The Chemistry of Peroxides;* S.Patai (Ed.), Wiely, New York **1983**, 161
13. K. A. Jorgenson, *Chem. Rev.*, **1989, 89,** 431
14. R. Hunter, P. Turner, S. Rimmer, *Synth. Commun.*, **2000**, 30, 4461
15. K-J. Kim, S-W. Park, S. S. Yoon, *J. Korean Chem. Soc.*, **2000, 44,** 286
16. W. Zhang, J. L. Loebach, S. R. Wilson, E. N. Jacobson, *J. Am. Chem. Soc.*, **1990**, 112, 2801
17. Z. Li, M. Fernandez, E. N. Jacobson, *Org. Lett.*, **1999**, 1, 1611
18. E. N. Jacobson, E. E. Schaus, a. G. Dosetter, T. F. Janison, *US Patent* - 1999 - 255480
19. W. Goertz, P. C. J. Kamer, P. W. N. M. van Leeuwen, D. Vogt, *Chem. Europ .J.*, **2001**, 7, 1614
20. G. R. Newkome, C. N. Moorefield, F. Vogtle, *Dendrimers and Dendrons: Concepts, Synthesis, Applications,* Wiely: Weinheim, **2001, 45**
21. D. M. Tomalia, P. R. Dvornic, *Nature* **1994**, 372, 617
22. S. M. Grayson, J. M. J. Frechet, *Chem. Rev.* **2001**, 101, 3819

23. P. Bhyrappa, J. K. Young, J. S. Moore, K. S. Suslick, *J. Am. Chem. Soc.* **1996,** *118,* 5708
24. S. B. Garber, J. S. Kingsbury, B. L. Gray, A. H. Hoveyda, *J. Am. Chem. Soc.,* **2000,** 122, 8168
25. R. Breinbauer, E. N. Jacobsen. *Angew. Chem. Int. Ed. Engl.,* **2000,** 39, 360
26. W. M. Mwier, D. H. Olson, *Zeolites,* **1992,** 12, 449
27. H. M. Leicester, *The Historical Background of Chemistry,* Dover, New York, **1971**
28. S. T. Sie, *Stud. Surf. Sci. Catal.,* **1994,** 85, 587
29. J. M. Thomas, *Angew. Chem. Int. Ed. Engl.,* **1994,** 33, 913,
30. W. Holderich, E. Galleli, *Chem. Ing. Tech.,* **1984,** 56, 908
31. R. A. Sheldon, *J. Mol. Catal. A,* **1996,** 107, 75
32. R. A. Sheldon, *Catal. Today,* **1994,** 19, 215
33. P. Kumar, R. Kumar, B. Pandey, *Synlett.,* **1995,** 289
34. J. Weitkamp, *Proc. Int. Zeolite. Conf. 9th 1992,* **1993,** Vol. 1, 13
35. W. J. Mortier, R. A. Schoonheydt, *Progr. Solid State Chem.,* **1985,** 16, 125
36. D.E. De Vos, P. -P. Knops-Gerrits. R. F. Parton, B. M. Weckhuysen, P. A. Jacobs, R. A. Schoonheydt, *J. Incl. Phenom. Mol. Rec. Chem.,* **1995,** 21, 185
37. K. J. Balkus, Jr. A. G. Gabrielov, *J. Incl. Phenom. Mol. Rec. Chem.,* **1995,** 21, 159
38. R. E. White, W. J. Coon, *Ann. Rev. Biochem.,* **1980,** 49, 315
39. D. Mansuy, P. Battioni, in *Bioinorganic Catalysis,* Ed: J. Reedijk, Marcel Dekker, New York, **1993,** 395
40. A. E. Shilov, *J. Mol. Catal.,* **1988,** 47, 351
41. B. R. Cook, T. J. Reinert, K. S. Suslick, *J. Am. Chem. Soc.,* **1986,** 108, 7281
42. J. P. Collman, X. Zhang, V. J. Lee, U. S. Uffelman, J. Brauman, *Science,* **1993,** 261, 1404
43. N. Herron, *J. Coord. Chem.,* **1988,** 19, 25
44. N. Herron, *Chemtech,* **1989,** 542
45. D. Mansuy, *Coord. Chem. Rev.,* **1993,** 125, 129
46. R. Parton, D. De Vos, P. A.Jacobs in *Zeolite Microprous Solids: Synthesis, Structure and Reactivity* Eds: E. G. Derouane, F. Lemos, C. Naccache, F. R. Ribeiro, Kluwer Academic Publishers, **1992,** 555
47. L H. Lunsford, *Catal. Rev. - Sci. Eng.,* **1975,** 12,137
48. N. Herron, *Inorg. Chem.,* **1986,** 25, 4714
49. W. H. Quayle, G. Peeters, G. L. De. Roy, E. F. Vansant, J. H. Lunsford, *Inorg. Chem.,* **1982,** 21, 2226
50. P.-P. Knops- Gerrits, D.de. Vos, F. Thibault - Starzyk, P. A. Jacobs, *Nature,* **1994,** 369, 543
51. W. de. Wilde, J. H. Lunsford, *Inorg. Chim. Acta.,* **1979,** 34, L229
52. W. de. Wilde, G. Peeters, J. H. Lunsford, *J. Phys. Chem.,* **1980,** 84,2306
53. M. Nakamura, T. Tatsumi, H. Tominaga, *Bull. Chem. Soc. Jpn.,* **1990,** 63, 3334
54. Y. W. Chan, R. B. Wilson, *Preprints, Div. of Petroleum Chemistry,* ACS, **1988,** 33, 453
55. N. Herron, G. D. Stucky, C. A. Tolman, *J. Chem. Soc., Chem. Commun.,* **1986,** 1521

56. R. F. Parton, L. Uytterhoeven, P. A. Jacobs, *Stud. Surf. Sci. Catal.*, **1991**, 59, 395
57. R. F. Parton, G. J. Pere, P. E. Neys, P. A. Jacobs, R. Claussens, G. V. Baron, *J. Mol. Catal. A: Chemical*, **1996**, 113, 445
58. F. T. Starzyk, R. F. Parton, P. A. Jacobs, *Stud. Surf. Sci. Catal.* **1994**, 84, 1419
59. N. Herron, G. D. Stucky, C. A. Tolman, *J. Chem. Soc., Chem. Commun.*, **1986**, 1521
60. C. A. Tolman, N. Herron, *Catal. Today*, **1988**, 3, 235
61. E. P-Mozo, N. Gabriunas, R. Maggi, D. Acosta, P. Reiz, B. Delmon, *J. Mol. Catal.*, **1994**, 91, 251
62. E. P. Mozo, N. Gabriunas, F. Lucacioni, D. D. Acosta, P. Patrono, A. L. Ginestra, P. Reiz, B. Delmon, *J. Phys. Chem.*, **1993**, 97, 12819
63. R. Raja, P. Ratnaswamy, *J. Catal.*, **1997**, 170, 244
64. S. Seelan, A. K. Sinha, D. Sreenivas, S. Sivasankar, *J. Mol. Catal. A: Chem.*, **2000**, 157, 103
65. B. V. Romanovsky, A. G. Gabrielov, *J. Mol. Catal.*, **1992**, 74, 293
66. E. Ernst, Y. Traa, U. Deeg, *Stud. Surf. Sci. Catal.*, **1994**, 84, 925
67. S. Seelan, A. K. Sinha, *Appl. Catal. A: General*, **2003**, 238, 201
68. I. F. J. Vankelecom, R. F. Parton, M. J. A. Casselman, J. B. Uytterhoeven, P. A. Jacobs, *J. Catal.*, **1996**, 163, 457
69. T. Tatsumi, M. Nakamura, H. Tominaga, *Chem. Lett.*, **1989**, 419
70. T. Tatsumi, M. Nakamura, H. Tominaga, *Catal. Today*, **1989**, 6, 163
71. W. S. Swzulbinski, J. R. Kincaid, *Inorg. Chem.*, **1998**, 37, 5614
72. S. Deshpande, D. Srinivas, P.Ratnasamy, *J. Catal.*, **2000**, 188, 261
73. Z. Li, C-Gu Xis, X-Ming Zhang, *J. Mol. Catal., A: Chemical*, **2002**, 185, 47
74. S. Ernest, M. Selle, *Microp. Mater.*, **1999**, 27, 355
75. F. Algaura, M. A. Estever, V. Fornes, H. Garcia,, J. Primo, *New. J. Chem.*, **1998**, 333
76. C.Bowers, P. K. Dutta, *J. Catal.*, **1990**, 122, 271
77. L. Gaillon, N. Sajot, F. Bedioui, J. Devynck, K. J. Balkus Jr., *J. Electroanal. Chem.*, **1993**, 345, 157
78. K. J. Balkus Jr., A. A. Welch, B. E. Gnade, *Zeolites*, **1990**, 10, 722
79. S. Kowalak, R. C. Weiss, K. J. Balkus Jr., *J. Chem. Soc., Chem. Commun.*, **1991**, 57
80. C. R. Jacob, S. P. Varky, P. Ratnasamy, *Appl. Catal.*, **1998**, 168, 353
81. S. Koner, *Chem. Commun.*, **1998**, 595
82. S. P. Varkey, C. R. Jacob, *Ind. J. Chem.*, **1998**, 37A, 407
83. C. Ratnasamy, A. Murugkar, S. Padhye, *Ind. J. Chem.*, **1996**, 36A, 1
84. N. Ulagappan, V. Krishnasamy, *Ind. J. Chem.*, **1996**, 35A, 787
85. M. J. Sabater, A. Corma, A. Domenech, V. Fornes, H. Garcia, *Chem. Commun.*, **1997**, 1285
86. T. H. Bennur, D. Srinivas, P. Ratnasamy, *Microprous and Mesoprous Materials*, **2001**, 48, 111
87. J. Woltinger, J. E. Backvall, A. Zsigmond, *Chem. Eur. J.*, **1999**, 5, 1460
88. A. Zsigmond, F. Notheisz Z. Frater, J. E. Backvall, in *Heterogeneous Catalysis and Fine Chemicals IV*, (Eds.) H. U. Blaser, A. Baiker, R. Prins, **1997**, 453

89. I. Neves, C. Freire, A. N. Zakharavo, B. de Castro, J. L. Figueiredo, *Colloids Surfaces A: Physicochem. Eng. Aspects*, **1996**, 115, 249
90. K. Mizuno, J. H. Lunsford, *Inorg. Chem.*, **1983**, 22, 3484
91. B. N. Figgis, M. Gerloch, J. Lewis, F. E. Mabbs, G. A. Webb, *J. Chem. Soc. A*, **1968**, 2086
92. S. K. Tiwary, S. Vasudevan, *Inorg. Chem.*, **1998**, 37, 5239
93. G. Vanko, Z. Homonnay, S. Nagy, A. Vertes, G. Pal-Borbely, H. K. Beyer, *J. Chem. Soc. Chem. Commun.*, **1996**, 785
94. F. Farzanch, M. Majidian, M.Gandhi, *J. Mol. Catal., A: Chemical*, **1999**, 148, 227
95. M. Sykora, K. Maruszewski, S. M. Treffert-Ziemelis, J. R. Kincaid, *J. Am. Chem. Soc.*, **1998**, 120, 3490
96. M. Sykora, J. R. Kincaid, *Nature*, **1997**, 387, 162
97. P. K. Dutta, M. Ledney, *Progress in Inorganic Chemistry;* J. Wiley & Sons: New York, **1997**, Vol. 44, 209
98. A. A. Bhuiyan, J. R. Kincaid, *Inorg. Chem.* **1998**, 37, 2525
99. B. Meier, T. Werner, I. Klimat, O. S. Wolfbin, *Sensors and Actuators B.*, **1995**, 29, 240
100. M. Ledney, P. K. Dutta, *J. Am. Chem. Soc.*, **1995**, 117, 7687
101. B. M. Weckhuysen, A. A. Verberckmoes, I. P. Vannijvel, J. A. Pelgrims, P. L. Buskens, P. A. Jacobs, R. A. Schoonheydt, *Angew. Chem. Int. Ed. Engl.*, **1995**, 34, 2652
102. R. Grommen, P. Manikandan, Y. Gao, T. Shane, J. J. Shane, R. A. Schoonheydt, B. M. Weckhuysen, D. Goldfarb, *J. Am. Chem. Soc.*, **2000**, 122, 11488
103. B. M. Weckhuysen, A. A. Verberckmoes, L. Fu, R. A. Schoonheydt, *J. Phys. Chem.*, **1996**, 100, 9456
104. P. Jacobs, in *Metal Clusters in Catalysis*, Eds. B. C. Gates, L. Guezi, H. Knozinger, Elsevier, Amsterdam, **1986**
105. P.-L. Zhou, B. C. Gates, *J. Chem. Soc., Chem. Commun.*, **1989**, 347
106. L.-F. Rao, A. Fukuoka, N. Kosugi, H. Kuroda, M. Ichikawa, B. J. Rode, M. E. Davis, B. E. Hanson, *J. Catal.*, **1985**, 96, 574
107. M. Iwamaoto, S. Kagawa, *J. Phys. Chem.*, **1986**, 90, 5244
108. G. Bergeret, P. Gallezot, F. Lefebore, *Stud. Surf. Sci. Catal.*, **1986**, 28, 401
109. L. Sheu, H. Knozinger, W. H. M. Sachtler, *Catal. Lett.*, **1989**, 2, 129
110. Y. Y-Sing, R. F. Howe, *J. Chem. Soc., Faraday Trans.*, **1986**, 82, 2887
111. L. F. Rao, A. Fukuoka, M. Ichikawa, *J. Chem. Soc., Chem. Commun.*, **1988**, 458
112. A. Fukuoka, L.-F Rao, N. Kosugi, H. Kuroda, M. Ichikava, *Appl. Catal.*, **1989**, 50, 245
113. G. A. Ozin, D. M. Haddleton, C. J. Gil., *J. Phys. Chem.*, **1989**, 93, 6710
114. P-L. Zhou, B. C. Gater, *J. Chem. Soc., Chem. Commun.*, **1989**, 347
115. M. Iwamoto, S. Nakamura, H. Kuseno, S. Kagava, *J. Phys. Chem.*, **1986**, 90, 5244
116. S. A. Chavan, D. Srinivas, P. Ratnasamy, *Chem. Commun.*, 2001, 1124
117. R. J. Taylor, R. S. Drago, J. E. George, *J. Am. Chem. Soc.*, **1989**, 111, 6610
118. R. J. Taylor, R. S. Drago, J. P. Hage, *Inorg. Chem.*, **1992**, 31, 253

119. S. P. Varkey, C. R. Jacob, *Ind. J. Chem.*, **1999**, 38A, 320
120. X. Hu, K. Meyer, *Inorg. Chim. Acta*, **2002**, 337, 53
121. Y.Ukisu, A. Kazusaka, M. Nomura, *J. Mol. Catal.*, **1991**, 70, 165
122. K. O. Xavier, J. Chacko, K. K. M. Yusuff, *J. Mol. Catal. A: Chemical*, **2002**, 178, 275
123. P. K. Dutta, Z. E. Zaykoski, *Inorg. Chem.*, **1985**, 24, 3490
124. R. F. Howe, J. H. Lunsford, *J. Phys. Chem.*, **1975**, 79, 1836
125. R. A. Schoonheydt, J. Pelgrims, *J. Chem. Soc. Dalton*, **1981**, 914
126. F. Bedioui, *Coord. Chem. Rev.*, **1995**, 144, 39
127. R. A. Augustine, S. Tanielyan, S. Anderson, H. Yang, *Chem. Commun.*, **1999**, 1257
128. C. Bianchini, P. Barbaro, *Top. Catal.*, **2002**, 19, 17
129. K. Mukhopadhyay, R. V. Choudari, *J. Catal.*, **2003**, 213, 73
130. A. Zsigmond, K. Bogar, F. Notheisz, *J. Catal.*, **2003**, 213, 103
131. C. N. Satterfield, *Heterogeneous Catalysis in Industrial Practice*, 2nd Edition, McGrea-Hill, Singapore, **1993**
132. H. Pines, W. O. Haag, *J. Am. Chem. Soc.*, **1960**, 82, 2471
133. K. Kunimori, T. Okouchi, T. Uchijima, *Chem. Lett.*, **1980**, 1513
134. A. Melchor, E. Garbowski, M-Vital Mathieu, *J. Chem. Soc. Faraday Trans.*, **1986**, 82, 3667
135. E. Garbowski, J-P. Candy, M. Primet, *J. Chem. Soc. Faraday Trans.*, **1983**, 79, 835
136. G. A. Olah, B. Gupta, M. Farina, J. D. Felberg, W. M. Ip, *J. Am. Chem. Soc.*, **1985**, 107, 7097
137. J. L. Rousset, L. Stievano, F. J. Cadete Santos Aires, C. Geantet, A. J. Renouprez, M. Pellarin, *J. Catal.*, **2001**, 197, 335
138. A. Ivanov, T. V. Vasina, E. G. Masloboishchikova, E. G. Khelkovskaya-Sergeeva, L. M. Kustov, J. I. Houzvicka, *Russ. Chim. Bl.*, **2000**, 49, 1726
139. X. Zuo, H. Liu, D. Guo, X. Yang, *Tetrahedron*, **1999**, 55, 7787
140. H. Okazaki, M. Soeda, Y. Ikefuji, R. Tamura, I. Mochida, *Bull. Chem. Soc. Jpn.*, **1989**, 62, 3622
141. H. Q. Dao, F. Pruchnik, *Pol. J. Chem.*, **1987**, 61, 537
142. G. Diaz, P. Esteban, L. Guczi, F. Grain, P. Bernhardt, *J. Chim. Phys. Chim. Biol.*, **1989**, 86, 1741
143. H. Osawa, T. Syzyki, K. Sugiyama, T. Matsuda, *Chem. Lett.*, **1982**, 1803
144. N. C. Kuhnen, S. J. Thomson, G. Webb, *J. Chem. Soc. Faraday Trans.1*, **1983**, 79, 835
145. Y. Iwasawa, H. Ichinose, S. Ogasawara, M. Soma, *J. Chem. Soc. Faraday Trans. 1*, **1981**, 77, 1763
146. K. P. Srivastava, K. L. Mahdok, *J. Ind. Chem. Soc.*, **1980**, 57, 80
147. R. Brown, C. Kemball, *J. Chem. Soc. Faraday Trans.*, **1990**, 86, 3815
148. J. Kobayashi, K. Kitaguchi, H. Tanaka, H. Tsuiki, A. Ueno, *J. Chem. Soc. Faraday Trans.1*, **1987**, 83, 1395
149. P. R. Jan Vissers, H. J. de Vincent, R. Prins, *J. Chem. Soc. Faraday Trans.1*, **1987**, 83, 2145
150. A. Drahoradova, M. Zdrazil, *Collect. Czech. Chem. Commun.*, **1986**, 51, 2770

151. R. P. Silvy, J. M. Beuken, P. Bertrand, B. K. Hodnett, F. Delannay, B. Delmon, *Bull. Soc. Chim. Belg.*, **1984**, 93, 775
152. N. A. Dhas, A. Ekhtiarzadeh, K. S. Suslik, *J. Am. Chem. Soc.*, **2001**, 123, 8310
153. S. T. Oyama, P. Clark, V. L. S. Teixeira da Silva, E. J. Lede, F. G. Requejos, *J. Phys. Chem.B*, **2001**, 105, 4961
154. Z. Pall, T. Koltai, K. Matusek, J-M. Manoli, C. Potvin, M. Muhler, U. Wild, P. Tetenyi, *Phys. Chem. Chem.Phys.*, **2001**, 3, 1535
155. M. Haneda, E. Joubert, J-C. Menezo, D. Duprez, J. Barbier, N. Bion, M. Daturi, J. Saussey, J-C. Lavalley, H. Hamada, *Phys. Chem. Chem. Phys.*, **2001**, 3, 1366
156. E. Lesage-Rosenberg, G. Vlaid, H. Dexport, P. Lagarde, E. Freund, *Appl. Catal.*, **1986**, 22, 211
157. H. Dexport, E. Freund, E. Lesage, J. P. Lynch in *Metal-Support and Metal-Additive effects in Catalysis*, B. Imelik (Ed), Elsevier, Amsterdam, **1982**, 53
158. A. J. van Hengstum, J. G. van Ommen, H. Bosch, P. Gellings, *Appl. Catal.*, **1983**, 5, 207
159. J. G. van Ommen, K. Hoving, H. Bosch,, A. J. van Hengstum, P. J. Gellings, *Z. Phys. Chem.*, **1983**, 134, 99
160. J. A. Rob van Veen, G. Jonkers, W. H. Hesselink, *J. Chem. Soc. Faraday. Trans.1*, **1989**, 85, 389
161. G. Agostini, M. J. Ledoux, L. Hilaire, G. Maire, *Preparation of Catalysts IV*, Elsevier, Amsterdam, **1987**, paper F6
162. J. C. Kenvin, M. G. White, M. B. Mitchell, *Langmuir*, **1991**, 7, 1198
163. M. G. White, *Catal. Today*, **1993**, 17, 73
164. P. Van Der Voort, I. B. Babitch, P. J. Grobet, A. A. Verberckmoes, E. F. Vansant, *J. Chem. Soc., Faraday. Trans.*, **1996**, 92, 3635
165. P. Van Der Voort, M. Baltes, E. F. Vansant, M. G. White, *Interface Sci.*, **1997**, 5, 209
166. M. Baltes, P. Van Der Voort, O. Collart, E. F. Vansant, *J. Porous Mater.*, **1998**, 5, 357
167. M. Baltes, P. van Der Voort, B. M. Weckhuysen, R. Ramachandra Rao, G. Catena, R. A. Schonhedyt, E. F. Vansant, *Phys. Chem. Chem. Phys.*, **2000**, 2, 2673
168. M. Baltes, O. Collart, P. Van der Voort, E. F. Vansant, *Langmuir*, **1999**, 15, 5841
169. D.D. Perrin, W. L. F. Armarego, D. R. Perrin, *Purification of Laboratory Chemicals*, 2nd Edn., Pergamon Press, New York, **1980**
170. C. L. Leese, H. N. Rydon, *J. Chem. Soc.*, **1955**, 303
171. A. Garg, J. P. Tandon, *Synth. React. Inorg. Metal. -Org. Chem.*, **1990**, 20, 707
172. Srinivasan, *J. Parm. Pharmacol.*, **1953**, 5, 4348
173. A. I. Vogel, *A Text book of Quantitative Inorganic Analysis*, Longmands-Green, London, **1978**
174. C. Tollman, N. Herron, *Symposium in Hydroc. Oxidation* 194th National meeting of American Chemical Society., New Orleans, LA, Aug 30- Sep. 4, **1987**
175. S. Brunauer, P. H. Emmet, E. Teller, *J. Am. Chem. Soc.*, **1938**, 60, 309

176. B. N. Figgis, R. S. Nyholm, *J. Chem. Soc.*, **1958**, 4190
177. D. W. Breck, *Zeolite Molecular Sieves Structure Chemistry and Use*, Vol.1, Wiley Interscience Publications, **1973**
178. H. G. Hecht, *Modern Aspects of Reflectance Spectroscopy*, W. W. Wendlandt (Ed.) Plenium Press, New York, **1968**
179. B. V. Agarwala, *Inorg. Chim. Acta.*, **1979**, 36, 209
180. *Catalysis - Science and Technology*, (Eds.) J. R. Anderson, M. Boudart, Vol. 11, Springer, **1996**
181. H. C. Liu, L. Yuan, S. W. Weller, *J. Catal.*, **1980**, 61, 282
182. K. O. Xavier, R. Sreekala, K. K. A. Rashid, K. K. M. Yusuff, B. Sen, *Catal. Today*, **1999**, 49, 17
183. K. Sato, O. Shiratori, K. Katagiri, *J. Antibiotic. Ser. A.*, **1967**, 20, 270
184. Y. Tadashi, K. Yasuo, K. Ken, *Progr. Antimicrob, Anticancer Chemother., Proc. Intl. Congr. Chemother.*, **1969**, 2, 1160
185. S. Mayadevi, K. K. M. Yusuff, *Synth. React. Inorg. Met. - Org. Chem.*, **1997**, 27, 349
186. K. K. M. Yusuff, R. Sreekala, *Synth. React. Inorg. Met. - Org. Chem.*, **1991**, 21, 563
187. D. H. Olson, *J. Phys. Chem.*, **1968**, 72, 4366
188. P. Gallezot, Y. B. Taarit, B. Imelik, *J. Catal.*, **1972**, 26, 295
189. P. G. Menon, S. Ramasheshan (Ed.)*Lecturers on Catalysis 41st Ann. Meet. Ind. Acad. Sci.*, **1975**
190. W. J. Mortier, *Compilation of Extra-framework Sites in Zeolites*, Butterworth, London, **1982**
191. W. M. Meier, D. H. Olson, C. Bacrlocher, *Atlas of Zeolite Structure Types*, fourth Ed., Elsevier, Amsterdam, **1996**
192. Y. Okamoto, *Catal. Today*, **1997**, 39, 45
193. E. M. Flasigen, H. Khatami, H. A. Szymanski, *"Molecular Sieve Zeolites", Advan. Chem. Ser., 101*, American Chemical Society, Washington D.C, **1971**, 201
194. W. H. Quayle, J. H. Lunsford, *Inorg. Chem.*, **1982**, 21, 97
195. H. Diegruber, P. J. Plath, G. Schulz-Ekloff, M. Mohal, *J. Mol. Catal.*, **1984**, 24, 115
196. A. Delabie, K. Pierloot, M. H. Groothaert, B. M. Weckhuysen, R. A. Schoonheydt, *Microporous and Mesoporous Materials*, **2000**, 37, 209
197. G. Kortum, *Reflectance Spectroscopy: Principles, Methods and Applications*, Springer-Verlag, Berlin, **1969**
198. R. Kellerman, *Diffuse Reflectance and Photoacoustic Spectroscopies*, W. N. Delgan, G. L. Haller, R. Kellerman, J. H. Lunsford (Eds), Spectroscopy in Heterogeneous Catalysis, Academic Press, New York, **1979**, 86
199. R. A. Schoonhydt, *Diffuse Reflectance Spectrocopy*, F. Delanny (Ed.), Characterization of Catalysis, Marcel Dekker, New York, 1984, p-220
200. N.N. Greenwood, A. Earnshaw, *Chemistry of the Elements*, Pergamon Press, Oxford, **1989**
201. A. B. P. Lever, *Inorganic spectroscopy*, 2nd Ed., Elsevier, New York, **1984**
202. B. J. Hathaway, A. A. G. Tomlinson, *Coord. Chem. Rev.*, **1970**, 5, 1

203. K. Sakata, H. Taziri, F. Yamaura, M. Hashimoto, *Synth. React. Inorg. Met. - Org. Chem.*, **1990**, 20, 757
204. B. N. Figgis, J. Lewis, "*The Magnetic properties of Transition Metal Complexes,*" (Ed) F. A. Cotton, "Progress in inorganic chemistry", Vol. 6, Interscience, New York, **1964.**
205. U. Sakaguchi, A. W. Addison, *J. Chem. Soc. Dalton Trans.*, **1979**, 600
206. S. J. Gruber, C. M. Harris, E. Sinn, *Inorg. Chem. Lett.*, **1967**, 3, 495
207. S. J. Gruber, C. M. Harris, E. Sinn, *Inorg. Chem.*, **1968**, 7, 268
208. U. Casellato, P. A. Vigato, *Coord. Chem. Rev.*, **1978**, 26, 85
209. A. B. P. Lever, I. M. Walker, P. J. McCarthy, *Inorg. Chim. Acta*, 1980, 39, 81
210. A. Earnshaw, *Introduction to Magnetochemistry,* Academic Press, London, **1968,**
211. J. Reedjik, In "*Comprehensive Coordination Chemistry, Vol.2*" R. D. Gillerd, J. A. McCleverty, Eds., Pergamon Press, Oxford, **1987**, 73
212. G. S. Basarab, M. Pifferitti, M. M. Bolinski, *Pestic. Sci.*, **1991**, 31, 403
213. K. C. Satpathy, A. K. Panda, R. Mishra, A. P. Chopdar, S. K. Pradhan, *Trans. Metal. Chem.*, **1991**, 16, 628
214. D. L. Cash, N. N. Ferguson, *J. Photogr. Sci.*, **1980**, 28, 12
215. D. L. Smith, H.L. Luss, *Photogr. Aci. Eng.*, **1976**, 20, 15
216. Kirk-Othmer, "*Encyclopedia of Chemical Technology,* 4th Edn. John Wiley, **1994**, 8, 590
217. G. Vos, R. A. le Febre, R. A. G. de Graff, J. G. Haasnoot, J. Reedijk, *J. Am. Chem. Soc.*, **1983**, 105, 1682
218. D. W. Engelfriet, G. C. Verschoor, *Acta Crystallogr.*, **1981**, B37, 237
219. L. R. Groenveld, R. A. le Febre, R. A. G. de Graff, J. G. Haasnoot, G. Vos, J. Reedijk, *Inorg. Chim. Acta*, **1985**, 102, 69
220. L. J. Bellamy, " *The Infrared Spectra of complex molecules*", Chapman and Hall, London, 3rd Edn. Vol.1, **1975**
221. M. K. Said, L. Mishra, A. Richaria, R. S. Dubey, *Ind. J. Chem.*, **1996**, 35A, 214
222. R. A. Palmer, W. C. Tenant, M. F. Dix, A. D. Rae, *J. Chem. Soc., Dalton*, **1976**, 2345
223. H. J. Stoklosa, G. L. Seebach, J. R. Wasson, *J. Phys. Chem.*, **1974**, 78, 962
224. H. Yokoi, *Bull. Chem. Soc. Jpn.*, **1974**, 47, 3037
225. L. Xu, Q. Ye, H. Li, K. Jiao, S. Zhang, *J. Chem. Crystallogr.*, **2000**, 30, 463
226. K. Iftikar, M. A. Sayeed, N. Ahmad, *Ind. J. Chem.* **1995**, 34A, 79
227. P. B. Chakrawarti, P. Khanna, *J. Ind. Chem. Soc.*, **1982**, 59, 828
228. A. Shahma, M. Athar, N. Ahmed, *Ind. J. Chem.*, **1982**, 21A, 185
229. P. B. Chakrawarti, K. Pramila, *J. Ind. Chem. Soc.*, **1985**, 62, 23]
230. P. B. Chakrawarti, K. Pramila, *J. Ind. Chem. Soc.*, **1984**, 61, 112
231. B. Dash, M. Patra, P. K. Mahapathra, *J. Ind. Chem. Soc.*, **1983**, 60, 772
232. R. M. Silverstein, G. C. Bassler, T. C. Mornill, *Spectrometric Identification of Organic Compounds*, Fourth Edn. John Wiley & Sons, New York, **1981**
233. R. A. Palmer, W. C. Tennant, M. F. Dise, A. D. Rae, *J. Chem. Soc., Dalton*, **1974**, 78, 962
234. T. A. Dahl, W. M. McGown, M. A. Shand, V. S. Srinivsan, *Arch. Microbiol.*, **1989**, 151, 183

235. W-J. Sye, C-C. Shen, M-J. Don, J-C. Ou, H-H. Lee, C-M Sun, *J. Nat. Prod.*, **1998**, 61, 1531
236. S. Nair, M. N. A. Rao, *Arzencim. Forsch.*, **1996**, 46, 169
237. M. Toshiya, J. Akiko, I. Junko, N.Nobuji, Y. Sigetomo, *Phytochemistry*, **1993**, 32, 1557
238. A. Mazumdar, N. Neamati, S. Sunder, J. Schulz, H. Partz, *J. Med. Chem.*, **1997**, 40, 3057
239. S-Y. Park, D. S. H. L. Kim, *J. Nat. Prod.*, **2002**, 65, 1227
240. A. Arrieta, F. Dietze, G. Mann, L. Beyer, J. Hartung, *J. Prakt. Chem.*, **1998**, 330, 111
241. H. Ulrich, *Raw Materials for Industrial Polymers*, Hanser Publishers, Munich, Oxford Univ. Press, Oxford, **1988**, 142
242. *Catalytic Oxidation, Principles and Applications*, R. A. Sheldon, R. A. van Santen, (Eds.) World Scientific Publishing, Singapore, **1995**
243. H. H. Szment, *Organic Building Blocks of the Chemical Industry*, Wiley, New York, **1989**
244. P. Gellin, C. Naccache, Y. B. Taarit, *Pure. Appl. Chem.*, **1988**, 8, 1315
245. A. Aurox, V. Bolis, P. Wierzechowski, P. Grazvelle, J. Vedrine, *J. Chem. Soc. Fraday Trans.*, **1979**, 2544
246. M. Iwamoto, H. Kusamo, S. Kagawa, *Inorg. Chem.*, **1983**, 22, 3366
247. R. A. Scheldon, *Stud. Surf. Sci. Catal.*, **1990**, 55, 1
248. T. G. Kaufmann, A. Kaldor, G. F. Stuntz, M. C. Kerby, L. L. Ansell, *Catal. Today*, **2000**, 62, 77
249. N. K. Nag, A. V. Sapre, D. H. Broderick, B. X. C. Gates, *J. Catal.*, **1979**, 57, 509
250. D. R. Kilanowski, H. Teeuiven, V. H. J. de Beer, B. C. Gates, H. Kwart, *Am. Chem. Soc., Div. Pet. Chem Prepr.*, **1977**, 22, 941
251. A. Stanislaus, B. H. Cooper, *Catal. Rev-Sci. Eng.*, **1994**, 36, 75
252. N. P. Martinez, P. C. H. Mitchell, P. Chiplunker, *J. Less-Common Met.*, **1977**, 54, 333.
253. B. Delmon, *Am. Chem. Soc. Div. Pet. Chem. Prepr.*, **1977**, 22, 503
254. P. Ratnasamy, A. V. Ramasamy, K. Banerjee, D. K. Sharma, N. Ray, J. Catal., **1975**, 38, 19
255. G. V. Smit, C. C. Hinckley, *J. Catal.*, **1973**, 30, 218
256. V. H. J de Beer, T. H. M. Van sint Fiet, G. H. A M. Van der Steen, A. C. Zwaga, G. C. A. Schuit, *J. Catal.*, **1974**, 35, 297
257. Y. Okamoto, H. Nakano, T. Shimokawa, T. Imanaka, Teranishi, *J. Catal.*, **1977**, 50, 447
258. V. H. J. de Beer, M. J. M. van der Aalst, C.J. Machiels, G. C. A. Schuit, *J. Catal.*, **1976**, 43, 78
259. H. Topsoe, B. S. Clausen, N-Y Topsoe, P. Zeuthen, *Stud. Surf. Sci. Catal.*, **1989**, 53, 77
260. M. Zdrazil, *Catal. Today*, **1988**, 3, 269
261. V. Prasad, K. Chary, K. S. Rao, P. K. Rao, *J. Chem. Soc. Che. Commun.*, **1989**, 1746
262. R. Cattaneo, T. Shido, R. Prins, *J. Catal.*, **1999**, 185, 199

263. G. Kishan, L. Coulier, V. H. J. de Beer, J. A. R. van Veen, J. W. Niemantsverdriet, *J. Catal.*, **2000**, 196, 180
264. F. W. Moore, M. L. Larson, *Inorg. Chem.*, **1967**, 6, 998
265. J. P. Fackler Jr., P. G. Holats, *Inorg. Nucl. Chem. Lett.*, **1966**, 2, 251
266. A. Stainsleus, M. Absi-Halabi, K. Al-Dolama, A. Katrib, M. Ismail, *Appl. Catal.*, **1988**, 41, 109
267. G. Muralidhar, B. E. Concha, G. L. Bartholomew, C. H. Bartholomew, *J. Catal.*, **1984**, 89, 274
268. S. J. Tanster, T. A. Pecorero, R. R. Chianelli, *J. Catal.*, **1980**, 63, 515
269. F. E. Massoth, G. Muralidher, J. Shabatai, *J. Catal.*, **1984**, 85, 53
270. S. J. Tanster, K. L. Riley, *J. Catal.*, **1981**, 67, 250
271. S. J. Tanster, K. L. Riley, *J. Catal.*, **1981**, 70, 230
272. T. A. Bodreo, C. H. Bartholomew, K. C. Pratt, *J. Catal.*, **1982**, 78, 253
273. J. -N. Park, J. -H. Kim, H. -I. Lee, *Bull. Korean Chem., Soc.*, **1998**, 19, 1363
274. P. T. Vasudevan, J. L. G. Fierro, *Catal. Rev. -Sci. Eng.*, **1996**, 38, 161
275. M. de Boer, A. J. van Dillen, D. C. Konigsberger, J. W. Geus, M. A. Vuurman, I. E. Waches, *Catal. Lett.*, **1991**, 11, 227
276. F. D. Hardcastle, I. E. Waches, *J. Raman. Spectrosc.*, **1990**, 21, 683
277. K. Y. S. Ng, E. Gulari, *J. Catal.*, **1985**, 92, 340
278. L. Wang, W. K. Hall, *J. Catal.*, **1982**, 77, 232
279. L. Wang, W. K. Hall, *J. Catal.*, **1980**, 66, 251
280. F. R. Brown, L. E. Makovsky, K. H. Ree, *J. Catal.*, **1977**, 50, 162
281. A. Iannibello, S. Marengo, F. Trifiro, P. L. Villa, "*Preparation of Catalysts II, Scientific Basis for the Preparation of Heterogeneous Catalysts*", B. Delmon, P. Grange, P. Jacobs, G. Poncelet, (Eds.), Elsevier, Amsterdam, **1979**
282. J.-N. Park, J.-H Kim, H.-I Lee, *Bull. Korean. Chem. Soc.*, **2000**, 21, 1239
283. F. E. Mascot, *J. Catal.*, **1975**, 36, 164
284. Y. W. Chen, M. C. Tsai, *Ind. Eng. Chem. Res.*, **1997**, 36, 2521

SUMMARY AND CONCLUSIONS

Heterogenisation of homogeneous systems are carried out to get the advantages of both homogenous and heterogeneous systems. One effective method of heterogenisation is encapsulation of homogenous metal complex catalysts inside zeolite Y cages. The work embodied in this thesis is mainly centered on the synthesis and characterization of some encapsulated transition metal complexes. The use of metal complexes for the preparation of well dispersed metal oxide catalyst for hydrodesulphurization reaction is also highlighted in this thesis. The thesis is divided into nine chapters. **Chapter 1** presents a general overview of the supported metal complex systems and the catalytic activity studies reported on such systems. The scope of the present investigation is also presented in this chapter.

Details regarding reagents and materials used, general procedures used for the preparation of the metal exchanged zeolites, synthesis and purification of the ligands, and the characterization techniques employed are given in **Chapter 2.** The characterization techniques used in the present study for the zeolite encapsulated complexes include chemical analysis, CHN analysis, TG, XRD, SEM, BET, surface area, magnetic moment measurements, diffuse reflectance, FTIR and EPR spectroscopies. Low temperature oxygen chemisorption, temperature programmed reduction and Laser Raman spectroscopy were used to characterize the hydrodesulphurization catalysts. Gas chromatograph equipped with FID detector was used to monitor the cyclohexanol oxidation. X-Ray fluorescence spectroscopy was used to estimate the sulphur content in the diesel.

Chapter 3 deals with the synthesis and characterization of zeolite encapsulated cobalt(II), nickel(II) and copper(II) complexes of the Schiff base N,N'-*bis*(quinoxaline-2-carboxalidene)-*o*-phenylenediamine (QOPD). The NaY zeolite used for encapsulating the complexes has the unit cell formula, $Na_{56}[(AlO_2)_{56}(SiO_2)_{36}]x.H_2O$. The Si/Al ratio of metal exchanged zeolite was found to be approximately in the range 2.3-2.4 and it is almost near to that of parent zeolite indicating that there is no collapse of the zeolite framework. XRD patterns also indicate the retention of zeolite framework. The elemental analysis of the zeolite encapsulated QOPD complexes indicate complex formation inside the zeolite cage. The unit cell formulae of the zeolite encapsulated complexes were also derived from the elemental data. The Si/Al ratio and the XRD patterns confirm that the crystallinity of the zeolite is maintained even after the encapsulation of the complex. Moreover the change in intensities of the characteristic peaks of XRD patterns indicate the redistribution of the cations due to encapsulation. Surface area and pore volume of the encapsulated metal complexes are found to be lower that that of the metal exchanged zeolite Y, which further confirms the effective encapsulation of complexes inside the pores of the zeolite Y. The scanning electron micrographs of the encapsulated complexes before and after Soxhlet extraction indicate the absence of surface adsorbed complexes. Some of the IR bands of the complex were obscured by the zeolitic peaks. However, the IR band at 1596 cm^{-1} due to $\nu_{(C=N)}$ of the QOPD is seen shifted to a lower energy (~1545 cm^{-1}) indicating coordination azomethine nitrogen to metal. Magnetic moment values calculated give a qualitative idea about the structure of the complex. A low spin octahedral structure in which metal is in the +3 oxidation state was assigned for the cobalt complex. The nickel(II) complex was also assigned to have the octahedral structure. Square planar structure was assigned for the copper(II) complex. EPR spectrum of the copper(II) complex taken at liquid nitrogen temperature also favour a square planar structure. The conclusions arrived from diffuse reflectance electronic spectra are in agreement with that of magnetic moment studies. The thermal stability of the complexes was ascertained from the TG/DTG data. However due to the small concentration of

the complex in the zeolite no quantitative inference could be drawn from the TG/DTG data.

Details regarding the studies on the metal complexes of the Schiff base, indole-3-carboxalidene semicarbazone are presented in **Chapter 4**. The Si/Al ratio of ~2.4 and XRD patterns of the complexes rules out the possibility of collapse of the crystalline nature of the zeolite Y due to encapsulation. The drop in surface area and pore volume further confirms the successful encapsulation of the metal complexes inside the zeolite cage. FT-IR spectra of the complexes reveal that the coordination takes place through the nitrogen of the azomethine and oxygen of the C=O group, and the presence of some of the ligand bands further confirms the encapsulation. The electronic spectra of the cobalt complex suggest a tetragonally distorted octahedron. An octahedral geometry was assigned for the nickel complex. The magnetic moment values of the complexes also supports the inferences arrived from the electronic spectra. A broad EPR spectrum was observed for the cobalt complex, suggesting a high spin octahedral geometry. The EPR spectrum of the copper complex suggests a flattened tetrahedral structure.

Chapter 5 of this thesis is on the synthesis and characterization of zeolite encapsulated cobalt, nickel and copper complexes of the Schiff base indole-3-carboxalidene-3-amino-1,2,4-triazole. Elemental analysis, surface area and XRD studies provide strong evidence for the encapsulation of the complex without loss of crystallinity. TG/DTG patterns show two decomposition stages, confirming the encapsulation inside the supercages of the zeolite. The FTIR spectra of the complex reveal that coordination of the ligand is through the azomethine nitrogen and the 4th nitrogen of the triazole ring. The electronic spectra of the complexes suggests an octahedral geometry for the cobalt and nickel complexes and a distorted tetrahedral geometry for the copper complex. Magnetic moment values of the complexes are also in agreement with structures arrived from the electronic spectra. A broad pattern was observed for the EPR spectrum of the cobalt complex. The hyperfine splitting observed in the EPR spectrum of the copper

complex suggest the coordination of nitrogen atom to the metal ion. The $g_{\parallel}/A_{\parallel}$ value of 150 cm suggest a flattened tetrahedral geometry.

Chapter 6 deals with the studies of the encapsulated cobalt(II), nickel(II) and copper(II) complexes of the Schiff base N,N'-*bis* (4-hydroxy-3-methoxy benzalidene)-*o*-phenylenediamine (VOPD). The elemental analysis and the drop in surface area and pore volume suggest successful encapsulation of the complexes inside the supercages of zeolite Y. XRD pattern shows that there is no change in crystalline nature of the zeolite support due to encapsulation. The changes in the intensities of the characteristic peaks of the XRD patterns indicate cation redistribution due to encapsulation. The $\nu_{(C=N)}$ band (azomethine) of the ligand was found to be shifted to the lower region in the case of complexes suggesting coordination through the azomethine nitrogen. Thermo gravimetric analysis exhibits two decomposition stages one corresponding to the removal of coordinated water and the other corresponding to the decomposition of complexes. The electronic spectra and the magnetic moment values suggest an octahedral geometry for the cobalt and nickel complexes. A broad EPR spectrum was observed for the cobalt complex. A high $g_{\parallel}/A_{\parallel}$ value of 220 cm obtained for the copper(II) complex suggest a tetrahedrally distorted square planar structure for the complex.

Details regarding the studies of metal complexes of curcumin, the pigment which impart yellow colour to the natural product turmeric, are given in **Chapter 7.** Curcumin was separated from the other curcuminoids by column chromatography. Only nickel(II) and copper(II) form stable encapsulated complexes of curcumin. Cobalt complex of curcumin formed was found to be leached out during soxhlet extraction. The analytical data, XRD patterns and surface area and pore volume data reveal that the crystalline nature of zeolite is intact after encapsulation. The FTIR spectra of the complexes shows that the -C=O group of the curcumine is coordinated to the metal. The electronic spectra and magnetic moment values of the nickel complex suggest an octahedral geometry

and the EPR parameters for the copper(II) complex suggest a square planar structure.

Chapter 8 deals with the studies on catalytic activity of the prepared complexes for the oxidation of cyclohexanol. *Tert*-butyl hydroperoxide was used as the oxidant. In order to optimize the reaction conditions, the effect of various parameters like oxidant to substrate ratio, temperature, amount of catalyst and the effect of various solvents were studied. The activity was found to increase with increase in temperature. The oxidant to substrate ratio of 2:1 was found to the be optimum condition for the reaction. The increase in amount of the catalyst does not appreciably much increase the conversion and in fact, it results in the decrease of the turn over number (TON). The copper complexes exhibit much higher activity than that of the cobalt and nickel complexes. The selectivity towards the product, cyclohexanone, was >98% in all the cases. The geometry of the complexes was found to influence the catalytic activity. The octahedral complexes are found to be less active than the four coordinate complexes. The vacant sites provided by the square planar/distorted tetrahedral structure of the copper complexes facilitate the coordination of the oxidant and substrate and thus increase the conversion. The catalysts were also found to be recyclable.

Sulphur emissions from the automobile exhaust create a lot of environmental problems. Hydrodesulphurization (HDS) is the technique used to remove sulphur compounds from the diesel. **Chapter 9** of the thesis deals with the studies on the preparation, characterization and hydrodesulphurization activity of some new HDS catalysts. The catalysts were prepared through molecular designed dispersion (MDD) method and also through the conventional wet impregnation method. In the MDD method, a neutral transition metal complex is anchored to the surface of a high surface area support and then the adsorbed complex is decomposed in an oxygen containing atmosphere at an elevated temperature yielding the supported transition metal oxide catalyst. Molybdenum and cobalt pyrrolidine-*N*-carbodithioate complexes were used as the catalyst precursors. The prepared catalysts were characterized using elemental analysis,

low temperature oxygen chemisorption, temperature programmed reduction and laser Raman spectroscopy. The studies indicate that the catalysts prepared through MDD method show high molybdenum dispersion, smaller molybdenum clusters and high reducibility of MoO_3 than those prepared though conventional methods. The catalysts prepared though the new method exhibits ~35% increase in activity, in comparison to that of the catalysts prepared through conventional method. Thus a superior hydrodesulphurization catalyst in all the respects was developed though the molecular designed dispersion method.

"If we knew what it was we were doing, it would not be called research, would it?"

- Albert Einstein